UNIVERSITY OF HAWAII
LIBRARY
FEB 19 53

The PHILOSOPHICAL MAGAZINE

FIRST PUBLISHED IN 1798

. 44 SEVENTH SERIES No. 348 January 1953

A Journal of Theoretical Experimental and Applied Physics

EDITOR
PROFESSOR N. F. MOTT, M.A., D.Sc., F.R.S.

EDITORIAL BOARD
SIR LAWRENCE BRAGG, O.B.E., M.C., M.A., D.Sc., F.R.S.
SIR GEORGE THOMSON, M.A., D.Sc., F.R.S.
PROFESSOR A. M. TYNDALL, C.B.E., D.Sc., F.R.S.

PRICE 15s. 0d.
Annual Subscription £8 0s. 0d. payable in advance

AND PUBLISHED BY TAYLOR & FRANCIS LTD., RED LION COURT, FLEET ST., LONDON, E.C.4.

ADVANCES IN PHYSICS

A QUARTERLY SUPPLEMENT OF THE PHILOSOPHICAL MAGAZINE

On 1st January, 1952, the first number of this new Quarterly Supplement to the Philosophical Magazine was published. The aim of this Supplement will be to give those interested in physics comprehensive and authoritative accounts of recent important developments. It is felt by the Editor that in view of the rapid advances in many branches of physics, scientists will welcome a journal devoted to articles of this type.

VOLUME 2 JANUARY 1953 NUMBER 5

The Unsaturated Helium Film. By Earl Long and Lothar Meyer, Institute for the Study of Metals, The University of Chicago, U.S.A.

The Thermal Conductivity of Metals at Low Temperatures. By J. L. Olsen and H. M. Rosenberg, The Clarendon Laboratory, Oxford.

The Diffraction of Radio Waves by the Curvature of the Earth. By M. H. L. Pryce, F.R.S., The Clarendon Laboratory, Oxford.

Tables of Functions occurring in the Diffraction of Electromagnetic Waves by the Earth. By C. Domb, The Royal Society Mond Laboratory, Cambridge.

The Thermal Conductivity of Dielectric Solids at Low Temperatures. By R. Berman, The Clarendon Laboratory, Oxford.

PRICE *per part* **15/-** *plus postage* **PRICE** *per annum* **£2 15s. 0d.** *post free*

Editor: PROFESSOR N. F. MOTT, M.A., D.Sc., F.R.S.
Editorial Board: SIR GEORGE THOMSON, M.A., D.Sc., F.R.S.
PROFESSOR A. M. TYNDALL, C.B.E., D.Sc., F.R.S.
SIR LAWRENCE BRAGG, O.B.E., M.C., M.A., D.Sc., F.R.S.

Printed and Published by
TAYLOR & FRANCIS, LTD., RED LION COURT, FLEET ST., LONDON, E.C.4

THE

PHILOSOPHICAL MAGAZINE

A JOURNAL OF THEORETICAL EXPERIMENTAL
AND APPLIED PHYSICS

First published in 1798

[SEVENTH SERIES—VOL. 44]

I. *Diffusion Problems Associated with the Growth of Crystals from Dilute Solution*

By Alfred Seeger*
H. H. Wills Physical Laboratory, University of Bristol†

[Received August 15, 1952]

Summary

Crystals growing from solutions with plane faces must have considerable supersaturation at some parts of the surface. A supersaturation number σ is introduced to give a measure of the maximum supersaturation. For two-dimensional growth in very dilute solutions a general method for evaluating σ is given ; it is applied to the growth of regular polygons, to the growth of a step on a surface, and to growth on the edge of a plate. For three-dimensional growth only a rough estimate for the supersaturation occurring with regular polyhedra can be given ; it is estimated that the maximum supersaturation on the surface of a cube or regular octahedron is between 0·25 and 0·4 of the concentration difference between the vertices and infinity.

---

§ 1. Introduction

It is known that crystals can grow from solutions with plane faces. We consider here only those cases in which there is no particularly large surface mobility for solute atoms, and in which the solution is dilute, and the diffusion coefficient independent of concentration. Then at any moment the flux of matter or the normal gradient of concentration has to be constant all over a face. This condition is the only one at the crystal surface that is required to specify the mathematical solution of the diffusion problem. This means that the concentration itself will not be uniform at a given face. All over a growing face, however, there must be at least a slight supersaturation ; therefore a considerable supersaturation will occur on parts of the faces, especially near corners and vertices. This conclusion is in agreement with experimental observations on growth of square or rectangular crystals between plates from $NaClO_3$ solutions (Berg 1938, Bunn 1949, Humphreys-Owen 1949). It is presumably this excess of supersaturation at crystal corners which in certain circumstances causes dendritic rather than polyhedral growth : it is therefore very desirable to estimate how this supersaturation excess depends upon crystal geometry.

---

* On leave from Technische Hochschule, Stuttgart, Institut für theoretisch und angewandte Physik.

† Communicated by F. C. Frank.

The fact of growth in plane faces (plane means here only macroscopically plane, not plane on a molecular scale), in spite of a certain amount of supersaturation, is in accordance with the view (Burton, Cabrera and Frank 1951) that below a certain supersaturation crystals can grow only by the screw dislocation mechanism and not by a nucleation process at the surface.

This paper is concerned with theoretical investigation of the diffusion problem and the supersaturation conditions at the crystal surface. This would be a very difficult task for three-dimensional growth and for non-dilute solutions. The problem, however, is tractable for two-dimensional growth in a simple shape at very small concentrations. The latter condition ensures (together with the reasonable assumption that surface migration is unimportant) that the flux has to be constant over any face, and that the growth rate is slow, so that the whole problem can be treated statically. This should give good results for the problem of the advancing step, because the characteristic length of this problem, the step-height a, does not exceed a few hundred ångströms, and is small compared with the ratio of diffusion-coefficient D and growth-rate v in a typical experiment. In the case, however, of regular polygons (a=length of a side) growing in two dimensions it will be more difficult to satisfy the condition $a \ll D/v$, and our treatment is to be regarded as giving the limiting case for very dilute solutions.

We cannot use any of the present observations on two-dimensional growth for comparison with the theory, because the conditions were not sufficiently symmetric and the solutions were far from being dilute. However, it is hoped that future experiments at moderate concentrations and under well-defined conditions will supplement the theory in finding the general dependence of supersaturation conditions on concentration and growth rate.

In §4 we give a few remarks on three-dimensional growth. They are meant only to give a very rough idea about the supersaturation conditions that are to be expected in three-dimensional growth of polyhedra.

§2. GENERAL METHOD FOR TWO-DIMENSIONAL GROWTH

The assumptions made in §1 permit the application of the methods of the theory of functions. The mathematical problem is to find the concentration c, satisfying the two-dimensional potential equation $\nabla^2 c=0$, to which the diffusion equation reduces, subject to the flux conditions stated above.

Two steps are involved in the solution of this problem. Firstly we consider the plane in which the two-dimensional crystal lies as a complex plane $w=u+iv$, and we map the exterior of the crystal by a conformal transformation on the upper half of a complex plane $z=x+iy$. During this transformation the concentration c remains invariant, the normal gradient at the surface, however, is changed. Secondly we solve the potential problem in the x–y-plane by means of Fourier integrals.

For a crystal with polygonal shape this can be done quite generally. The integrals involved can be evaluated only in simple cases. We are not, however, very much interested in the determination of the concentration $c(u, v)$ everywhere in the exterior of the crystal, but mainly in the supersaturation conditions at the crystal surface, especially in the largest supersaturation that occurs in a certain mode of growth. This can be characterized by a single number, the *supersaturation-number* σ, which we define as the difference between the highest and the lowest concentration at the crystal surface, divided by the integral of the normal gradient of the concentration, taken over the trace of the crystal surface in the w-plane. We shall evaluate σ for several crystal shapes.

According to the Schwarz–Christoffel transformation the interior of the polygon shown in fig. 1 in the w-plane is mapped on the upper half of the z-plane by a mapping function

$$w=\phi(z), \qquad (1)$$

which satisfies

$$\frac{dw}{dz}=\psi(z)=\mu(z-z_1)^{\beta_1-1}\dots(z-z_n)^{\beta_n-1}, \qquad (2)$$

or

$$w=\phi(z)=\int_0^z \psi(t)\,dt+\mu'. \qquad (3)$$

$z_1, \dots, z_n$, being points on the real z-axis, are the images of the corners of the polygon. It is mainly the difficulty in finding the z_i for a given polygon that limits the present method either to very symmetrical cases or polygons with only few corners.

The normal derivative $(\partial c/\partial y)_{y=0}=G(x)$ at the boundary in the z-plane can be expressed in terms of $\partial c/\partial n$ and $\psi(x)$ according to the formula

$$\frac{\partial c}{\partial y}=\frac{\partial c}{\partial n}\frac{\partial n}{\partial y}, \qquad (4)$$

and is therefore known. The general solution of the potential equation $\nabla^2 c=0$ with the right behaviour at infinity is given by

$$c(x, y)=\int_{-\infty}^{\infty} g(k)e^{ikx}\,e^{-|k|y}\,dk. \qquad (5)$$

From

$$G(x) = -\int_{-\infty}^{\infty} g(k)\,|k|\,\mathrm{e}^{ikx}\,dk \quad . \quad . \quad . \quad . \quad . \quad . \quad . \qquad (6)$$

$g(k)$ is determined by

$$g(k) = -\frac{1}{2\pi\,|k|}\int_{-\infty}^{\infty} G(x)\,\mathrm{e}^{-ikx}\,dx. \quad . \quad . \quad . \quad . \quad . \quad . \qquad (7)$$

The equations (3), (5) and (7) contain the solution of the problem, and practical applications are solely a question of evaluating these integrals.

Fig. 1

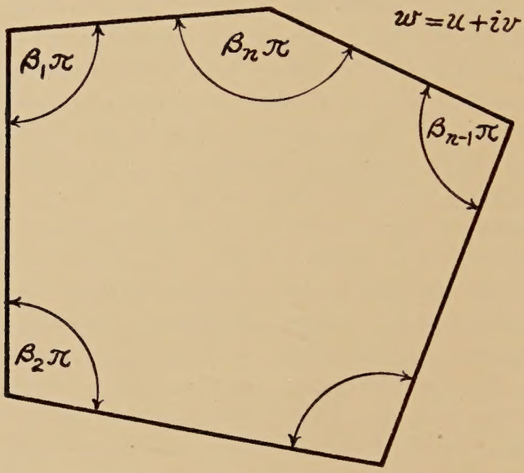

Notation for the angles of an arbitrary polygon.

§3. EXAMPLES

(i) *Regular Polygons* (fig. 2 (*a*))

By symmetry it is sufficient to consider the polygon ABCD with the interior angles $\alpha_1=\alpha_2=\pi(\frac{1}{2}+1/n)$ if the regular polygon has n corners. The upper half of the z-plane (fig. 2 (*b*)) is mapped on the interior of ABCD by

$$w=\mu\int_0^z (1-t^2)^{(1/n-1/2)}\,dt. \quad . \quad . \quad . \quad . \quad . \quad . \quad . \qquad (8)$$

The factor μ is to be determined from the fact that $z=-1$ should correspond to $w=-\frac{1}{2}a$, $z=1$ should correspond to $w=\frac{1}{2}a$ (a being the length of a side of the regular polyhedron). Using the formula (Groebner–Hofreiter 1950)

$$\int_0^1 x^{\kappa-1}(1-x)^{\lambda-1}\,dx = B(\lambda,\kappa) = \Gamma(\kappa)\Gamma(\lambda)/\Gamma(\kappa+\lambda), \quad . \quad . \quad . \qquad (9)$$

we obtain

$$a=\mu B\left(\frac{1}{2}, \frac{1}{2}+\frac{1}{n}\right). \quad . \quad . \quad . \quad . \quad . \quad . \quad . \quad . \quad . \qquad (10)$$

Fig. 2

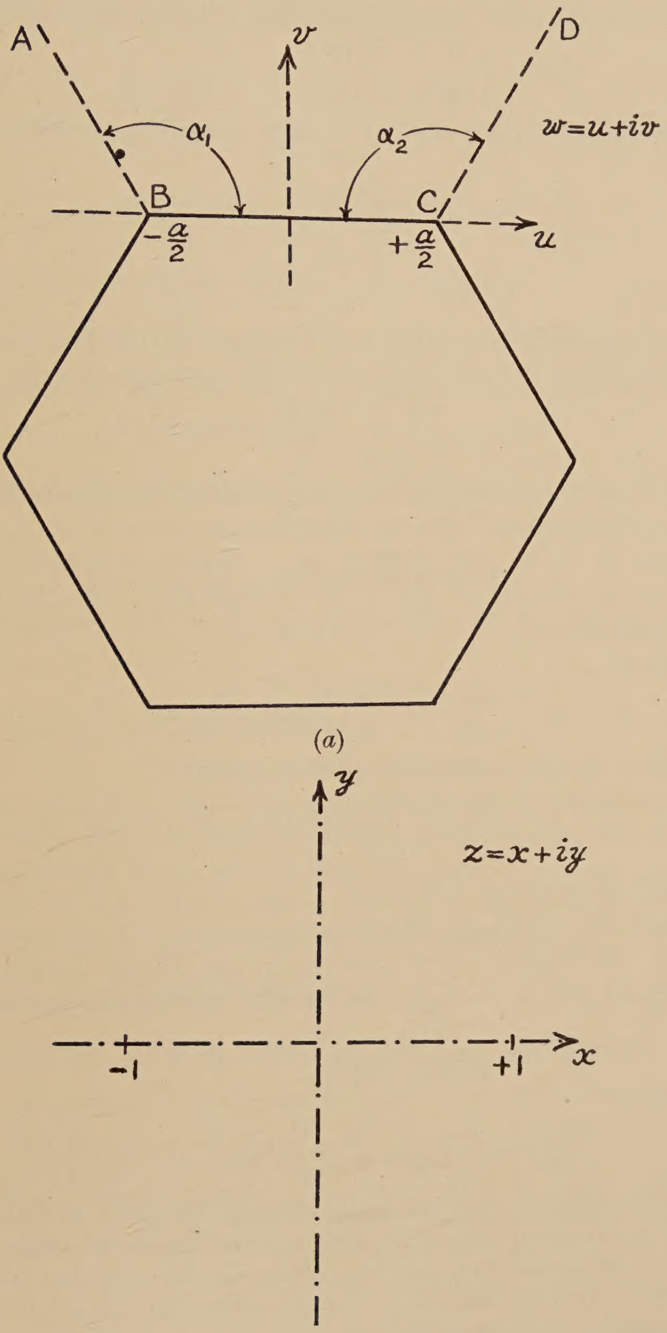

(*a*)

(*b*)

The region within ABCD of fig. 2 (*a*) is mapped upon the region $y>0$ of fig. 2 (*b*).

Let the concentration gradient at the boundary of the regular polyhedron be $\partial c/\partial n = q$. Then the boundary conditions in the z-plane are given by

$$G(x) = \left\{ \begin{array}{ll} 0 & |x| > 1, \\ q\mu(1-x^2)^{(1/n-1/2)} & |x| > 1. \end{array} \right\} . \quad . \quad . \quad . \qquad (11)$$

Due to the symmetry of $G(x)$ we may write the general solution for $c(x, y)$ as

$$c(x, y) = 2\int_0^\infty g(k)\cos kx\, \mathrm{e}^{-ky}\, dk, \quad . \quad . \quad . \quad . \quad . \quad . \qquad (12)$$

where
$$g(k) = -\frac{1}{\pi k}\int_0^\infty G(\xi)\cos k\xi\, d\xi. \quad . \quad . \quad . \quad . \quad . \quad . \qquad (13)$$

It is a mathematical convenience to introduce the complex function $\mathbf{c}(z)$, whose real part is the physically significant concentration $c(x, y) = \mathscr{R}\mathbf{c}(z)$.

Then
$$\mathbf{c}(z) = -\frac{2}{\pi}\int_0^\infty\int_0^\infty \frac{\cos k\xi}{k}\, \mathrm{e}^{ikz} G(\xi)\, d\xi\, dk. \quad . \quad . \quad . \quad . \qquad (14)$$

In order to obtain known functions we consider $d\mathbf{c}(z)/dz$, interchange the order of integration, and use the formula

$$\int_0^\infty \cos k\xi\, \mathrm{e}^{ikz}\, dk = -\frac{iz}{\xi^2 - z^2}, \quad . \quad . \quad . \quad . \quad . \quad . \quad . \qquad (15)$$

which holds for $y > 0$.

This gives

$$\frac{d\mathbf{c}(z)}{dz} = -\frac{2}{\pi}\int_0^\infty G(\xi)\frac{z}{\xi^2 - z^2}\, d\xi, \quad . \quad . \quad . \quad . \quad . \quad . \qquad (16)$$

and (apart from an unessential additive constant)

$$\mathbf{c}(z) = \frac{1}{\pi}\int_0^\infty G(\xi)\ln(z^2 - \xi^2)\, d\xi. \quad . \quad . \quad . \quad . \quad . \quad . \qquad (17)$$

Using eqn. (11), eqn. (16) becomes

$$\frac{d\mathbf{c}(z)}{dz} = -\frac{2q\mu}{\pi}\int_0^1 (1-\xi^2)^{(1/n-1/2)}\frac{z}{\xi^2 - z^2}\, d\xi. \quad . \quad . \quad . \qquad (18)$$

This integral can be evaluated in terms of the hypergeometric function

$$F(a, b, c, z) = \frac{\Gamma(c)}{\Gamma(b)\Gamma(c-b)}\int_0^1 t^{b-1}(1-t)^{c-b-1}(1-tz)^{-a}\, dt. \quad . \qquad (19)$$

The result is

$$\frac{d\mathbf{c}(z)}{dz} = \frac{q\mu}{\pi z} B\left(\frac{1}{2}, \frac{1}{2} + n\right) F\left(1, \frac{1}{2};\ 1 + \frac{1}{n};\ \frac{1}{z^2}\right). \quad . \quad . \qquad (20)$$

By analytic continuation this holds not only for $y > 0$, but also for $y = 0$. We did not succeed in expressing $\mathbf{c}(z)$ in terms of well-investigated functions. It is, however, possible to express the minimum concentration $\mathbf{c}(0)$ at $w = 0$ and the maximum concentration $\mathbf{c}(1)$ at $w = \frac{1}{2}a$ in terms of the logarithmic derivative of the factorial

$$\Psi(z) = \frac{d\ln \Pi(z)}{dz} = \frac{d\ln \Gamma(z+1)}{dz} \quad . \quad . \quad . \quad . \quad . \quad . \qquad (21)$$

by using the formula (Groebner–Hofreiter 1950)

$$\int_0^1 x^{\kappa-1}(1-x)^{\lambda-1}\ln(1-x)\,dx=B(\kappa,\lambda)[\Psi(\lambda-1)-\Psi(\kappa+\lambda-1)].$$

This gives

$$\mathsf{c}(1)=\frac{q\mu}{2\pi}B\left(\frac{1}{2},\frac{1}{2}+\frac{1}{n}\right)\left[\Psi\left(-\frac{1}{2}+\frac{1}{n}\right)-\Psi\left(\frac{1}{n}\right)\right], \quad . \quad (23)$$

and

$$\mathsf{c}(0)=\frac{q\mu}{2\pi}B\left(\frac{1}{2},\frac{1}{2}+\frac{1}{n}\right)\left[\Psi\left(-\frac{1}{2}\right)-\Psi\left(\frac{1}{n}\right)\right]. \quad . \quad . \quad . \quad (24)$$

The saturation number is

$$\sigma=\frac{\mathsf{c}(1)-\mathsf{c}(0)}{nqa}=\frac{1}{2\pi n}\left[\Psi\left(-\frac{1}{2}+\frac{1}{n}\right)-\Psi\left(-\frac{1}{2}\right)\right]. \quad . \quad . \quad (25)$$

An approximately valid formula for large n is obtained from the leading term,

$$\sigma=\pi/4n^2, \quad . \quad . \quad . \quad . \quad . \quad . \quad . \quad . \quad . \quad (26)$$

of the Taylor expansion in powers of $1/n$. It gives values for σ (in table 1 given as σ_2) which are too large, the correction term being of the order $1/n^3$.

Another upper bound for σ was suggested by F. C. Frank. If the concentration field were that of a line-sink of unit strength (so having circular symmetry despite the polygonal form of the crystal boundary), giving

$$c=(1/2\pi)\ln r, \quad . \quad . \quad . \quad . \quad . \quad . \quad . \quad . \quad . \quad (27)$$

the supersaturation number would be

$$\sigma=-(1/2\pi)\ln\cos(\pi/n). \quad . \quad . \quad . \quad . \quad . \quad . \quad . \quad (28)$$

The actual value for σ (which we give in table 1 as σ_1) must be between 0 and the value given by eqn. (28). For large n eqn. (28) reduces to eqn. (26), the next term being of the order $1/n^4$.

We refer to the approximation that gives eqn. (28) as the 'circle-approximation'; corresponding values of σ appear in table 1 as σ_3. The corresponding 'sphere-approximation' may be applied to regular polyhedra and will be dealt with in § 4.

Table 1

n	2	3	4	6	8	10	20
σ_1	0·111	0·0570	0·0349	0·0171	0·0101	0·00674	0·00177
σ_2	∞	0·1103	0·0551	0·0229	0·0126	0·00798	0·00198
σ_3	0·196	0·0822	0·0492	0·0218	0·0123	0·00785	0·00196

As it is difficult to give the concentration along one of the faces of the polygons by evaluation of eqns. (8) or (17), we shall now derive a simple interpolation formula for the concentration along the faces. We denote this concentration as a function of u by $C(u)$, and we express $C(u)$ by an interpolation formula giving the correct value for σ and for $dC(u)/du$ at $u=\tfrac12 a$ (which we denote by $C'(\tfrac12 a)$). Such an interpolation formula is

$$C(u)-C(0)=\{2C(\tfrac12 a)-2C(0)-\tfrac14 aC'(\tfrac12 a)\}(2u/a)^2 \\ +\{\tfrac14 aC'(\tfrac12 a)-C(\tfrac12 a)+C(0)\}(2u/a)^4. \quad . \quad (29)$$

In order to evaluate $C'(\tfrac12 a)$ we apply to eqn. (20) the formula

$$F(a,b\,;\,c\,;\,z)=\frac{\Gamma(c)\Gamma(c-a-b)}{\Gamma(c-a)\Gamma(c-b)}F(a,b\,;\,a+b-c+1\,;\,1-z) \\ +(1-z)^{c-a-b}\frac{\Gamma(c)\Gamma(a+b-c)}{\Gamma(a)\Gamma(b)}F(c-a,c-b\,;\,c-a-b+1\,;\,1-z) \quad . \quad (30)$$

and proceed then to the limit $u=\tfrac12 a\,(z=1)$ in the equation for $C'(u)$. This gives after some calculation

$$C'(\tfrac12 a)=\frac{q}{\pi}\,\frac{\Gamma\left(\frac12+\frac1n\right)\Gamma\left(\frac12-\frac1n\right)}{\Gamma(1)}=\frac{q}{\cos(\pi/n)}. \quad . \quad . \quad . \quad . \quad (31)$$

Our interpolation formula (31) becomes now

$$\frac{C(u)-C(0)}{qa}=\left\{2\sigma n-\frac{1}{4\cos(\pi/n)}\right\}\left(\frac{2u}{a}\right)^2+\left\{-\sigma n+\frac{1}{4\cos(\pi/n)}\right\}\left(\frac{2u}{a}\right)^4. \\ . \quad . \quad . \quad (32)$$

This method can of course be extended to include higher derivatives, for instance d^2C/du^2 at the centre of an edge.

(ii) *Growth of Steps on Crystal Surfaces*

Crystals showing growth-spirals grow in steps of a step-height equal to the Burgers vector of the screw-dislocation which forms the axes of the spiral. One does not know anything about the actual shape of the step. We assume here that it is a plane, but we do not make any assumptions about the angle γ (see fig. 3). We can treat this problem along the lines indicated in § 2. We introduce a complex variable $w=u+iv$ as shown in fig. 3. The mapping function of the (degenerate) polygon formed by the trace of the crystal surface on the z-plane is

$$w=\mu\int_0^z\left(\frac{1+t}{1-t}\right)^{\gamma/\pi}dt+\mu'. \quad . \quad . \quad . \quad . \quad . \quad . \quad . \quad (33)$$

From the condition that the distance between A and B is equal to a, μ is determined by

$$a=\mu\int_{-1}^{1}\left(\frac{1+t}{1-t}\right)^{\gamma/\pi}dt=\frac{2\mu\gamma}{\sin\gamma}. \quad . \quad . \quad . \quad . \quad . \quad . \quad (34)$$

The function $(\partial c/\partial y)_{y=0}=G(x)$ is, if the normal gradient of the concentration along the step is denoted by q,

$$G(x)=\left\{\begin{array}{ll} 0 & |x|>1, \\ q\mu\{(1+x)/(1-x)\}^{\gamma/\pi} & |x|\leqslant 1. \end{array}\right\} \quad . \quad . \quad . \quad (35)$$

By calculations similar to those in the first example one finds for the concentration

$$c(x,\,y)=\mathscr{R}\mathbf{c}(z)=\frac{q\mu}{\pi}\,\mathscr{R}\int_{-1}^{+1}\ln\,(z-\xi)\left(\frac{1+\xi}{1-\xi}\right)^{\gamma/\pi}d\xi. \qquad . \quad . \quad (36)$$

The difference Δc between the concentrations at $z=-1$ and $z=1$ is given by

$$\Delta c=\frac{q\mu}{\pi}\int_{-1}^{+1}\left(\frac{1+\xi}{1-\xi}\right)^{\gamma/\pi}\ln\left(\frac{1+\xi}{1-\xi}\right)d\xi=qa\left(\frac{1}{\gamma}-\cot\gamma\right), \qquad . \quad . \quad (37)$$

and the saturation number is

$$\sigma=\frac{\Delta c}{qa}=\frac{1}{\gamma}-\operatorname{ctg}\gamma=\frac{1}{3}\gamma+\frac{1}{45}\gamma^3+\frac{2}{945}\gamma^5+\cdots \qquad . \quad . \quad (38)$$

σ is plotted as a function of γ in fig. 4. A remarkable feature is that σ is approximately a linear function of γ for small γ but that it rises sharply if the angle becomes an obtuse one.

We should mention that the problem solved in this example also provides the solution for a crystal growing in the shape shown in fig. 5.

Fig. 3

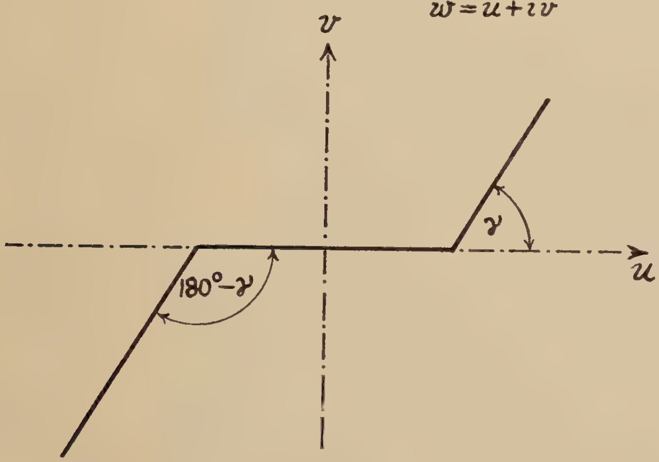

Coordinates for a stepped crystal surface.

§4. THREE-DIMENSIONAL GROWTH OF REGULAR POLYHEDRA

Quantitative observations during growth of crystals suitable for checking the theory are most likely to be made for two-dimensional growth. For natural growth of crystals, however, the growth in three dimensions is most important. The simplest cases of growth in polyhedral shape are growth in the form of a cube or of a regular octahedron. These cases cannot be treated exactly even under the idealized conditions which we introduced into the earlier parts of this paper. These idealizations allow one to replace the diffusion problem by a problem of heat conduction; we have to find the temperature outside a solid body with zero thermal conductivity and with a uniform distribution of heat sinks on

Fig. 4

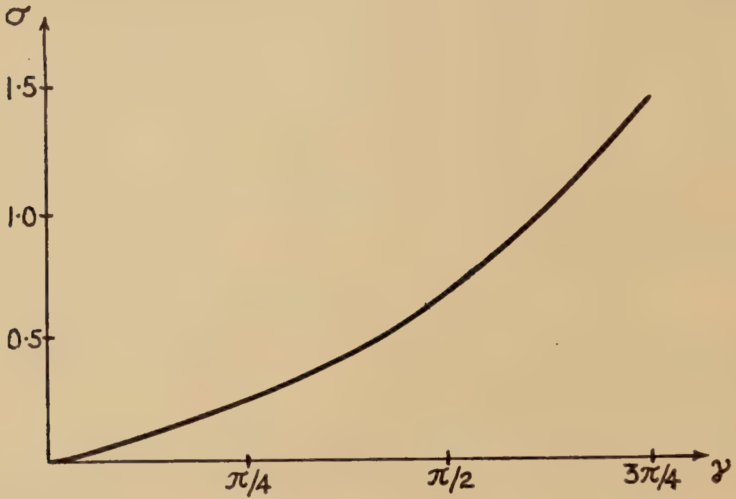

Dependence of the supersaturation range at a step upon its steepness, γ.

Fig. 5

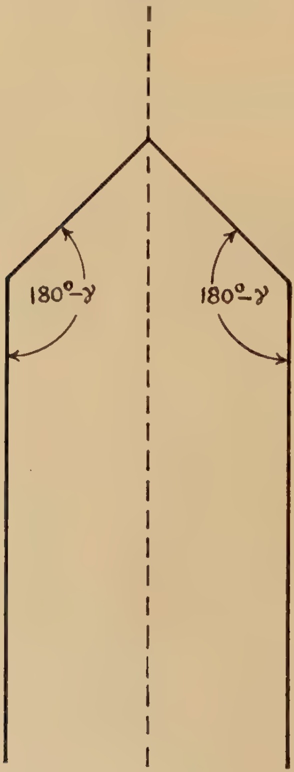

Another crystal form to which the step solution applies.

its surface. In this heat-conduction problem we can ask for the solution of this problem not only for octahedron, cube and tetrahedron (these are the only regular solids that are possible growth shapes of crystals), but also for icosahedron, dodecahedron and for the dihedra. These dihedra (Klein 1924) are improper regular solids with zero volume; they consist of two regular polygons as the only faces.

We shall apply the sphere-approximation to the proper regular polyhedra, and we may expect from the results in §3 that this will give an overestimate for σ of about 10 to 20% for the icosahedron and the dodecahedron. On the other hand we can solve the heat-conduction problem accurately in a simple way for one of the dihedra, namely the limiting case of a large number of corners, the circular disk. So we get for the sequence of regular solids two numerical values for the saturation number comparatively accurately, and we may interpolate for the other regular solids. (We continue to give the discussion in terms of concentration rather than in terms of temperature.)

We denote the radius of the circumscribed sphere of the regular polyhedra by R_1, the radius of the inscribed sphere by R_2, and the length of the edges by d. In order to get a dimensionless quantity for the supersaturation number σ we adopt a definition slightly different from the one used in two dimensions. We define σ/R_1 as the difference between the maximum and the minimum concentration divided by the integral of the normal gradient of concentration, taken over the whole surface.

The concentration field of a unit point-sink is given by

$$c=-1/4\pi r. \qquad (39)$$

In the sphere-approximation we assume this to be the concentration also in the presence of the solid. The supersaturation number is then given by

$$\sigma=(1/4\pi)(-1+R_1/R_2). \qquad (40)$$

In table 2 we give a list for R_1, R_2 (Buerklen–Ringleb 1936) and for σ, calculated from eqn. (40).

For the circular disk the sphere-approximation would give an infinite supersaturation number. We can, however, solve this problem exactly. If ρ, z, ϕ are cylindrical polar coordinates, $\rho=R_1$, $z=0$ correspond to the circumference of the disk, and q is equal to $|\partial c/\partial z|$ on the disk, then the concentration is given by

$$c(\rho, z)=-qR_1\int_0^\infty J_0(\lambda\rho)J_1(\lambda R_1)\,e^{-\lambda z}\,d\lambda/\lambda. \qquad (41)$$

J_ν is the Bessel function of order ν. The minimum concentration at the centre of the disk is

$$c(0, 0)=-qR_1\int_0^\infty J_1(\lambda R_1)\,d\lambda/\lambda=-qR_1\,; \qquad (42)$$

the maximum concentration at the circumference is

$$c(R_1,\ 0)=-qR_1\int_0^\infty J_0(\lambda R_1)J_1(\lambda R_1)\,d\lambda/\lambda=-2qR_1/\pi. \quad . \quad . \quad (43)$$

The supersaturation number is

$$\sigma=\frac{1}{2\pi}-\frac{1}{\pi^2}=0{\cdot}0579. \quad . \quad . \quad . \quad . \quad . \quad . \quad . \quad (44)$$

This is less than the value of σ in table 2 for the tetrahedron, cube and octahedron. Comparing with $n=2$ in two dimensions one would expect the proper solids to have smaller supersaturation numbers than an improper one. This shows that we have to reduce these values of σ to a considerable extent. We think that it might be a good estimate to assume that σ is between 0·025 or 0·03 for cube and octahedron, and between 0·03 and 0·04 for the tetrahedron.

Table 2

	R_1/d	R_2/d	R_1/R_2	σ
Icosahedron	$\frac{1}{4}\sqrt{}2(5+\sqrt{}5)$	$\frac{1}{2}\sqrt{}[(7+3\sqrt{}5)/6]$	1,258	0·0205
Dodecahedron	$\frac{1}{4}(1+\sqrt{}5)\sqrt{}3$	$\frac{1}{4}\sqrt{}[(50+22\sqrt{}5)/5]$	1,258	0·0205
Octahedron	$\frac{1}{2}\sqrt{}2$	$\frac{1}{2}\sqrt{}6$	1,732	0·0587
Cube	$\frac{1}{2}\sqrt{}3$	$\frac{1}{2}$	1,732	0·0587
Tetrahedron	$\frac{1}{4}\sqrt{}6$	$\frac{1}{2}\sqrt{}6$	2,000	0·0796

In three dimensions it is possible to relate the concentration difference $\Delta_1 c$ between infinity and the surface of the crystal to the supersaturation Δc at the surface. If the concentration field were really that given by eqn. (39), and if $\Delta_1 c$ were taken at the vertices of the solid, this relation would be

$$\Delta c=4\pi\sigma\Delta_1 c. \quad . \quad . \quad . \quad . \quad . \quad . \quad . \quad . \quad (45)$$

In the case of the disk the corresponding relation is

$$c=0{\cdot}571\Delta_1 c, \quad . \quad . \quad . \quad . \quad . \quad . \quad . \quad . \quad (46)$$

if $\Delta_1 c$ is taken between the edge of the disk and infinity, and

$$c=0{\cdot}364\Delta_1 c, \quad . \quad . \quad . \quad . \quad . \quad . \quad . \quad . \quad (47)$$

if $\Delta_1 c$ is taken between the centre of the disk and infinity.

For the disk the numerical factor $4\pi\sigma$ in eqn. (45) would be 1·23 times the correct factor given by eqn. (46), so that both give the same order of magnitude. A rough estimate for a cube and a regular octahedron would be that under symmetrical conditions Δc is between 25% and 40% of $\Delta_1 c$.

ACKNOWLEDGMENTS

My thanks are due to Dr. F. C. Frank for suggesting the problem and for valuable suggestions, to Professor N. F. Mott for the opportunity to work in the H. H. Wills Physical Laboratory, and to the British Council for the award of a scholarship.

REFERENCES

BERG, W. F., 1938, *Proc. Roy. Soc.* A, **164,** 79.
BUNN, C. W., 1949, *Discussions Faraday Soc.* No. 5 (Crystal Growth), p. 132.
BUERKLEN, O. TH., and RINGLEB, F., 1936, *Mathematische Formelsammlung, Berlin.*
BURTON, W. K., CABRERA, N., and FRANK, F. C., 1951, *Phil. Trans.* A, **243,** 299.
GROEBNER, W., and HOFREITER, N., 1950, *Intejraltafeln,* Zweiter Teil (Wien: Springer).
HUMPHREYS-OWEN, S. P. F., 1949, *Proc. Roy. Soc.* A, **197,** 218.
KLEIN, F., 1924, *Elementarmathematik vom höheren Standpunkt aus.* 3rd ed. (Berlin: Springer), p. 129.

II. *Further Observations on the Helium II Film by an Optical Method*

By L. C. Jackson and D. G. Henshaw*
H. H. Wills Physical Laboratory, University of Bristol†

[Received October 15, 1952]

Abstract

Further studies of the helium film have been made using the optical method of Burge and Jackson. Evidence has been obtained that there is a film of helium I at 2·3° K about 10 atoms thick, but accurate values of this thickness have not yet been obtained. It has been shown that the thickness of the creeping film of helium II does not change when the volume of liquid flowing per second in the film decreases considerably and that the thickness is equal to that of the stationary film under the same conditions.

Bulk liquid is seen to form when the helium II film flows on to a surface (i) which is below the highest liquid level and (ii) which has a perimeter smaller than that which controls the rate of creep. The bulk liquid returns to the film if the latter then flows on to a surface with a perimeter at least as great as the controlling perimeter.

§ 1. Introduction

In a previous paper (Jackson and Henshaw 1950)‡ a description was given of simultaneous measurements of the transfer rate of liquid helium II from a stainless steel beaker and of the thickness of the moving film on the outside of the beaker by the optical method of Burge and Jackson (1951). These observations have been continued for the investigation of certain specific problems. A preliminary account of part of the work was given at the Oxford Conference on Low Temperature Physics, 1951 (Jackson and Henshaw (1951)).

§ 2. Observations of Helium I Film

The work of Kistemaker (1947) and Long and Meyer (1949) has shown that one may expect to observe a film 15–30 atomic layers thick on any solid substance in contact with liquid helium I at temperatures immediately above the λ-point. Such a film was not observed by Burge and Jackson but their technique was, however, as follows. Readings of the position of the nicol prism were made at some temperatures below the λ-point. The temperature was then allowed to rise above the λ-point and was maintained constant at, say 2·3° K. Readings of the position of the nicol prism were again made, after which the radiation from a small electric lamp held close to the cryostat was allowed to fall on the mirror for a few minutes. After switching off the lamp the position of the nicol prism was read once more. The averages of the readings of the second and third sets were always found to be the same within the accuracy of the observations. This could mean (i) that no film was present at the temperature 2·3° K or (ii) that a film was initially present at 2·3° K and was evaporated by absorption of radiation from the lamp but was reformed completely either from the bulk liquid or from the vapour phase, after the lamp had been switched off, during the period of 1–2 minutes required to take the first few observations of the third set. The first alternative was assumed by Burge and Jackson and the difference between the first and second sets of nicol readings was taken as a measure of the total thickness of film present at the temperature of the first set of observations.

---

* On leave of absence from the National Research Council of Canada. Now at Atomic Energy of Canada Limited, Chalk River, Ontario.

† Communicated by the Authors.

‡ The values of $\bar{v}$ in this paper are incorrect. The values should be 69, 69, 68, 59 and 44 cm/sec.

The second alternative has now been investigated and found to be the correct one. For this purpose a small electric heater was attached to the top of the mirror used by Burge and Jackson, the current leads being taken down into the liquid helium and then up the support. Thus no heat was conducted down the leads directly to the mirror and the helium film on it. Observations were then made of the nicol position (i) below the λ-point (no heat input), (ii) at 2·3° K (no heat input) and (iii) at 2·3° K (heat on). For a dissipation of 50 milliwatts or more the nicol setting was seen to change from (ii) and take on a new constant value. On switching off the current in the heater the setting returned to the value (ii) within about one minute. The nicol shift between settings (ii) and (iii) corresponded to the presence of a film at 2·3° K of the order of magnitude of 10 atomic layers* and so all film thicknesses given by Burge and Jackson (1951) and Henshaw and Jackson (1950)† have to be increased by this amount. Owing to circumstances accidentally present, these observations could not be made with the accuracy usually obtained. We shall therefore not give any table of corrected values here but shall postpone publication until the results of definitive experiments now in progress are available.

Calculations of the velocity of the helium II film as given by Jackson and Henshaw (1950, 1951) involve not only the measured film thickness but also the measured creep rate and the geometric internal perimeter of the beaker. The recent observations of Chandrasekhar and Mendelssohn

---

* Taking the value $4{\cdot}0 \times 10^{-8}$ cm (Keesom and Schweers) for the thickness of one atomic layer, as used by Kistemaker (1947).

† Also thickness measurements quoted by Henshaw and Jackson at the Conference on Low Temperature Physics at the National Bureau of Standards, Washington, 1951.

(1952) with highly polished stainless steel appear to show that the higher creep rates observed on less highly polished metals under clean conditions are a mixture of true film flow at a universal rate depending only on the temperature and a flow in cracks and other channels. Until the present controversy as to the interpretation of the observed creep rates is finally settled it is perhaps inopportune to publish values of the calculated film velocities.

§ 3. THICKNESS OF THE TRANSFER FILM AT SUBCRITICAL VELOCITIES

In the experiments of Jackson and Henshaw (1950) in which the thickness of the helium film was measured during transfer into or out of a cylindrical stainless steel beaker, the observations were made on the film on the outside of the beaker. The liquid helium in the film at the point of observation was necessarily moving with a subcritical velocity. It was, however, not known whether variation of the velocity within the subcritical range had any influence on the thickness of the moving film. To decide this question and to obtain visual evidence of the production of bulk liquid as described in the next section, the beaker shown in fig. 1 (*a*) was constructed. It was again of stainless steel and consisted of two cylindrical portions, the upper of internal diameter 0·7 cm and external diameter 0·8 cm, the lower of 0·3 cm and 0·4 cm respectively. It was provided with a glass capillary tube to observe the level of the liquid in the beaker and with a radiation shield as shown in fig. 1 of the previous paper. A strip of plane mirror, 2 mm wide, was ground and polished on the outside of each portion of the beaker and barium stearate films were deposited as usual so that there was a 1–3 boundary at A and a 3–5 boundary at B.

Fig. 1

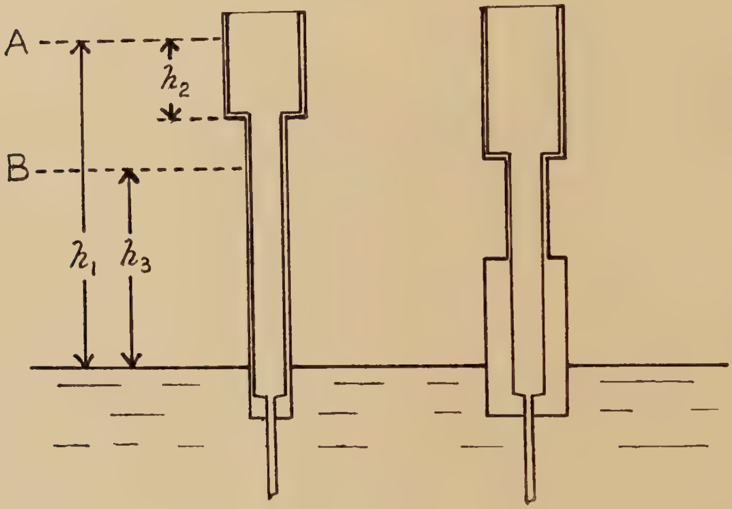

(*a*) (*b*)

Observations were then made at the 1–3 boundary at various temperatures below the λ-point after the beaker had been filled and withdrawn almost entirely from the liquid helium. The thickness of the film at A was found to be the same within the accuracy of the observations when the inner liquid level was in the upper wider part of the beaker or in the lower narrower part and was equal to that of the stationary film present when the transfer had ceased. Thus since the volume of liquid transferred per second decreased by a factor of more than 2 when the inner level entered the narrow part, the velocity of the helium in the film must have decreased by the same factor. For subcritical velocities of flow the film thickness therefore depends only on the temperature, the height of the point of observation above the main liquid surface and (presumably) on the nature of the substrate. The velocity of the flowing helium adapts itself to the amount of helium transferred per second.

§ 4. PRODUCTION OF BULK LIQUID FROM THE FILM AND VICE VERSA

When observations were made at point B on the lower part of the beaker the results were as follows. When the inner liquid level was in the wider part of the beaker the appearance at B was that of a waterfall or a stream of liquid with large local variations of thickness. When the inner level was in the narrower part the usual film was observed with a thickness corresponding to the height h_3. Bulk liquid was therefore formed when the film carrying a volume of liquid per second proportional to the internal diameter of the upper part of the beaker flowed on to the narrower part of the beaker. Since however the thickness of the film at A was that for the height h_1 and not the much smaller height h_2 (the distance to the point at which bulk liquid first appeared) the film must have been continuous over the whole beaker and the bulk liquid represented the excess liquid which could not be carried by the film on the surface of reduced perimeter.

Mendelssohn and Chandrasekhar (Mendelssohn (1951), Chandrasekhar (1952)) have studied the formation of bulk liquid from the helium II film with a glass beaker of varying internal diameter and provided with external ‘ skirts ’. They interpreted their observations as showing that bulk liquid is formed from the film at points below the level of the liquid in the beaker when the film flows on to a surface with a perimeter smaller than that governing the rate of transfer and that film is reformed if the total liquid flowing then encounters a surface of perimeter larger than (or equal to) that originally governing the rate of transfer.

The above observations by the optical method give a complete visual confirmation of the correctness of the first part of their conclusions. To test the second part a further beaker of the shape shown in fig. 1 (*b*) was constructed.* The observations on the upper and middle portions were exactly as recorded for the beaker of fig. 1 (*a*) as was to be expected. Observations on the lower portion of the new beaker showed the presence of a film of a thickness corresponding to the height of the lower boundary above the outer liquid level independent of the position of the inner liquid level. The helium, which appeared as bulk liquid on the narrow part of the beaker, had therefore returned to the film form on the wider lower part of the beaker.

---

* We are indebted to Mr. A. C. Ham for these observations.

A further simple observation* is of interest. A beaker was filled with helium II and partly withdrawn from the liquid. An accidental disturbance to the support caused some of the contents to splash over. This liquid was seen to run down the mirror in the form of separate drops (diameter $\frac{1}{5}$–$\frac{1}{2}$ mm). In spite of the fact that the beaker was covered with a thick film of helium II the drops showed no tendency to spread. This may seem strange at first sight but it is what must be expected when the surface is covered by the creeping film of helium II which can carry only a certain maximum flow at any temperature. Liquid in excess of this flow cannot enter the film and remains as bulk liquid in the form of separate drops. When the observations were repeated at a temperature above the λ-point the results were quite different. The liquid splashing over was seen to drain down and spread sideways in the manner to be expected with any normal viscous liquid which wets the substrate.

REFERENCES

Burge, E. J., and Jackson, L. C., 1951, *Proc. Roy. Soc.* A, **205,** 270.

Chandrasekhar, B. S., 1952, *Thesis,* Oxford.

Chandrasekhar, B. S., and Mendelssohn, K., 1952, *Proc. Phys. Soc.* A, **65,** 226.

Jackson, L. C., and Henshaw, D. G., 1950, *Phil. Mag.,* **41,** 1081 ; 1951, *Proc. Conf. Low Temp. Physics,* Oxford, 65.

Kistemaker, J., 1947, *Physica,* **13,** 81.

Long, E. A., and Meyer, L., 1949, *Phys. Rev.,* **76,** 440.

Mendelssohn, K., 1951, *Proc. Conf. Low Temp. Physics,* Oxford, 66.

---

* We are indebted to Mr. A. C. Ham for these observations.

III. *The Polarization Fields and the Resonance Frequencies of the Alkali Halide Crystals*

By Sir K. S. Krishnan, F.R.S., and S. K. Roy
National Physical Laboratory of India, New Delhi*

[Received August 7, 1952]

Abstract

The effect of the polarization field on the dielectric constant of a medium can be taken into account in two alternative ways, which are equivalent. It may be regarded as enhancing the actual field that produces the polarization, or as determining the resonance frequencies of the medium, which will be different from the frequencies of the individual oscillators that constitute the medium. The dispersions of the alkali halides are discussed from the latter point of view. Though the polarization factors defining the interactions between the infra-red oscillators have the Lorentz value $4\pi/3$, those defining the interactions of the *electronic* oscillators are found to be zero. The electronic overlap between the neighbouring ions in their equilibrium positions seems to be just the one that corresponds to negligible interactions between the electronic oscillators.

§1. Introduction

The part played by the polarization field in dielectric phenomena has been discussed in detail by Lorentz (1908), and following him by several authors. (For a good account of the subject see Debye 1928, Fröhlich 1949, or Rosenfeld 1951.) An obvious method of considering the influence of the polarization field on the dielectric constant is to regard the effective field that produces the polarization as including the polarization field in addition to ' the field in the medium ', to which the polarization field will naturally be proportional. The result will be an enhanced susceptibility and a correspondingly enhanced dielectric constant. This method of calculating the effect of the polarization field is the one usually adopted.

The polarization field is also known (Krishnan and Roy 1951) to play an important part in determining the observed resonance frequencies of the medium. Hence its effect on the dielectric constant may also be regarded as exercised indirectly through its influence on the resonance frequencies. The dispersion of the dielectric constant of the alkali halide crystals is discussed in the present paper from the latter point of view. The alkali halides are particularly suitable for this purpose.

---

* Communicated by the Authors.

The point of view adopted here throws also some light on the relation between the different types of dispersion formulae, and in particular on the relation between the characteristic frequencies that appear in these formulae.

§ 2. THE EFFECT OF THE POLARIZATION FIELD ON THE PRINCIPAL LATTICE OSCILLATION OF AN ALKALI HALIDE CRYSTAL

In a recent paper (Krishnan and Roy 1951) the frequency of the principal mode of oscillation of an alkali halide crystal, in which the lattice of the alkali ions oscillates with respect to the lattice of the halide ions, was calculated on the basis of the simple Born model. It was found that the electric polarization of the crystal due to the separation of the charges accompanying the oscillation, plays an important part in determining the frequency. Separating the two lattices by a small distance r one can obviously express the potential energy of the crystal thus deformed as a power series in r, in which owing to the centre of symmetry of the lattice points of the undeformed crystal, terms involving odd powers of r will naturally be absent. We shall confine attention at present to the r^2 term, which is the first non-vanishing, and also the predominant, term involving r, and which determines the frequency. We shall denote this term in the potential energy per *pair* of ions by

$$W=ar^2=\tfrac{1}{2}\mu\omega_i^2r^2, \quad . \quad . \quad . \quad . \quad . \quad . \quad . \quad . \quad (1)$$

where μ is the reduced mass of the pair given by $1/\mu=1/m_1+1/m_2$ and m_1 and m_2 are the masses of the two ions, and ω_i is the angular frequency of the principal mode of oscillation.

The essential part of the problem is to evaluate the contributions to a from the different types of interactions. This has been done in the paper referred to, and we shall merely quote here the relevant results. It will be seen immediately, in view of the centre of symmetry of all the lattice points, that the electrostatic interactions contribute nothing to a. As regards the repulsion interactions, they may be taken to be of the form $Ae^{-R/\varrho}$, where R is the distance between the interacting ions, and they are of short range, since ρ is found to be much shorter than the equilibrium distance d between the neighbouring ions. Hence these interactions may be regarded as confined to the immediate neighbours only. Their contribution to a is found to be equal to

$$\frac{3}{2N\beta\, d^2}=\frac{\alpha e^2(\delta-2)}{6d^3}=a_1 \text{ say}, \quad . \quad . \quad . \quad . \quad . \quad . \quad . \quad (2)$$

where N is the number of ion-pairs per unit volume, β is the compressibility of the crystal, α is the Madelung constant, d is the equilibrium distance between neighbouring ions, $\delta=d/\rho$ and e is the electronic charge. The interactions of the van der Waals type involving the dipole moments induced in the ions contribute relatively little to a, and they are neglected throughout.

Had a_1 been the *whole* of the contribution to a, the frequency of the principal lattice oscillation of the crystal would be given by

$$a_1=\tfrac{1}{2}\mu\Omega_i^2. \quad \ldots \quad (3)$$

But actually the contribution to a from the polarization field is considerable. For a given relative displacement r between the two lattices the polarization per unit volume is given by

$$P=Ner. \quad \ldots \quad (4)$$

In the paper referred to it was shown (1) that owing to the electronic overlap between the neighbouring ions, this polarization does not induce any *electronic* polarization in the ions, and (2) that the polarization field acting on an ion and tending to displace it as a whole, has just the Lorentz value, namely $(4\pi/3)P$, and hence (3) that the corresponding contribution to a is given by

$$a_2=-\tfrac{2}{3}\pi Ne^2. \quad \ldots \quad (5)$$

This term is negative since the polarization field is in a direction that tends to *increase* the relative displacement r between the two lattices.

In NaCl, for example, a_2 is found to be numerically nearly half of a_1 and since they are of opposite signs, a_2 is of almost the same magnitude as a, the net coefficient of the r^2 term, namely

$$a=a_1+a_2. \quad \ldots \quad (6)$$

For most of the alkali halide crystals the frequency ω_i calculated in this manner by taking the polarization field into account, agrees well with the observed reststrahlen frequency (Krishnan and Roy 1951).

§3. THE MAGNITUDE OF THE POLARIZATION FIELD

As is well known the internal field F in a dielectric may differ considerably from the field E in the medium, the difference between them being the polarization field

$$F=E+p\chi E, \quad \ldots \quad (7)$$

in which χ is the susceptibility of the medium, i.e., the polarization per unit volume per unit field in the medium, and p is the polarization factor, which is rather difficult to evaluate except under certain simple conditions. When the elementary dipoles in the medium, which together make up the polarization of the medium, are *point*-dipoles, and when they are arranged in a cubic lattice, or are distributed at random, p, as Lorentz has shown, will be equal to $4\pi/3$ (see also Van Vleck 1937).

But actually, as was shown in the paper referred to, the dipoles concerned in refraction phenomena, for which Lorentz's theory was originally intended to apply, are by no means point-dipoles ; they are due primarily to the displacement of the electrons in an atom with respect to its positively charged nucleus, and the separation of charges will be of atomic dimensions, and comparable with the distances between neighbouring dipoles. Thus the Lorentz polarization factor $p=4\pi/3$ may fail just where it was originally intended to apply, namely to electronic polarization as is involved in refraction phenomena in the visible and in the ultra-violet regions of the spectrum. But the polarization produced in ionic crystals like the alkali halides by a small relative displacement of the two lattices, with which we are concerned here, is in a different category altogether, since we can now regard the polarization as due to dipoles of small dimensions of the order of r located at the lattice points. This can be readily seen from the following considerations. Electrostatically the effect of deforming the original lattice, which we shall designate by A, into B will be equivalent to superposing on A the following two lattices: the lattice A' obtained from A by changing the signs of all the ions in it, and the lattice B. The superposition of A' and B will be equivalent to locating a small dipole of moment er at each of the positive, *or* each of the negative lattice points, which again will be equivalent to locating a dipole $er/2$ at every lattice point, whether positive or negative. Since r can be made as small as we desire, these dipoles will be practically point-dipoles, and the corresponding polarization factor p will therefore be expected to approximate closely to the Lorentz value $4\pi/3$, and this is just the value which we have used in the calculation of ω_i and which, as we mentioned, is confirmed experimentally.

§4. THE RESONANCE FREQUENCY OF AN ASSEMBLAGE OF HARMONIC OSCILLATORS

Coming back to the calculation of the energy ar^2 per pair of ions from which the resonance frequency ω_i of the crystal is evaluated using relation (1), it may appear at first sight that when the electrostatic interactions between all the ions of the positive and the negative lattices displaced relatively to each other by r are taken into account, the effect of the polarization field also, which is a direct result of this displacement, gets included in it automatically, and it should not therefore be necessary to invoke separately the effect of the polarization field. But actually the necessity arises from the following circumstance. It was shown just now that separating the two lattices by a small distance r is equivalent to developing small dipoles at the lattice points. The oscillating crystal will be equivalent to harmonic oscillators, all of the same moment, located one at each of the lattice points of the crystal. The frequency Ω_i which we would have obtained from a_1 with the help of relation (3), i.e. the frequency which we would have obtained by ignoring the polarization field, would be the frequency of these *individual* oscillators, whereas the frequency ω_i that we are trying to calculate is the resonance frequency of the assemblage of these oscillators, which will be different from Ω_i, and the difference is determined by the polarization field. (That Ω_i is itself dependent on the density of the medium does not affect the argument.)

Anticipating the results concerning the energies associated with the polarization of the medium to be given in § 6, we may mention immediately that

$$Nar^2 = \tfrac{1}{2}N\mu\omega_i^2r^2 = \tfrac{1}{2}PE,$$

where E is the field in the medium, whereas the energy that is obtained from the Coulomb and the repulsion interactions is equal to $PF/2$, where F is the internal field, which includes in addition to E the polarization field pP. Hence one has to subtract from Na_1r^2 the work done by the polarization field, namely $pP^2/2$ ($=2\pi P^2/3$ in the case of the alkali halides), before it can be equated to $\frac{1}{2}N\mu\omega_i^2r^2$.

§5. THE DIELECTRIC CONSTANT OF THE CRYSTAL AND THE DRUDE AND THE LORENTZ FORMULAE

Let us for the present ignore the electronic polarization, i.e. the polarization due to the displacements of the electrons in the ions with reference to their respective nuclei, and regard the medium as consisting of ions that can only be bodily displaced. For any given relative displacement r of the positive and the negative lattices the polarization per unit volume will be given by (4), namely $P=Ner$. This polarization may also be regarded as produced by a field E in the medium, such that

$$Ee=2ar=\mu\omega_i^2r. \quad \text{. . . . .} \quad (8)$$

The corresponding internal field F will be given by

$$Fe=Ee+\frac{4\pi}{3}Ne^2r=2a_1r=\mu\Omega_i^2r, \quad \text{. . . . .} \quad (9)$$

where, as we have seen, Ω_i is the frequency which we would have obtained for the principal oscillation of the crystal if we had neglected the effect of the polarization field, as distinguished from the actual resonance frequency ω_i.

It will be seen from (8) that the susceptibility χ_0 of the medium for static electric fields will be given by

$$\epsilon_0-1=4\pi\chi_0=\frac{C_i}{\omega_i^2}, \quad \text{. . . . .} \quad (10)$$

where

$$C_i=\frac{4\pi Ne^2}{\mu} \quad \text{. . . . .} \quad (11)$$

and ϵ_0 is the corresponding dielectric constant. Equation (10) can be readily identified with the well-known expression of Born's (see *Handbuch der Physik*). The two frequencies Ω_i and ω_i are connected by the relation

$$\Omega_i^2=\omega_i^2+\frac{C_i}{3}, \quad \text{. . . . .} \quad (12)$$

or

$$\Omega_i^2=\omega_i^2\frac{\epsilon_0+2}{3}. \quad \text{. . . . .} \quad (13)$$

Similarly

$$\left.\begin{aligned} a_1&=a\frac{\epsilon_0+2}{3}, \\ a_2&=-a\frac{\epsilon_0-1}{3}. \end{aligned}\right\} \quad \text{. . . . . .} \quad (14)$$

Hence eqn. (10) can also be written in the form

$$\frac{\epsilon_0-1}{\epsilon_0+2}=\frac{C_i/3}{\Omega_i^2}. \qquad (15)$$

Similarly the dielectric constant at any frequency ω can be expressed either in the form

$$\epsilon_\omega-1=\frac{C_i}{\omega_i^2-\omega^2} \qquad (16)$$

or, in view of (12), in the form

$$\frac{\epsilon_\omega-1}{\epsilon_\omega+2}=\frac{C_i/3}{\Omega_i^2-\omega^2}, \qquad (17)$$

which are indeed identical relations (Livens 1912).

Just as the equivalence of (10) and (15) is based on relation (13), the equivalence of (16) and (17) corresponds to a relation which is analogous to (13), and which is a corollary to it, when we are concerned, as we are now, with only one frequency that influences the polarization, the relation being

$$\Omega_i^2-\omega^2=(\omega_i^2-\omega^2)\frac{\epsilon_\omega+2}{3}. \qquad (18)$$

It can be readily seen that (16) and (17) reduce to (10) and (15) respectively when $\omega \to 0$.

In (16) resonance occurs obviously when $\omega=\omega_i$ and in (17) when the right hand side tends to unity, i.e. when $\Omega_i^2-\omega^2=C_i/3$ which in view of (12) corresponds again to $\omega=\omega_i$ as it should.

One may thus take into account the effect of the polarization field on the dielectric constant explicitly by taking the field that is effective in producing the polarization as $(1+4\pi\chi_\omega/3)$ times E or $(\epsilon_\omega+2)E/3$ where E is the field in the medium, in which case the formula obtained is of the Lorentz type, and the characteristic frequency appearing in the expression is the frequency Ω_i; or *alternatively*, one may regard the effect of the polarization field as confined to changing Ω_i to the actual resonance frequency of the crystal ω_i such that the relation (18) is satisfied, in which case the formula is of the Drude type.

§6. THE ELECTRIC FIELDS ASSOCIATED WITH THE SEPARATION OF THE LATTICES

Now the potential energy Nar^2 per unit volume, due to separating the two lattices by a small distance r can also be regarded as due to the incidence of a ‘ field E in the medium ’ such that eqn. (8) is satisfied, or such that

$$Nar^2=\frac{E^2}{8\pi}(\epsilon_0-1)$$
$$=\tfrac{1}{2}EP. \qquad (19)$$

Similarly

$$Na_1r^2=\tfrac{1}{2}FP, \qquad (20)$$

and the energy per unit volume associated with the occurrence of the polarization field will be given by

$$Na_2r^2 = -\tfrac{1}{2}pP^2, \quad . \quad . \quad . \quad . \quad . \quad . \quad . \quad . \quad (21)$$

where pP is the polarization field. In the alkali halides, as we have seen, $p = 4\pi/3$.

As is well known, the field in the medium E at any given lattice point O includes not only the field due to all the surrounding dipoles, but also a certain averaged field at O due to the dipole at O also, i.e., the averaged self-field of the dipole at O also, whereas the inner field F does not include the latter (Fröhlich 1949). Though we refer to the latter field for convenience as the self-field, it depends very much on the polarization of the surroundings, which will be realized immediately when we remember that the self-field will be just compensated by the field that would obtain at the point O in the cavity produced by removing from the medium the doublet located at O.

Now the effect at O of all the dipoles including the one at O will be equivalent to the field at O due to the charges developed on the surface of the medium due to polarizing it. Hence the averaged self-field of the doublet at O will be just the difference between the field at O due to the charges developed on the surface of the medium as a result of polarizing it, and the field at the same point due to all the surrounding dipoles in the medium. Since the difference between F and E is the polarization field, the latter field can be regarded as equal to the averaged self-field, but of opposite sign to it.

Now the self-field of a dipole should depend only on the fine structure of the medium, and in particular should be independent of the external shape. One may, therefore, use any convenient shape like a sphere or an infinite parallel plate, and show that the self-field is equal to

$$-\left(\frac{4\pi}{3} + f\right)P = -pP, \quad . \quad . \quad . \quad . \quad . \quad . \quad . \quad (22)$$

where fP is the field at O due to all the surrounding doublets in an infinite medium. In the case of the alkali halides f will obviously be zero.

§7. THE DISPERSION FORMULAE FOR A DENSE MEDIUM

We have specifically discussed till now the case when the only frequency affecting the dielectric constant is that of the principal lattice oscillation of the crystal. One good reason for confining ourselves to this case is that the polarization factor involved here is very definite, and is known to be equal to $4\pi/3$. But the main results obtained are applicable equally well to the case when the medium has more than one resonance frequency, and when some or all of these are electronic frequencies, instead of lattice frequencies. Let us denote these frequencies and the physical constants associated with them by the subscripts $i, j, k, \ldots n$. The polarization factor p_{ij} defining the polarization field acting on any oscillator i due to the dipole moments of all the oscillators j in the medium will not in general be equal to $4\pi/3$ but will depend on both i and j. The dielectric constant of the medium will then be given by

$$\epsilon-1=4\pi\chi=4\pi\sum_i\chi_i, \tag{23}$$

where χ_i is the contribution to the susceptibility, i.e. to the polarization per unit volume per unit field in the medium, from the oscillators of type i.

$$4\pi\chi_i=\frac{C_i}{\Omega_i^2-\omega^2}(1+\sum_j p_{ij}\chi_{ij}), \tag{24}$$

in which the summation extends over all values of j namely $i, j, \ldots n$.

$$C_i=\frac{4\pi n_i f_i e^2}{\mu_i}, \tag{25}$$

where n_i is the number of oscillators of type i present per unit volume of the medium, f_i is the oscillator strength, and μ_i is the effective mass of the oscillator. Ω_i is the frequency of the oscillator in the free state, to be more precise, the frequency which it will have if the influence of the interactions of the surrounding dipoles is eliminated.

In the special case when all the p_{ij}'s have the same value, say p, eqns. (23) and (24) reduce to

$$\frac{\epsilon-1}{\epsilon+\alpha}=\sum_i\frac{B_i}{\Omega_i^2-\omega^2}, \tag{26}$$

where

$$B_i=\frac{pC_i}{4\pi};\quad \alpha=\frac{4\pi}{p}-1. \tag{27}$$

When further all the polarization factors have just the Lorentz value, namely $p=4\pi/3$, it will be seen from (27) that α reduces to 2, and eqn. (26) to the well-known Lorentz formula.

Herzfeld and Wolf (1925) have shown that the simple Lorentz formula

$$\frac{\epsilon-1}{\epsilon+2}=\sum_i\frac{B_i}{\Omega_i^2-\omega^2}, \tag{28}$$

is mathematically convertible into the Drude formula

$$\epsilon-1=\sum_i\frac{C_i}{\omega_i^2-\omega^2} \tag{29}$$

and *vice versa*. Using the same method it can be readily shown that the more general formula corresponding to (23) and (24) in which the polarization factors p_{ij} may all be different, can also be reduced to the Drude formula (28) or to the simple Lorentz formula, and conversely the Drude or the simple Lorentz formula can also be transformed to a formula of the type (24), *with any specified values of* p_{ij}.

It will be seen immediately, whatever may be the actual polarization fields that may obtain in the medium, and even if there is no polarization field at all, that the dispersion data can be fitted, as may be desired, into a Drude formula, or a simple Lorentz formula, or a generalized Lorentz formula of the type (23) and (24) with any postulated set of polarization factors p_{ij}. The characteristic frequencies that appear in these alternative formulae with which the same set of observational data can be fitted, will naturally be different ; those that appear in the Drude formula will be the actual resonance frequencies ω_i of the medium, and in the other formulae the frequencies will differ from ω_i by amounts which are determined by the polarization fields postulated on which the formulae are based. Hence dispersion data by themselves can yield information regarding only the resonance frequencies of the medium and their oscillator strengths, and none at all regarding the polarization field.

It may not be out of place here to emphasise these results. Though the mathematical equivalence of the Drude and the simple Lorentz formulae, which was demonstrated long ago by Herzfeld and Wolf, is generally conceded, the agreement between the characteristic frequencies appearing in these formulae, and the observed absorption frequencies is sometimes invoked in order to decide between the alternative formulae as regards their experimental validity. On considerations of convenience, the Drude dispersion formula, in which the characteristic frequencies that appear are also the observed absorption frequencies, is naturally preferable to any alternative formulae, but the latter formulae too should be regarded as having the same experimental validity as Drude's.

It should be mentioned immediately that the equivalence between the different alternative formulae relates to the formulation of the dielectric constant as a function of the frequency of the incident electromagnetic waves, with which we are concerned here, and *does not extend to the expressions for the dielectric constant as a function of the density of the medium.* Since the polarization field will depend on the density the latter formula will be conditioned by the actual polarization field. Even here, the frequencies Ω_i of the individual oscillators, and the polarization field factors p_{ij} may also be dependent on the degree of close-packing. We shall postpone consideration of these aspects to a later section of the paper.

§8. THE CASE OF THE ALKALI HALIDES

The case of the alkali halides is exceptional, as we have mentioned already. The only infra-red resonance frequency that is involved in the dispersion formula is that of the principal lattice oscillation of the crystal. Making the subscript i refer to this frequency, p_{ii} as we have seen, has just the Lorentz value $4\pi/3$. The other frequencies, denoted by the subscripts j, k, . . . , will all be electronic and the separation of the charges in the corresponding dipoles will be comparable with the distance between the neighbouring ions. Hence the distribution of the field in the neighbourhood of any of the latter dipoles will differ considerably from that of a point-dipole. Indeed, even the order of magnitude of the field may become different when the approach to the dipole is close.

In other words, when there is considerable overlap of the electronic clouds of neighbouring ions, as is the case with the neighbouring ions in the alkali halide crystals, the polarization factors of the type p_{ij}, p_{ik}, . . . will be much less than $p_{ii}=4\pi/3$, and the factors p_{jj}, p_{kk}, . . . may be still smaller.

In the paper referred to, it was shown that in the alkali halides all the p's except p_{ii} have practically zero values. This circumstance, namely, that only one of the p's has a finite value, and the rest have zero value renders the case of the alkali halides exceptional.

The expression for the dielectric constant of these halides will, therefore, be of the form

$$\epsilon_\omega-1=\frac{C_i}{\omega_i^2-\omega^2}+\sum_j\frac{C_j}{\omega_j^2-\omega^2}, \quad . \; . \; . \; . \; . \; . \quad (30)$$

where the electronic resonance frequencies ω_j, ω_k, . . . will be practically the same as for the individual (not isolated) atoms, namely, Ω_j, Ω_k, . . . respectively, whereas the lattice frequency ω_i will naturally be very different from Ω_i.

In particular, in the region of very long wavelengths in which the contribution to the dispersion from the electronic frequencies, namely

$$n_\omega^2-1=\sum_j\frac{C_j}{\omega_j^2-\omega^2}, \quad . \; . \; . \; . \; . \; . \; . \; . \quad (31)$$

is practically independent of ω, and is nearly the same as for $\omega=0$, we obtain

$$\epsilon_\omega-n_0^2=\frac{C_i}{\omega_i^2-\omega^2}, \quad . \; . \; . \; . \; . \; . \; . \; . \quad (32)$$

or alternatively,

$$\frac{\epsilon_\omega-n_0^2}{\epsilon_\omega-n_0^2+3}=\frac{C_i/3}{\Omega_i^2-\omega^2}, \quad . \; . \; . \; . \; . \; . \; . \quad (33)$$

the relation between Ω_i and ω_i being given as before (see (12) and (13)) by

$$\Omega_i^2=\omega_i^2+\frac{C_i}{3}=\omega_i^2\left(\frac{\epsilon_0-n_0^2+3}{3}\right). \quad . \; . \; . \; . \quad (34)$$

In particular one obtains from (31) for the dielectric constant in a static field, the well-known expression of Born

$$\epsilon_0=n_0^2+\frac{C_i}{\omega_i^2}. \quad . \; . \; . \; . \; . \; . \; . \; . \; . \quad (35)$$

§ 9. DISCUSSION OF THE AVAILABLE EXPERIMENTAL DATA

The available experimental data for the refractive indices of the alkali halides, which extend over a wide spectral range, have been discussed by Herzfeld and Wolf (1925), by Fuchs and Wolf (1928), and more recently by Ramachandran (1947) and by Radhakrishnan (1948). Attention may be drawn in particular to the following results.

(1) When the data are fitted into a dispersion formula of the Drude type, the characteristic frequencies that appear in the formulae are found to agree well with the observed resonance frequencies. Since the fitting is done empirically, it will be more correct to say that the available experimental data can be fitted satisfactorily into a Drude dispersion formula, using the *observed* resonance frequencies of the crystal as the characteristic ones that should appear in the formula. For details regarding the fitting with the experimental data reference may be made to the original papers. The formula in general, involves three frequencies in the far ultra-violet, and the principal lattice frequency in the infra-red.

(2) Since the only infra-red frequency involved in the formula is that of the principal lattice oscillation of the crystal the corresponding oscillator strength C_i will be that defined by (16), and given by (11). Hence it will be possible to compare the values of C_i calculated from (11) with the numerical values appearing in the empirical formulae given by Ramachandran and Radhakrishnan. They are collected together in table 1 which includes all the crystals for which experimental dispersion formulae are available.

Table 1

Crystal	LiF	NaF	NaCl	KCl	KBr
$C_i \times 10^{-26}$ from (11)	210	68	28	15	10
$C_i \times 10^{-26}$ from dispersion	230	74	33	18	11

(3) Now the measurements on dispersion usually extend at the infra-red end to about 22 μ for some of the crystals, and to about 9 μ only for most others. Since even at the former limit the contribution to n^2-1 from the infra-red term in the dispersion formula is very small, the experimental value of C_i appearing in the infra-red terms is slightly uncertain, except where the value of the dielectric constant for either steady fields or for the usual radio frequencies has also been utilized in determining the constants of the dispersion formula. Actually this has been done only for a few crystals, by Radhakrishnan. Hence it will be of interest to compare the calculated and observed values of $k_0-n_0^2$ in which k_0 is the dielectric constant for static fields, and n_0^2 is the square of the refractive index extrapolated to $\omega \to 0$. The experimental value of n_0^2 is readily obtained from the dispersion formula by taking the contributions at $\omega=0$ from all the terms except the infra-red one. The experimental values of $k_0-n_0^2$ thus calculated are given in table 2 along with the values calculated from (34), in which we have used for the frequency of the principal lattice oscillation of the crystal the values calculated by us in an earlier paper, on the basis of Born's model, from

the known Coulomb and repulsion interactions between the ions (Krishnan and Roy 1951). The value as was shown in the paper agrees well with the observed reststrahlen frequency.

Table 2

Crystals	k_0	n_0^2	$k_0 - n_0^2 = Ne^2/\pi\mu\nu^2$	
			Observed	Calculated
LiF	9·3	1·9	7·4	7·6
NaF	6·0	1·7	4·3	4·5
NaCl	5·6	2·3	3·3	3·2
KCl	4·7	2·2	2·5	2·4
KBr	4·8	2·4	2·4	2·2

§10. DEPENDENCE ON DENSITY

Extensive data are also available for the temperature variation of the refractive index of the alkali halides, and for some of them for the variation of the refractive index with the density also. One may therefore compare the observed values of $(\partial n/\partial t)$ and $-\rho(\partial n/\partial \rho)\alpha$ where α is the coefficient of thermal expansion, in order to find whether the change of refractive index with temperature is due wholly to the change of density accompanying the temperature change, or whether there is in addition a pure temperature effect due to the thermal agitations of the ions. From the values of $\partial n/\partial t$ and of $-\alpha\rho(\partial n/\partial \rho)$ given in table 3 it will be seen that the pure temperature effect, if any, is practically negligible.

Table 3

Crystals	$10^5\alpha$	$\rho(\partial n/\partial \rho)$	$10^5(dn/dt)$	
			Observed	Calculated
NaCl	12·0	0·24	−3·8	−2·9
KCl	11·4	0·23	−3·6	−2·6
KBr	12·0	0·35	−3·6	−4·2
KI	13·5	0·43	−5·0	−5·8

Now the available data for the temperature variation of the refractive index which extend from the extreme quartz ultra-violet to the infra-red in most crystals, have been analysed by Ramachandran and by Radhakrishnan. They find that the temperature variation can be expressed empirically in the form*

$$2n\frac{dn}{dt}=-\alpha(n^2-1)+\Sigma\frac{2C_j\psi_j}{(\omega_j^2-\omega^2)^2}+\frac{2C_i\psi_i}{(\omega_i^2-\omega^2)^2}+\frac{D}{\omega_i^2-\omega^2}, \quad . \quad (36)$$

where

$$\psi_j=-\omega_j\frac{\partial\omega_j}{\partial t}. \quad . \quad . \quad . \quad . \quad . \quad . \quad . \quad . \quad . \quad . \quad (37)$$

The first term on the right hand side of (36) is due directly to the change in density, since the expression for n^2-1 will contain a factor proportional to ρ, and this term accounts for the bulk of the temperature variation. Attention may be drawn here to the extra term involving the infra-red frequency and proportional to $1/(\omega_i^2-\omega^2)$.

We have referred to the experimental finding that in the alkali halides all the polarization factors are zero except p_{ii}, which is equal to $4\pi/3$. Any change of density is not likely to affect p_{ii}. If the other factors also remain unchanged, i.e. continue to be zero, it will be difficult to explain either the change in the ω_j's suggested by the analysis of the experimental data, or the extra infra-red term proportional to $1/(\omega_i^2-\omega^2)$ which corresponds to a change of the oscillator strength with temperature. The obvious inference is that though all the p's except p_{ii} are quite small, their variations with density, and therefore also with temperature, are considerable. Further the form of the empirical formula suggests that coefficients of the type $(\partial p_{jj}/\partial t)$, $(\partial p_{kk}/\partial t)$ . . . relating to the interactions of the electronic oscillators of the same frequency, and terms like $\partial p_{ij}/\partial t$ which define the interaction of the infra-red frequency with the other frequencies, are the predominant ones. These differential coefficients can be calculated from the experimental data. We shall merely mention that $\partial p/\partial t$ is of the order of 10^{-4}.

§11. FURTHER REMARKS ON THE ELECTRONIC OVERLAP OF THE NEIGHBOURING IONS

In the previous sections the effect of the electronic overlap between the neighbouring ions has been regarded as affecting the polarization field, and rendering it almost nothing when the ions are at their equilibrium positions. Alternatively, the effect of the overlap can also be regarded as reducing the effective charge on an ion from e to fe where f is a factor which is determined by the degree of overlap, and is less than unity, while the polarization field is allowed to have the Lorentz value (Fröhlich 1949). The former point of view, in which the overlap is regarded as reducing the polarization field to nothing, has certain advantages over the alternative point of view, and has therefore been adopted here.

---

* Actually these authors use wave-lengths instead of frequencies, but the latter are used here for convenience.

That in all the alkali halides the electronic polarization field is found to be practically zero when the ions are at their equilibrium positions may be theoretically significant. According to the simple Born model on which the foregoing discussions are based, the ions in the lattice are held in their equilibrium positions by the Coulomb electrostatic interactions between the charges carried by the ions, and the repulsion interactions between the neighbouring ions. When the ions have taken their equilibrium positions under the corresponding attractive and repulsive forces respectively, there will be a certain optimum overlap between the neighbouring ions, and this overlap is apparently also the one that corresponds to zero polarization field. This view receives strong support from the observation referred to in the previous section, namely this: though the polarization field is zero for the equilibrium positions of the ions, it varies rapidly about this value with change of density.

References

Born, M., and Mayer, G. M., 1933, *Handbuch der Physik*, **24 2,** 623.
Debye, P., 1928, *Polar Molecules* (New York: Dover Publication).
Fröhlich, H., 1949, *Theory of Dielectrics* (Oxford: Clarendon Press), pp. 21–36.
Herzfeld, F. F., and Wolf, K. L., 1925, *Ann. d. Physik*, **78,** 35.
Krishnan, K. S., and Roy, S. K., 1951, *Proc. Roy. Soc.* A, **207,** 447.
Livens, G. H., 1912, *Phil. Mag.*, **24,** 268.
Lorentz, H. A., 1908, *Theory of Electrons* (Leipzig: Teubner), Section 117 and note 54.
Radhakrishnan, T., 1948, *Proc. Ind. Acad. Sci.* A, **27,** 165.
Ramachandran, G. N., 1947, *Proc. Ind. Acad. Sci.* A, **25,** 481.
Rosenfeld, L., 1951, *Theory of Electrons* (Amsterdam: North Holland Publishing Co.).
Van Vleck, J. H., 1937, *J. Chem. Phys.*, **5,** 556.

IV. *The Nuclear Spins and Magnetic Moments of* ^{24}Na, ^{42}K, ^{86}Rb, ^{131}Cs *and* ^{134}Cs

By E. H. Bellamy* and K. F. Smith
Cavendish Laboratory, Cambridge†

[Received September 23, 1952]

Summary

The atomic beam magnetic resonance method has been used to find the nuclear spins and the ground state hyperfine structure splittings of the radioactive alkali atoms ^{24}Na, ^{42}K, ^{86}Rb, ^{131}Cs and ^{134}Cs. The spins and $\Delta\nu$ values were obtained by observing $\Delta F=0$, $\Delta m=\pm 1$ transitions in weak and intermediate fields, and the Fermi–Segre relation was used to calculate the magnetic moments from the results. More accurate $\Delta\nu$ values were also found for ^{24}Na and ^{42}K by locating $\Delta F=\pm 1$, $\Delta m=\pm 1$ transitions. The results are tabulated below.

Isotope	I	H.F.S. (Mc/s)	μ (NM)
^{24}Na	4	1139·35 ± 0·10	+1·688 ± 0·005
^{42}K	2	1258·9 ± 0·1	−1·137 ± 0·005
^{86}Rb	2	3960 ± 20	−1·69 ± 0·01
^{131}Cs	5/2	13200 ± 110	+3·48 ± 0·04
^{134}Cs	4	10440 ± 30	+2·95 ± 0·01

§1. Introduction

The experiments performed by Davies, Nagle and Zacharias (1949) using ^{22}Na, ^{40}K, ^{135}Cs and ^{137}Cs, showed that the atomic beam magnetic resonance method is suitable for the measurement of nuclear spins and ground state hyperfine structure splittings of alkali atoms when only small quantities in samples of low concentration are available. This paper contains an account of experiments in which ^{24}Na, ^{42}K, ^{86}Rb, ^{131}Cs and ^{134}Cs were used in a similar apparatus. The ^{86}Rb, ^{131}Cs and ^{134}Cs beam intensities were measured with a mass-spectrometer detector, and the ^{24}Na and ^{42}K beam intensities were found by collecting the ionized atoms on a target which was then removed from the apparatus to find the activity deposited.

§2. The Experimental Procedure

2.1. *The Method*

The atomic beam magnetic resonance method developed by Rabi and his collaborators (Zacharias 1942) makes use of the fact that the nuclear spin and the ground state hyperfine structure splitting of an alkali atom can be deduced from the way the energy difference between a pair of magnetic levels varies with the magnitude of the external magnetic field H. This is found experimentally by inducing transitions between the levels by applying an oscillating magnetic field perpendicular to H; the energy change associated with the transition (or ‘ flop ’) is then h times the frequency at which the transition probability is a maximum.

---

* Now at Glasgow University.

† Communicated by Professor O. R. Frisch, F.R.S.

The experimental arrangement given in fig. 1 is used to detect the flopped atoms. The beam of neutral atoms, defined by the oven and collimating slits, passes through three magnetic fields as shown. The intense inhomogeneous deflecting fields A and B produce large equal deflections in the plane of the detector, while the field C, on which the oscillating field is superimposed by the RF loop, is homogeneous and produces no additional deflection. The three fields are in the same direction and there is no region where H is zero or varies rapidly, so the atoms move adiabatically from one magnet to the next. Under these conditions, the deflections due to the A and B magnets add up and the unflopped beam is split into two Stern–Gerlach components which fall on either side of the detector. When the oscillating field induces transitions between states associated with opposite effective magnetic moments in intense fields, the B magnet deflections oppose those due to the A magnet and the flopped atoms are refocused on the detector. The measured beam intensity is, therefore, a maximum when the frequency of the oscillating field satisfies the resonance condition for a transition between states with opposite intense field effective magnetic moments, providing the transition is allowed by the selection rules.

Fig. 1

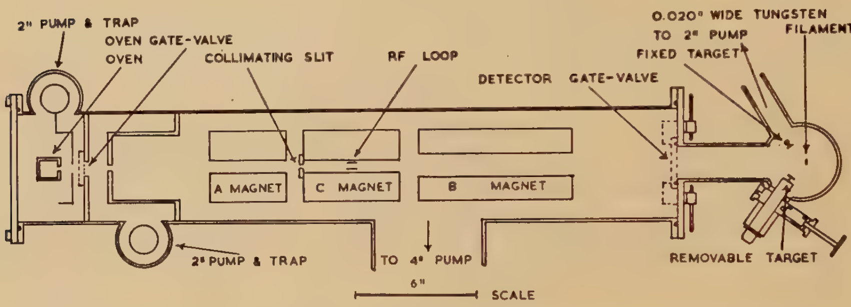

A schematic diagram of the atomic beam magnetic resonance apparatus with the ^{24}Na detector in position.

2.2. *The Energy Levels*

It is convenient to describe the energy levels of an atom in a magnetic field in terms of the total angular momentum quantum number F and the resolved component m in the direction of the field. When the total electronic angular momentum is 1/2, as it is for the $^2S_{1/2}$ ground state of an alkali atom, F takes on the two values $(I\pm\frac{1}{2})$, and the way in which the magnetic level W_{Fm} varies with magnetic field is given by the Breit–Rabi (1931) formula,

$$W_{Fm}=-\frac{h\Delta\nu}{2(2I+1)}+mg_I\mu_0H\pm h\Delta\nu\left(1+\frac{4mx}{2I+1}+x^2\right)^{1/2}, \quad . \quad . \quad . \quad (1)$$

where $h\Delta\nu$ is the hyperfine structure splitting in zero field, $g_I=-\mu_I/I$, μ_I is the nuclear magnetic moment, μ_0 is the Bohr magneton, $x=(g_J-g_I)\mu_0H/h\Delta\nu$ and g_J is the Lande factor for the $^2S_{1/2}$ electronic ground state. The positive sign refers to the magnetic levels associated with the $F=(I+\frac{1}{2})$ zero field level and the negative sign to those associated with $F=(I-\frac{1}{2})$. The form of the level scheme for an alkali atom with $I=4$ and μ_I positive is shown in fig. 2 ; the diagram is inverted when the magnetic moment is negative.

Fig. 2

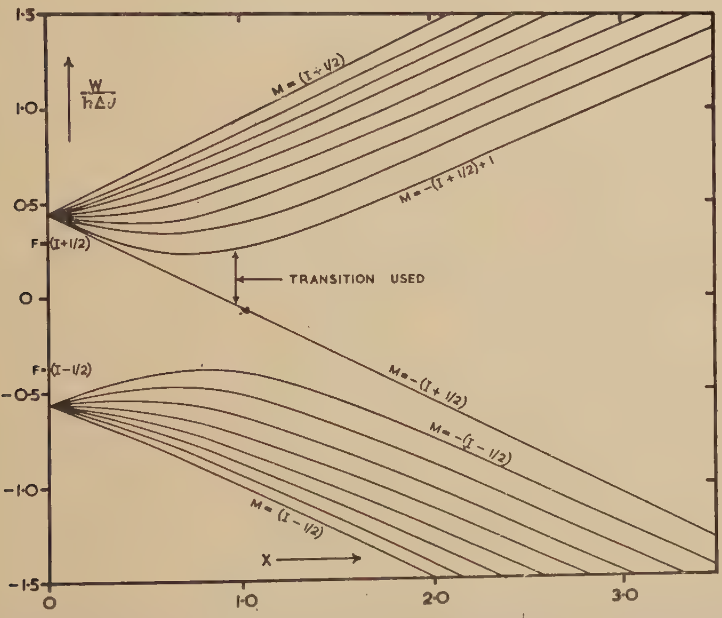

The energy levels of $J=1/2$, $I=4$ atom in a magnetic field. The parameter x is equal to $(g_J-g_I)\mu_0H/(h\Delta\nu)$ and the magnetic moment has been assumed to be positive ; the diagram is inverted when μ_I is negative.

2.3. *The Measurement of Nuclear Spin*

Since the effective magnetic moment is equal to $-dW/dH$ and the transitions are subject to the selection rules $\Delta F=0, \pm1$, $\Delta m=\pm1$ when they are induced by an oscillating field perpendicular to H, the only low frequency transition which satisfies both the selection rules and the refocusing condition, is the one from $F=(I+\frac{1}{2})$, $m=-(I+\frac{1}{2})$ to $F=(I+\frac{1}{2})$, $m=-(I+\frac{1}{2})+1$, shown in fig. 2.

The frequency associated with this transition, if H is small ($x \ll 1$) and terms involving $\Delta\nu$ and μ_I are neglected, is,

$$\nu = 2\mu_0 H/[(2I+1)h] = 2{\cdot}8H/(2I+1)\ \text{Mc/s}. \quad . \quad . \quad . \quad (2)$$

When ν is less than 10 Mc/s, the μ_I and $\Delta\nu$ terms are small compared with the resonance half-width given by the uncertainty relation $\nu_{1/2} \sim 1/t \sim 0{\cdot}1$ Mc/s, where t, the time spent by the atom in the RF field, is about 10^{-5} seconds. The resonance frequency is seen to depend only on H and I, and the frequencies associated with two isotopes in the same magnetic field are related by,

$$\nu_1(2I_1+1) = \nu_2(2I_2+1). \quad . \quad . \quad . \quad . \quad . \quad . \quad . \quad (3)$$

The frequencies associated with the different spin values differ by several resonance half-widths when ν is a few megacycles per second, so the method is capable of giving an unambiguous value for the nuclear spin.

2.4. *The Measurement of $\Delta\nu$ and μ_I*

When the magnetic field is increased until the terms involving $\Delta\nu$ and g_I are larger than the resonance half-width, the magnitudes of both $\Delta\nu$ and μ_I can be deduced. If the resonance occurs at frequency ν in a magnetic field H, $\Delta\nu$ is given by the following relation which was derived from eqn. (1),

$$\Delta\nu = \frac{(\nu - 1{\cdot}4g_I H)(2{\cdot}800H - \nu)}{\left(\nu - \dfrac{2{\cdot}800H}{2I+1} - \dfrac{2{\cdot}8Ig_I H}{2I+1}\right)}\ \text{Mc/s}. \quad . \quad . \quad . \quad . \quad (4)$$

The value of H is found by observing the resonance associated with an isotope of known I, μ_I and $\Delta\nu$ in the same magnetic field H, and g_I is calculated from $\Delta\nu$ using the following form of the Fermi–Segre (1930) relation,

$$\frac{\Delta\nu_1}{\Delta\nu_2} = \frac{g_1(2I_1+1)}{g_2(2I_2+1)}, \quad . \quad . \quad . \quad . \quad . \quad . \quad . \quad . \quad . \quad (5)$$

which connects the values of I, g_I and $\Delta\nu$ for two isotopes of the same element. The resonance frequency is found at several values of H and the sign of g_I which gives a constant set of $\Delta\nu$ values is assumed to be the correct one.

Some accurate independent measurements of g_I and $\Delta\nu$ of stable isotopes have shown that eqn. (3), which is based on the assumption that the nuclear dipole is concentrated at a point, gives g_1/g_2 ratios which can be in error by as much as 0·5% (Eisinger 1952). This hyperfine structure anomaly does not effect the determination of the sign of g_I, however, since the terms in eqn. (2) are small, but it does set a lower limit to the accuracy of a μ_I value which is deduced from a measurement of $\Delta\nu$.

2.5. *The $\Delta F = \pm 1$ Transitions*

Several $\Delta F = \pm 1$ transitions which satisfy both the refocusing condition and selection rules can also be observed in the apparatus. The pattern expected when H is small consists of $2I$ equally spaced lines with a frequency difference between alternate lines of $5{\cdot}6H/(2I+1)$ Mc/s. The lower

$(2I-1)$ lines have the same intensity and are centred on the frequency $\Delta\nu$, while the other line, which comes at the high frequency end, is only half as intense. When I is integral, one line occurs at the frequency $\Delta\nu$ and is almost frequency independent; this line was located for ^{24}Na and ^{42}K and plotted out in detail so that an accurate $\Delta\nu$ value could be obtained. No corrections were made for the higher order terms which come into the exact expression for the frequency of this field independent line, since they are small compared with the error due to the wavemeter and the 0·1 Mc/s half-width of the resonance curve.

§3. THE APPARATUS

3.1. *General*

The general arrangement of the deflecting system is shown in fig. 1. The oven and magnets are built into a 6 in. diameter brass tube and gate-valves are provided so that the oven and detector chambers can be let up to atmospheric pressure without effecting the vacuum in the magnet chamber.

3.2. *The Oven*

The oven used with ^{24}Na and ^{42}K is made of monel metal and is large enough to contain a 2 g charge of alkali metal. Radiation heating is arranged so that the 0·002 in. slit is at a higher temperature than the cavity, and the oven block, which contains the cavity and slit, can be removed without disturbing the heater coils and thermocouple. The block is replaced by one with a small cavity and a long channel, similar to that used by Davies (1949), when working with ^{86}Rb, ^{131}Cs and ^{134}Cs.

3.3. *The* ^{24}Na *and* ^{42}K *Detector*

After being collimated by an 0·010 in. slit mounted on the C magnet, the beam falls on a 0·025 in. wide hot oxidized tungsten strip, one end of which is grounded. The positive ions are attracted to a 1 cm diameter brass target mounted on an insulated support which can be removed from the vacuum system through a gate-valve (fig. 1). The target, which is 100 v negative with respect to the ground, is connected to the input of a d.c. amplifier and current integrator. A second similarly situated, normally grounded collector is mounted in the detector chamber; it can be switched to the d.c. amplifier input in place of the target which is then grounded. This collector is used when setting the C field and making other adjustments, to avoid depositing unwanted activity on the target. The ratio of the activity collected on the removable target during a run at a particular frequency to the total beam current integrated over the same period is used as a measure of the active isotope beam intensity. Since the time taken to plot out a resonance curve by this method is comparable with the half-lives of ^{24}Na and ^{42}K, allowance for decay in the source is made by monitoring the counter with a standard made from the material in the oven.

3.4. *The Mass-Spectrometer Detector*

The mass-spectrometer detector is shown diagrammatically in fig. 3. The 1 cm high beam enters the liquid-air cooled box and falls obliquely on a hot 0·020 in. wide tungsten strip kept at a potential which can be varied from +2 500 v to +4 000 v with respect to ground. The positive ions which leave the strip are accelerated in the uniform field and pass through the two slits into the 6 in. radius, 90° magnetic field, which focuses the ions, according to mass, in the neighbourhood of the 0·010 in. final slit. The ions which pass through the slit are accelerated through a further 4 000 v on to the first dynode of an electron multiplier detector, connected to the usual amplifier and discriminator. The adjustable slit in front of the final slit considerably improves the resolution by defining the angle at which the ions are allowed to enter the final slit. An enrichment factor of 4 000 per mass number is obtained at the 133 setting of the spectrometer. The change over from one isotope to another is done by altering the voltage between the tungsten strip and ground.

Fig. 3

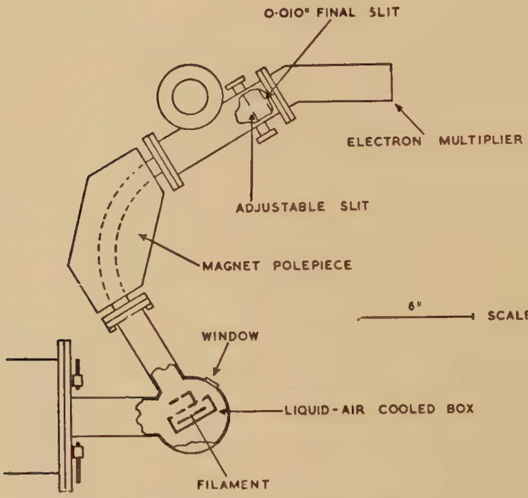

The mass-spectrometer detector.

A switching circuit is arranged so that a cycle of RF-on for 15 seconds and then RF-off for 15 seconds is repeated automatically. The RF-on and RF-off counts are added in separate scalers and the resonance curves are plotted out by finding the variation of RF-on/off ratio with frequency.

3.5. *The Deflecting System*

The A, B and C magnets have soft iron polepieces and yokes, energized by copper tube windings insulated with degreased glass fibre tape. The A and B magnets have the usual cylindrical polepieces (Rabi 1934) and for the A magnet, the distance between the wires of the equivalent two wire magnet is 0·340 in., the male polepiece radius is 0·170 in., the female polepiece radius is 0·186 in., the gap is 0·081 in., the undeflected beam passes 0·025 in. from the male poleface and the length of the polepiece is 4·0 in. The B magnet dimensions are all twice as large. The remaining dimensions of the apparatus are as follows : from the oven to the A magnet is 8·0 in., the C magnet is 5·0 in. long with a 0·250 in. gap and the detector surface is 12·0 in. from the end of the B magnet.

3.6. *The Oscillating Field*

Although the C magnet length is about 12·5 cm, an oscillating field which extends over the central 0·5 cm is used. The resonance curve half-widths is then about 0·15 Mc/s, which is smaller than the separation between the possible low field resonances due to different spins, but large enough for the effects of A and B magnet current drifts to be small compared with the resonance half-widths, providing the C field is checked every few minutes. The RF used to set the C field is obtained from a crystal controlled 10 Mc/s oscillator followed by doubler stages and a standard signal generator provides the variable frequency. A thermocouple near the loop is used to measure the RF current which is always set to the optimum value found when setting the C field. The frequencies are measured to about 1 part in 10^4 with a hetrodyne wavemeter.

§ 4. RESULTS

4.1. ^{24}Na *Results*

The oven was loaded with a one gram sample of sodium metal which had been in a slow neutron flux of 5×10^{11} n/cm^2/sec for one week. The ^{24}Na/^{23}Na ratio in the source was then about 2×10^{-8} and the specific activity 200 mc/g. The oven end of the apparatus was shielded by lead to reduce the radiation hazard. A refocused ^{23}Na beam with an RF (on/off) ratio of between 5 and 6 was obtained. Under these conditions, the target activity after collecting the beam for 20 to 30 minutes was generally about 50 counts/minute ; this rose to 150 counts/minute when the RF was set to a ^{24}Na resonance frequency. The results of the first successful run are shown in fig. 4, where the positions expected for resonances associated with spins of 3, 4 and 5 are marked. The region between 1·3 Mc/s and 1·4 Mc/s was studied in more detail later and the peak was located at 1·33 Mc/s, the position expected for a nuclear spin of 4.

The ^{24}Na resonances in magnetic fields associated with ^{23}Na resonances at 30·00 Mc/s, 60·00 Mc/s, 100·00 Mc/s and 120·00 Mc/s were also found at the frequencies tabulated below, together with the calculated $\Delta\nu$ values associated with both positive and negative g_I ; the frequencies are in megacycles per second and the magnetic fields in gauss.

The $\Delta\nu$ values associated with negative g_I are more constant than the others, so the magnetic moment is probably positive. Since the $\Delta\nu$ value of 1139 Mc/s came within the range of an available oscillator, an attempt was made to find $\Delta F=\pm1$ transitions and a more accurate result for $\Delta\nu$. The C field was set so that the expected spacing between the adjacent low field $\Delta F=\pm1$ peaks was 0·5 Mc/s and the frequency was reduced in steps of about 0·1 Mc/s, starting at 1142·0 Mc/s, until a resonance was obtained at 1141·40 Mc/s. Other resonances were found at intervals of 0·5 Mc/s and the one which was field independent was plotted out in detail (fig. 5). The $\Delta\nu$ value obtained from this run is 1139·35±0·10 Mc/s; the magnetic moment calculated using the Fermi–Segre formula with values of $\Delta\nu_{23}=1771{\cdot}61$ Mc/s and $\mu_{23}=+2{\cdot}215$ NM is then $+1{\cdot}688\pm0{\cdot}005$ NM. The error given is large enough to include the effect of the hyperfine structure anomaly.

Fig. 4

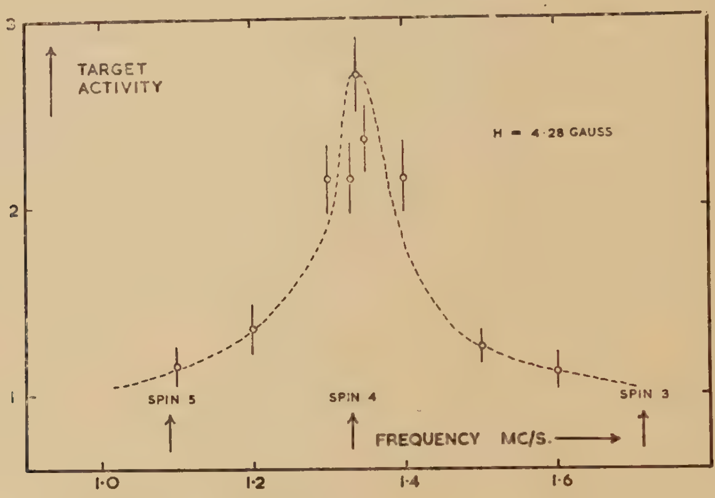

The ^{24}Na low frequency resonance in a magnetic field associated with a ^{23}Na resonance at 3·00 Mc/s.

Table 1. The ^{24}Na Results

ν_{23}	H	ν_{24}	$\Delta\nu(+ve\, g_I)$	$\Delta\nu(-ve\, g_I)$
30·00	13·93	13·93±0·02	1142±23	1129±18
60·00	78·12	29·12±0·03	1148± 7	1142± 7
100·00	123·23	51·60±0·02	1148± 2	1139± 2
120·00	144·13	63·82±0·03	1143± 2	1139± 2

4.2. ^{42}K *Results*

A one gram sample of potassium which had been in a slow neutron flux of 5×10^{11} n/cm^2/sec for one week was used in the oven. The ^{42}K/^{39}K ratio in the source was then about 2×10^{-9} and the specific activity 20 mc/g. The procedure was the same as with ^{24}Na; since the count rates were down by about a factor of ten, a scintillation counter was used to measure the activity deposited on the targets. The results are shown below.

The four $\Delta F=\pm 1$, $\Delta m=\pm 1$ peaks were also located and the frequency of the field independent line was found to be 1258·9±0·1 Mc/s. This is in agreement with the $\Delta\nu$ values associated with positive g_I so the magnetic moment of ^{4}-K (calculated assuming $\Delta\nu_{42}=1258{\cdot}9$ Mc/s, $\Delta\nu_{39}=461{\cdot}75$ Mc/s and $\mu_{39}=0{\cdot}391$ NM) is $-1{\cdot}137\pm 0{\cdot}005$. The error given is large enough to include the hyperfine structure anomaly effect.

Fig. 5

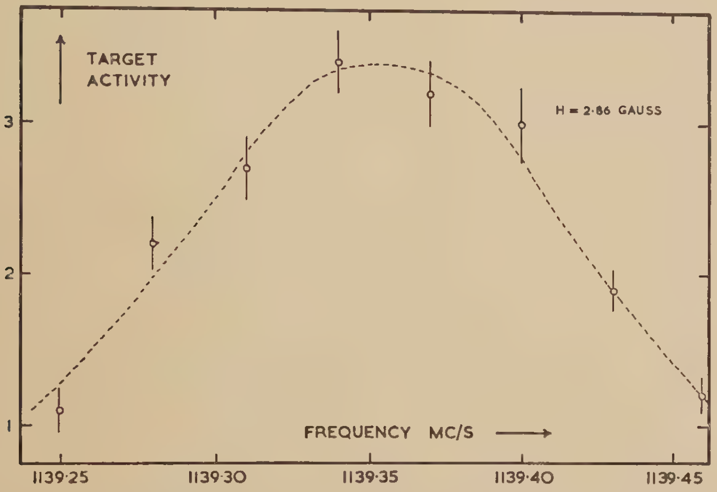

The field independent $\Delta F=\pm 1$ ^{24}Na resonance in a weak magnetic field.

Table 2. The ^{42}K Results

ν_{39}	H	ν_{42}	$\Delta\nu(+ve\, g_I)$	$\Delta\nu(-ve\, g_I)$
3·00	4·3	2·40±0·02	Consistent	with $I=2$
20·00	25·41	14·90±0·02	1255±38	1233±36
40·00	46·12	28·10±0·02	1262±10	1239±10
80·00	79·21	51·33±0·02	1260± 4	1251± 4
120·00	105·91	72·20±0·03	1260± 3	1254± 3

4.3. ^{86}Rb *Results*

This isotope was prepared by the ^{84}Sr (dα) ^{86}Rb reaction using 15 MEV deuterons on a thick target. After a 2 500 μamp hour bombardment, about 0·5 mc of ^{86}Rb was separated chemically, using 1 mg of KCl as carrier and placed in the oven with 1 μg of natural RbCl. This was added so that the mass spectrometer and C field could be set using ^{85}Rb and ^{87}Rb beams ; the ^{86}Rb/^{85}Rb expected in the source was then about 5×10^{-3}. The rubidium beam was produced by displacing the rubidium atoms with sodium as described by Davies (1949).

The low frequency resonance shown in fig. 6 was found at 2·36 Mc/s when the ^{87}Rb resonance was at 3·00 Mc/s, so the spin of ^{86}Rb is 2. The frequencies of the higher field resonances located are tabulated below.

The $\Delta\nu$ values associated with positive g_I are consistent so the magnetic moment of ^{86}Rb (calculated assuming $\Delta\nu_{87}=6834{\cdot}1$ Mc/s, $\mu_{87}=2{\cdot}733$ NM and $\Delta\nu_{86}=3950\pm20$ Mc/s) is $-1{\cdot}69\pm0{\cdot}01$ NM.

Fig. 6

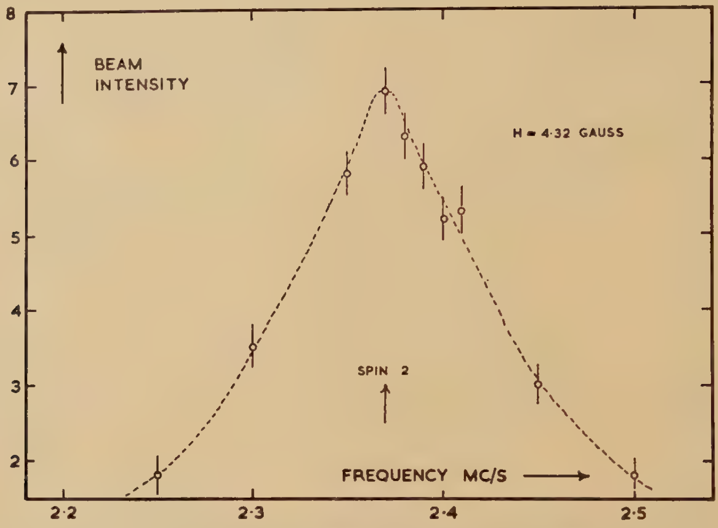

The ^{86}Rb low frequency resonance in a magnetic field associated with a ^{87}Rb resonance at 2·96 Mc/s.

Table 3. The ^{86}Rb Results

ν_{87}	H	ν_{86}	$\Delta\nu(+ve\ g_I)$	$\Delta\nu(-ve\ g_I)$
20·00	28·37	16·13±0·02	4330±350	3990±330
40·00	56·25	32·55±0·02	3980± 70	3770± 70
60·00	83·66	49·20±0·02	3950± 30	3820± 30
120·00	163·21	100·51±0·04	3970± 20	3900± 20

4.4. ^{131}Cs *Results*

A few milligram sample of ^{131}Cs, prepared by irradiating 100 g of barium nitrate for three weeks in a slow neutron flux of 5×10^{11} n/cm^2/sec, was extracted chemically using 5 mg of KCl as carrier. This was placed in the long channel oven with 0·1 mg of natural CsCl and the sodium used to produce the beam, giving a ^{131}Cs/^{133}Cs ratio in the source of about 3×10^{-4}.

Since the ^{133}Cs, ^{135}Cs and ^{137}Cs spins are all 7/2, a search was made for a significant change in RF (on/off) ratio when the oscillating field was set to the frequency corresponding to $I=7/2$ and the mass spectrometer was varied through the 131 setting. An RF (on/off) ratio of $4{\cdot}0\pm0{\cdot}5$ was found, but it was almost constant from the 130 to the 132 setting and then began to rise steadily as the 133 position was approached, so the increase was contributed to ^{132}Cs atoms which had been scattered into the 131 position. At the frequency corresponding to $I=5/2$, however, an RF (on/off) ratio, which fell away to unity on either side of the 131 position, was found and contributed to the ^{131}Cs atoms in the beam. A second run was done to find resonances at higher frequencies and two were found before the experiment was abandoned because of trouble with the electron multiplier.

Table 4. The ^{131}Cs Results

ν_{133}	H	ν_{131}	$\Delta\nu(+ve\, g_I)$	$\Delta\nu(-ve\, g_I)$
40·00	111·07	52·78±0·02	16750±450	13050±250
60·00	164·02	78·75±0·02	15265±145	13200±100

The $\Delta\nu$ values associated with negative g_I agree so the magnetic moment of ^{131}Cs (calculated assuming $\Delta\nu_{131}=13\,200\pm100$ Mc/s, $\Delta\nu_{133}=9\,192{\cdot}6$ Mc/s and $\mu_{133}=+2{\cdot}558$ NM) is $+3{\cdot}48\pm0{\cdot}04$ NM.

4.5. ^{134}Cs *Results*

A sample of CsCl in which the ^{134}Cs/^{133}Cs ratio was about 2×10^{-5} was obtained from A.E.R.E. Harwell where the ^{134}Cs had been made by the ^{133}Cs (nγ) ^{134}Cs reaction. A caesium beam was produced using 10 mg of CsCl in the long channel oven.

The RF (on/off) ratio was measured as a function of mass-spectrometer setting near the mass number 134 position, at frequencies corresponding to $I=0$, 1, 2, 3, 4 and 5, and the only significant increase occurred at the $I=4$ frequency. Four higher frequency resonances were also located at the frequencies shown below.

Table 5. The ^{134}Cs Results

ν_{133}	H	ν_{134}	$\Delta\nu(+ve\, g_I)$	$\Delta\nu(-ve\, g_I)$
20·00	56·37	17·75±0·02	13750±1500	10350±850
40·00	111·07	34·56±0·02	12030± 300	10525±220
60·00	164·20	53·06±0·02	11375± 125	10440±100
120·00	314·88	105·62±0·02	10975± 30	10440± 30

The $\Delta\nu$ values associated with negative g_I are consistent so the magnetic moment of ^{134}Cs (calculated assuming $\Delta\nu_{134}=10\,440\pm30$ Mc/s, $\Delta\nu_{133}=9\,192{\cdot}6$ Mc/s and $\mu_{133}=+2{\cdot}558$ NM) is $+2{\cdot}95\pm0{\cdot}01$ NM.*

§ 5. DISCUSSION

5.1. *The Shell Model*

It has been shown (Feenberg 1949, Talmi 1950) that the known magnetic moments of odd-odd nuclei are generally in agreement with those calculated using j–j coupling and Schmidt's values for the magnetic moments of the odd–proton and odd-neutron states. This agreement is not so good when the odd-proton and odd-neutron are in different states, though it can be improved by using experimental values for the moments of the proton and neutron states. The magnetic moment μ_I of a nucleus with spin I is then,

---

* Similar results have been reported in a private communication, by V. Jaccarino, B. Bederson and H. H. Stoke, of Massachusetts Institute of Technology.

$$\mu_I=\mu_\mathrm{P}[J_\mathrm{P}(J_\mathrm{P}+1)+I(I+1)-J_\mathrm{N}(J_\mathrm{N}+1)]/[2(I+1)J_\mathrm{P}]$$
$$+\mu_\mathrm{N}[J_\mathrm{N}(J_\mathrm{N}+1)+I(I+1)-J_\mathrm{P}(J_\mathrm{P}+1)]/[2(I+1)J_\mathrm{N}], \quad . \quad . \quad . \quad (6)$$

where J_P and J_N are the total angular momentum quantum numbers and μ_P and μ_N are the effective magnetic moments of the proton and neutron states.

Table 6. A Comparison between the Observed Magnetic Moments of the Isotopes Investigated and the Values Calculated for some of the Possible Nuclear Configurations

Isotope	I	μ (observed)	Configuration		μ(S)	μ(E)
			Proton	Neutron		
^{131}Cs	5/2	+3·48	$\mathrm{d}_{5/2}$	—*	+4·79	+3·6
^{24}Na	4	+1·69	$\mathrm{d}_{(5/2)}{}^{3}{}_{3/2}$	$\mathrm{d}_{5/2}$	+0·97	+1·26
			$\mathrm{d}_{5/2}$	$\mathrm{d}_{5/2}$*	+2·30	+2·14
			$\mathrm{d}_{3/2}$	$\mathrm{d}_{5/2}$	−1·78	−0·36
			$\mathrm{d}_{5/2}$	$\mathrm{d}_{3/2}$	+5·94	+2·72
^{42}K	2	−1·14	$\mathrm{d}_{3/2}$	$\mathrm{f}_{7/2}$*	−1·73	−1·05
^{86}Rb	2	−1·69	$\mathrm{f}_{5/2}$	$\mathrm{g}_{9/2}$*	−2·14	−1·79
			$\mathrm{p}_{3/2}$	$\mathrm{p}_{1/2}$	+4·43	+3·35
^{134}Cs	4	+2·95	$\mathrm{g}_{7/2}$	$\mathrm{d}_{3/2}$*	+2·17	+2·79
			$\mathrm{g}_{7/2}$	$\mathrm{h}_{11/2}$	−1·39	−0·67
			$\mathrm{g}_{7/2}$	$\mathrm{s}_{1/2}$	−0·19	+1·66
			$\mathrm{d}_{5/2}$	$\mathrm{d}_{3/2}$	+5·94	+4·31
			$\mathrm{d}_{5/2}$	$\mathrm{h}_{11/2}$	−2·96	−1·77

The observed and calculated magnetic moments of some of the possible configurations of the nuclei investigated have been tabulated below. The magnetic moments under the heading μ(S) were calculated assuming Schmidt values for μ_P and μ_N, while those under the heading μ(E) were evaluated using values of μ_P and μ_N found experimentally (Mach 1950) for neighbouring odd-proton and odd-neutron nuclei in corresponding states. When these had not been measured, an average value taken from the plot of magnetic moments given by Klinkenberg (1952) was used. The odd-proton nucleus ^{131}Cs is also included.

The configurations given in the literature by Mayer (1951) and Klinkenberg (1952) are marked with asterisks. It is seen that in the cases of

^{41}K, ^{86}Rb and ^{134}Cs, the $\mu(E)$ values for the states are closer to the observed magnetic moments than the $\mu(S)$ values and the agreement is sufficiently good to be used as evidence in favour of these configurations which were suggested because they are most consistent with the shell model. The ^{24}Na agreement, however, is not good enough to decide between the $d_{5/2}$ proton state predicted by Mayer (1951) and the $(d_{5/2})^3{}_{3/2}$ state which is the most likely for the odd-proton nucleus ^{23}Na. This second configuration has a μ(E) value of 2·18 NM which is close to the observed ^{23}Na magnetic moment (2·22 NM) and has been justified theoretically (Kurath 1950, Talmi 1952).

5.2. *Decay Schemes*

The spin values found for the isotopes suggested are all consistent with the decay schemes given in the literature ((*Nuclear Data*). The ^{86}Rb result is of interest since the β-decay to the ground states of ^{86}Sr has an ‘ a ’ type first forbidden shape (Zaffarano 1948, Muether 1950) which predicts $I=2$ and even parity for ^{86}Rb, assuming that ^{86}Sr, being an even–even nucleus, has spin 0 and even parity. Since the configuration $(f_{5/2}, g_{9/2})_2$, which gives a good magnetic moment agreement, has odd-parity, this prediction is verified.

ACKNOWLEDGMENTS

The authors wish to express their gratitude to Professor O. R. Frisch for his interest and advice in the course of the work. They also wish to thank Dr. D. Nagle for his practical assistance with the design of the apparatus, P. Nutter for help with the activity measurements and the RF supplies, Professor W. E. Burcham and Dr. W. I. B. Smith for providing cyclotron irradiation facilities at Birmingham, the Isotope Section, A.E.R.E., Harwell, for the slow neutron irradiations and Dr. A. G. Maddock of the Radiochemical Laboratory, Cambridge, for the chemical separations.

REFERENCES

Breit, G., and Rabi, I. I., 1931, *Phys. Rev.*, **38,** 2082.
Davies, L., Nagle, D. E., and Zacharias, J. R., 1949, *Phys. Rev.*, **76,** 1068.
Eisinger, J. T., Bederson, B., and Feld, B. T., 1952, *Phys. Rev.*, **86,** 73.
Feenberg, E., 1949, *Phys. Rev.*, **76,** 1275.
Fermi, E., 1930, *Zeits. f. Physik*, **60,** 320.
Klinkenberg, P. F. A., 1952, *Rev. Mod. Phys.*, **24,** 63.
Kurath, D., 1950, *Phys. Rev.*, **80,** 98.
Mack, J. E., 1950, *Rev. Mod. Phys.*, **22,** 64.
Mayer, M. G., 1950, *Phys. Rev.*, **78,** 16.
Mayer, M. G., Moskowski, S. A., and Nordheim, L. W., 1951, *Rev. Mod. Phys.*, **23,** 315.
Muether, H. R., and Ridgeway, S. L., 1950, *Phys. Rev.*, **80,** 750, L.
Nuclear Data, National Bureau of Standards.
Rabi, I. I., Kellog, J. M. B., and Zacharias, J. R., 1934, *Phys. Rev.*, **46,** 157.
Talmi, I., 1950, *Phys. Rev.*, **83,** 1248 ; 1952, *Helv. Phys. Acta.*, **25,** 185.
Zacharias, J. R., 1942, *Phys. Rev.*, **61,** 270.
Zaffarano, D. J., Kern, B. D., and Mitchell, A. C. G., 1948, *Phys. Rev.*, **74,** 682.

V. *The Use of Neutron Counters to Obtain Cloud-Chamber Photographs of V-Particle Decays*

By K. H. Barker, R. D. Sard, and M. G. Sowerby
The Physical Laboratories, University of Manchester*

[Received October 30, 1952]

Abstract

In an attempt to increase the rate at which cloud-chamber photographs of *V*-particle decays can be obtained a number of triggering arrangements incorporating BF_3 neutron counters have been used on the Pic-du-Midi (2867 m).

The yields of *V*-particle decays are found to be comparable with the yield of a typical multiple Geiger counter system.

§1. Introduction

One of the main problems in obtaining cloud-chamber photographs of *V*-particle decays lies in detecting the interactions in which they are produced as efficiently as possible. Several teams are working at mountain altitudes, where the flux of nuclear interacting particles is considerably greater than that at sea-level, but the yield of photographs of *V*-particle decays is small. Most control systems employed in this work are conventional arrays of Geiger counters dependent for their operation on the showers of penetrating particles produced in energetic nuclear interactions. The most serious limitation of such arrangements is the difficulty of detecting interactions in which only small numbers of mesons are produced, because of the large background of unwanted μ-meson knock-on and air showers. It is probable that the majority of the penetrating shower detectors that have been used to trigger cloud chambers do not respond efficiently to the interactions of particles of energy less than about 10 Bev. Of the interacting cosmic ray particles with energies greater than 1 Bev less than 2% have energies above 10 Bev. It is therefore important to consider ways in which the lower energy interactions can be efficiently detected.

Methods dependent on the properties of the evaporation star accompanying a nuclear interaction would appear to be the most hopeful, since the size of the star is not very dependent on the energy expended in meson production for primary energies greater than about 1 Bev (Camerini *et al.* 1951). A cloud-chamber experiment has been reported (Salvini 1951) in which the chamber was triggered by particles whose total ionization loss within a crystal of sodium iodide exceeded a few Mev.

---

* Communicated by G. D. Rochester.

The ionization in these cases was due to the evaporation particles from single nuclear interactions. This method might be rather troublesome to operate in a magnetic field and will probably only be useful for detecting interactions produced in a scintillating material. Recently workers at Washington University (Fowler *et al.* 1950, Althaus 1951 a) have reported the use of neutron counters, filled with enriched BF_3, in coincidence with Geiger counters to control the operation of a cloud chamber. The interactions occurred in lead nuclei, which give a copious yield of slow neutrons. The yield of pictures showing recognizable mesons and V-particles was promising (Althaus 1951 b, Fowler 1951) and further trials seemed appropriate. The Blackett magnet chamber at the Pic-du-Midi (735 g/cm^2) has been used. Two major changes have been made from the triggering system used in the earlier neutron experiments: a large mass of lead on the roof of the chamber and the requirement that more than one evaporation neutron be detected. As a result of the first change, evaporation neutrons are detected from a nucleonic cascade in the lead, instead of from just one star. The second change effectively eliminates electron–photon cascades, which contribute appreciably to the single neutron rate. The results obtained with the neutron triggering system are compared with those obtained using a conventional Geiger counter system on the same chamber.

§2. A BRIEF DESCRIPTION OF THE SELECTION SYSTEMS

(i) *The Arrangement Using Neutron Counters*

Four neutron counters connected in parallel were used and the electronic circuits, following the design of Crouch, counted events in which a number of neutron pulses, n, ($n \geqslant 1$, 2 and 3) were detected in a 400 μ-sec coincidence gate. The gate was opened 5 μ-sec after a coincidence pulse from a simple Geiger counter array. The relative dispositions of the counters, the paraffin wax moderator, the lead absorbers and the cloud chamber are shown in fig. 1 (a). The division of the Pb producer into two parts, with the C tray between them instead of being right on top of the chamber, was required mechanically in order to avoid altering the present thermal jacket of the cloud chamber.

Various triggering arrangements were tried, such as ($A_1B_1 \,.\, N_3$), ($C_1D_1 \,.\, N_2$), ($C_1D_1 \,.\, N_3$). Here the number gives the minimum number of pulses, e.g., ($A_1B_1 .\, N_3$) means one or more pulses in the A tray coincident with one or more pulses in the B tray, associated with three or more neutron pulses in the delayed coincidence gate.

The efficiencies of neutron detection were measured with a calibrated Ra—α—Be source. The results averaged over the volumes in question and corrected for the loss of neutrons captured after termination of the neutron coincidence gate, were 3·7% for the top layer, 2·0% for the layer immediately above the chamber, and 0·8% for the tungsten-copper plate inside the chamber. These figures show that when multiple neutron coincidences are required, the efficiency of detection of nucleonic cascades starting in the top layer will be much greater than for the lower layers.

(ii) *The Geiger Counter Arrangement*

For comparison the Geiger counter arrangement used most recently to control the cloud chamber is also described. The geometry of the system is shown in fig. 1 (*b*). Two combinations in parallel have been used, the first requiring the discharge of at least two counters in both trays C and D and the second at least one in tray C and two in each of trays D and E.

Fig. 1

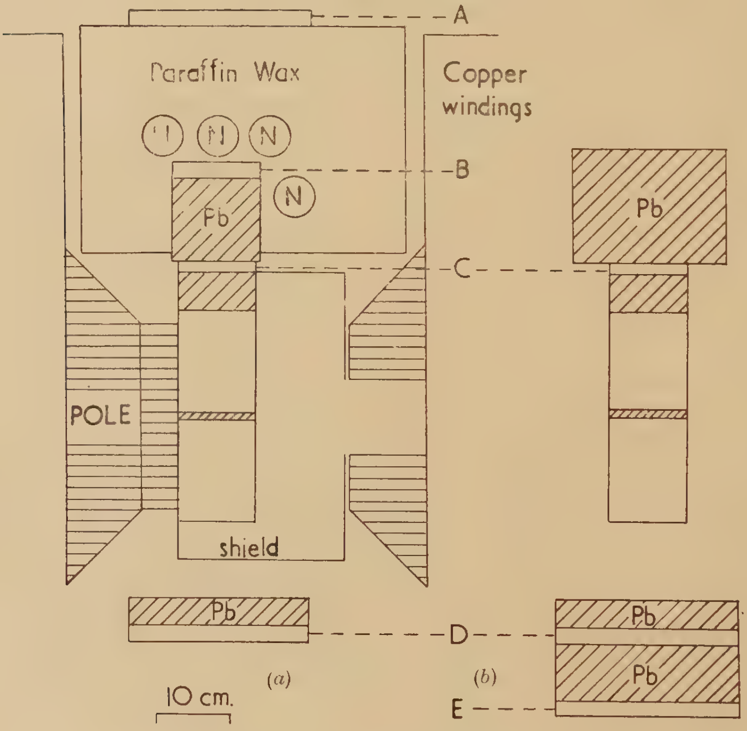

(*a*) The neutron counter control system.
(*b*) The Geiger counter control system.
Areas of the counter trays: A 1000 cm^2, B 240 cm^2, C 150 cm^2, D 1000 cm^2, E 800 cm^2.

§3. Discussion of Results

Data relevant to the various counter arrangements described in the previous section are presented in the table. During the tests of the neutron triggering arrangements, the resetting time of the chamber was two minutes. The data obtained with the multiple Geiger systems have been corrected to this resetting time.

The first neutron counting arrangement ($A_1B_1 . N_3$), is insensitive to neutron-induced events, and responds mainly to interactions produced by protons of several Bev energy. The geometrical efficiency of the chamber for the detection of the products of such interactions when they occur in the top producing layer is small. In order to increase the yield of events giving particles in the chamber, an arrangement with the Geiger telescope below the main producing layer was used. One energetic secondary particle was then required below the cloud chamber. This change raised the average energy of the events detected, and also made the arrangement sensitive to interactions initiated by neutrons as well as protons. The second, third and fourth rows of the table give the results. Several other neutron triggering arrangements were tried briefly, but the results were not considered to be of sufficient significance to tabulate. The last row combines the results of two runs with a penetrating shower selector of the conventional type, between which the neutron trials were made.

Comparison of Various Control Systems

(1) Counter arrangement.	(2) No. of photographs.	(3) Rate per hr.*	(4) Total time (hrs.)	(5) No. p.p. per hr.	(6) (a) No. of *V*°-particles. (b) No. of *V*±-particles.	(7) No. hrs. per *V*-particle.	(8) No. p.p. per *V*-particle.
$A_1B_1 . N_3$	587	11	53·5	3·6±0·2	(*a*) 2 (*b*) 0	~27	~97
$C_1D_1 . N_3$	1946	9·1	214·0	6·0±0·1	(*a*) 11 (*b*) 0	19±6	114±38
$C_1D_1 . N_2$	1328	13·6	97·6	10·0±0·3	(*a*) 6 (*b*) 0	16±7	160±70
$C_2D_1 . N_2$	804	6·3	127·5	5·0±0·2	(*a*) 6 (*b*) 1	18±7	90±35
C_2D_2 and $C_1D_2E_2$	3923	8·0	490·4	6·4±0·1	(*a*) 30 (*b*) 7	13±3	83±20

* Resetting time of chamber was 2 min.

No definite conclusions can be drawn regarding the absolute yields of *V*-particle decays, given in column (7) of the table, since the numbers recorded are small. The first arrangement may have the lowest efficiency while the other neutron arrangements give yields comparable to those obtained with the multiple Geiger systems.

The yields of shower particles (p.p.) penetrating the plate across the chamber are shown in column (5) and the numbers of penetrating particles for each *V*-decay in column (8). Although a significantly larger number of shower particles per hour are detected with the arrangement ($C_1D_1 . N_2$) there is probably no significant increase in the rate of *V*-particle decays in the chamber. Moreover there are no obvious differences in the energies of the *V*-particles recorded by the neutron counter and Geiger counter arrangements. It thus appears that there is no great advantage in using a neutron counter triggering system at mountain altitudes unless the chamber resetting time can be considerably reduced. However, even for large chambers the neutron detection system can probably increase the rate of recording *V*-particle decays at sea level.

Acknowledgments

We wish to express our thanks to Professor P. M. S. Blackett for his encouragement and for the laboratory facilities provided, and to Dr. C. C. Butler for many discussions. R. D. Sard is indebted to the U.S. Education Commission in the United Kingdom for a Fulbright research grant and M. G. Sowerby to the Department of Scientific and Industrial Research for the award of a maintenance grant.

References

Althaus, E. J., 1951 a, *Phys. Rev.*, **81,** 647 ; 1951 b, *Ibid.*, **83,** 896.

Camerini, U., Davies, J. H., Fowler, P. H., Franzinetti, C., Muirhead, H., Lock, W. O., Perkins, D. H., and Yekutieli, G., 1951, *Phil. Mag.*, **42,** 1241.

Fowler, W. B., 1951, *Thesis*, Washington University, St. Louis.

Fowler, W. B., Sard, R. D., Fowler, E. C., and Street, J. C., 1950, *Phys. Rev.*, **78,** 323.

Salvini, G., 1951, *Nuovo Cimento*, **8,** 798.

VI. *A Theoretical Examination of the Plastic Deformation of Crystals by Glide*

By J. F. W. Bishop
H. H. Wills Physical Laboratory, University of Bristol, and
Mechanical Engineering Research Organisation, D.S.I.R.*

[Received September 17, 1952]

Summary

Proofs are given of theorems stated in the Bishop–Hill theory of crystal distortion. Mathematical relations are established for the deformation of crystals by simultaneous shears, and the possibility of enforcing an arbitrary strain by glide is examined. The uniform stress states not exceeding the critical shear stresses in the glide-directions are discussed, and a geometrical picture of stress and strain states is developed. It is proved that it is always *physically* possible to enforce a given strain by glide provided it is *geometrically* possible. The uniform elongation of a face-centred cubic crystal is examined.

§ 1. Introduction

Experimental investigation of the plastic deformation of metallic and ionic crystals has led to the conclusion that two basic processes are involved, namely, gliding and twinning. In glide, planes of atoms slide relative to each other through integral numbers of lattice spaces. This preserves the lattice structure, but constitutes a *discontinuous* shear at the atomic level. Mechanical twinning can be regarded as a *continuous* shear in portions of the crystal, which results in the atoms taking up a symmetrical position with regard to the atoms in the original lattice. The magnitude of the shear is such that the lattice structure is again preserved. Both processes are commonly observed to occur in plastically deformed crystals. Strictly speaking, these processes are not directly applicable to real crystals, which are only perfectly ordered over small regions. However, the departure from the idealized model is sufficiently small to allow of real crystals being treated as perfect. The spacing between the individual slip-planes, and the amount of slip occurring on each, is such that a uniform *macroscopic* shear can conveniently be regarded as a uniform *continuous* shear for the purposes of a mathematical theory of crystal distortion. Assuming that glide alone is a sufficient mechanism for deformation, it has been shown (Bishop and Hill 1951 a) that two extremum principles hold for single crystals. The extension of these principles to a polycrystalline aggregate leads to the mathematically important result that the plastic potential and the yield function coincide for an aggregate (as they do for single crystals). This in turn enables the yield to be computed. In this paper, the circumstances under which glide alone is, in fact, a sufficient mechanism, are investigated.

---

* Communicated by the Author.

§ 2. GLIDE–STRAIN RELATIONS

It is known that the atomic planes on which relative sliding occurs in crystals are closely related to the lattice structure. In metals containing close-packed planes, glide occurs on these planes, and the close-packed directions are glide-directions. The glide-planes and directions can be determined from suitable surface markings on test specimens (see, for example, Taylor and Elam 1925).

If glide is regarded as a continuous shear parallel to a glide plane, the displacement of an arbitrary point due to a given shear can be found by simple geometry. Knowing the displacement components, the strains are immediately obtainable by differentiation.

Considering the general problem, let there be r glide planes with normals n_i^α, $\alpha=1, 2, \ldots r$; i takes the values 1, 2, and 3 and gives the direction-cosines of the normal in an orthogonal Cartesian space. Let the glide plane α contain s glide-directions $l_i^{\alpha\beta}$, $\beta=1, 2, \ldots s$. (Generally s will be different for each plane.) The displacement components u_i at a point P, position x_i, due to a uniform shear of magnitude $d\gamma^{\alpha\beta}$ parallel to the α plane in the β direction, are

$$u_i=\sum_j d\gamma^{\alpha\beta} n_j^\alpha x_j l_i^{\alpha\beta},$$

where $d\gamma^{\alpha\beta}$ is the engineering shear equal to twice the mathematical shear, and the origin is chosen to be a point of zero displacement. The summation convention of summing over repeated indices does not apply.

The total displacement components due to shears on all planes are therefore

$$u_i=\sum_{\alpha\beta j} d\gamma^{\alpha\beta} n_j^\alpha x_j l_i^{\alpha\beta}. \qquad (1)$$

Since the strain components and displacements are related by

$$d\epsilon_{ij}=\frac{1}{2}\left(\frac{\partial u_i}{\partial x_j}+\frac{\partial u_j}{\partial x_i}\right),$$

the strain components corresponding to (1) are

$$d\epsilon_{ij}=\sum_{\alpha\beta} \tfrac{1}{2}\, d\gamma^{\alpha\beta}(l_i^{\alpha\beta} n_j^\alpha + l_j^{\alpha\beta} n_i^\alpha). \qquad (2)$$

Equation (2) represents six relations since $d\epsilon_{ij}=d\epsilon_{ji}$. In shearing, no volume change occurs, and it follows that $d\epsilon_{11}+d\epsilon_{22}+d\epsilon_{33}=0$. An arbitrary strain in an incompressible material is therefore specified by five independent strain components. Equation (2) can be considered as a set of linear algebraic equations expressing the strains $d\epsilon_{ij}$ in terms of the shears $d\gamma^{\alpha\beta}$.

If the column vectors $[d\epsilon]$, $[d\gamma]$ have components

$$\{d\epsilon_{11}, d\epsilon_{22}, d\epsilon_{33}, 2d\epsilon_{23}, 2d\epsilon_{31}, 2d\epsilon_{12}\} \text{ and } \{d\gamma^{11}, d\gamma^{12}, \ldots d\gamma^{r1}, d\gamma^{r2}, \ldots\},$$

and $[E]$ is the matrix of the coefficients of $d\gamma^{\alpha\beta}$, eqn. (2) becomes

$$[d\epsilon]=[E][d\gamma]. \quad \ldots \ldots \ldots \ldots \quad (3)$$

Omitting one of the equations in $d\epsilon_{ii}$, ($d\epsilon_{11}$ say), if a (5×5) minor of $[E]$ has a non-zero determinant, eqns. (2) contain a linear independent set of five. This implies that an arbitrary strain can be imposed geometrically in terms of five independent shears, i.e. by glide alone. (A distinction between *geometrically* and *physically* possible sets of shears will be made later.) Since only five independent strain components exist, only five shears can be linearly independent.

Normally it is necessary to examine $[E]$ to find whether a non-zero minor exists, but some general remarks can be made. Since only two independent shears can occur on one plane, at least three non-parallel glide planes must be available. (The existence of three such planes, each with two independent shears does *not*, however, imply that a general strain can be imposed by glide alone.)

§ 3. STRESS IN A SINGLE CRYSTAL

It is known that glide can occur when the resolved shear stress on a glide plane in a glide direction reaches a specific value, the critical shear stress. This value may differ for different glide directions and for opposite senses of shear in the same glide direction. In considering the variation of the critical value with strain, two types of glide systems must be differentiated, *active* systems on which slip is actually occurring, and *latent* systems which are not slipping. The experimental evidence as to how the critical values on the two types of system depend on strain is slight. Taylor and Elam in their work on aluminium (1925) have concluded that both active and latent systems harden by *approximately* the same amount. More recently, Röhm and Kochendörfer (1950), on the basis of their experiments on aluminium crystals, have proposed an empirical law relating the hardening on active and latent systems through the lattice geometry. Any applied stress system must be such that the resolved shear stress in each of the glide directions does not exceed the *current* critical value.

Let $\tau^{\alpha\beta}$ be the resolved shear stress on the α plane in the positive β direction. If σ_{ij} is the current uniform stress state,

$$\begin{aligned}\tau^{\alpha\beta}&=\sum_{ij}\sigma_{ij}n_i^{\alpha}l_j^{\alpha\beta},\\ &=\sum_{ij}\tfrac{1}{2}\sigma_{ij}(n_i^{\alpha}l_j^{\alpha\beta}+n_j^{\alpha}l_i^{\alpha\beta}). \quad \ldots \ldots \ldots \quad (4)\end{aligned}$$

This set of equations expresses the resolved shear stresses in terms of the stress components. If $\tau_c^{\alpha\beta}$, $\tau_c'^{\alpha\beta}$ are the critical shear stresses in the positive and negative senses of shear,

$$-\tau_c'^{\alpha\beta} \leqslant \tau^{\alpha\beta} \leqslant \tau_c^{\alpha\beta},$$

i.e.
$$-\tau_c'^{\alpha\beta} \leqslant \sum_{ij} \tfrac{1}{2}\sigma_{ij}(n_i^{\alpha} l_j^{\alpha\beta} + n_j^{\alpha} l_i^{\alpha\beta}) \leqslant \tau_c^{\alpha\beta}, \quad \ldots\ldots \quad (5)$$

for all α and β.

If column vectors $[\tau]$ and $[\sigma]$ have components $\{\tau^{11}, \tau^{12}, \ldots \tau^{r1}, \tau^{r2}, \ldots\}$ and $\{\sigma_{11}, \sigma_{22}, \sigma_{33}, \sigma_{23}, \sigma_{31}, \sigma_{12}\}$, and $[S]$ is the matrix of coefficients of the σ_{ij} in (4),

$$[\tau] = [S][\sigma]. \quad \ldots\ldots\ldots\ldots \quad (6)$$

(It will be realized that the coefficient of σ_{xy}, say, will contain the terms in both σ_{xy} and σ_{yx}.) Comparison of (2) and (4) shows that the matrix $[E]$ is the transpose of $[S]$. This can be predicted from a different viewpoint. The virtual work theorem states that the work done in a strain by a stress system, is equal to that done by an equivalent set of shear stresses in an equivalent set of shears, i.e.

$$\sum_{ij} \sigma_{ij}\, d\epsilon_{ij} = \sum_{\alpha\beta} \tau^{\alpha\beta}\, d\gamma^{\alpha\beta}.$$

The stresses and strains do not necessarily correspond. In matrix notation this becomes

$$[\sigma]'[d\epsilon] = [\tau]'[d\gamma],$$

where the prime denotes transpose.

Now $[d\epsilon] = [E][d\gamma]$ and $[\tau] = [S][\sigma]$. Hence $[\sigma]'[E][d\gamma] = [\sigma]'[S]'[d\gamma]$. This is true for all $[\sigma]$ and $[d\gamma]$ and hence

$$[E] = [S]'.$$

§ 4. Geometrical Representation

So far, we have seen that for a general strain to be geometrically possible, five independent shears must exist, and that mathematically this requires a (5×5) minor of a certain matrix to have a non-zero determinant; further that a set of inequalities places conditions on possible combined stress states which may be imposed on the crystal. In this section it is proposed to develop a geometrical picture illustrating the relations between stress, strain, shear, etc.

Consider an orthogonal space of six dimensions with $(d\epsilon_{11}, \ldots 2d\epsilon_{12})$, $(\sigma_{11}, \ldots \sigma_{12})$ plotted along the co-ordinate axes. Stress and strain states appear as six-vectors in this space. Since the work done by a stress σ_{ij} in a strain $d\epsilon_{ij}$ is

$$dW = \sigma_{11}\, d\epsilon_{11} + \sigma_{22}\, d\epsilon_{22} + \sigma_{33}\, d\epsilon_{33} + 2\sigma_{23}\, d\epsilon_{23} + 2\sigma_{31}\, d\epsilon_{31} + 2\sigma_{12}\, d\epsilon_{12},$$

the work done is the scalar product of the stress and strain vectors. Since each glide direction can be operated in two senses, twice as many vectors corresponding to unit shears will exist as glide directions. Any five independent vectors corresponding to *incompressible* strains (taken in both senses) will map the entire subspace defined by $d\epsilon_{11}+d\epsilon_{22}+d\epsilon_{33}=0$. Hence *all* sets of five independent shears can constitute an arbitrary strain from purely geometrical considerations. Any five independent shears operating in one sense only will map a region of the subspace.

Now let us consider stresses. From eqns. (2) and (4) it can be seen that the resolved shear stress in a glide direction is the scalar product of the stress vector with a vector corresponding to a unit shear in the glide direction. Each of the stress states which achieves the critical value in a glide direction will therefore lie in a hyperplane normal to the unit shear vector and given by either

$$\tau_c{}^{\alpha\beta}=\sum_{ij}\sigma_{ij}n_i{}^{\alpha}l_j{}^{\alpha\beta} \quad \text{or} \quad -\tau_c{}'^{\alpha\beta}=\sum_{ij}\sigma_{ij}n_i{}^{\alpha}l_j{}^{\alpha\beta}.$$

The set of these planes constitutes a bounding surface called the yield surface, within or upon which all stress states not exceeding the critical shear value in any glide direction must lie. If n such planes meet in a point, the corresponding stress vector will achieve the critical shear stress in all n glide directions, and will make the simultaneous operation of all n shears possible. Since a pure hydrostatic pressure gives no shearing stress on any plane, the yield surface will be cylindrical with generators in the direction (1, 1, 1, 0, 0, 0). A stress vector can always be found to achieve the critical value in five independent shears, but in general it will lie outside the yield surface. We have seen that under certain conditions sufficient shears will be available to impose an arbitrary strain from purely geometrical considerations. It remains to show that a stress system satisfying the yield conditions can always be found to operate such a set of shears.

Geometrically the problem appears as follows. If there are N glide directions there will be $2N$ vectors corresponding to unit shears (regarding positive and negative shearing along a glide direction as separate). Suppose several sets of five independent vectors exist. All *positive* combinations of the vectors in a set will map a region of the space, within which all strain states imposable by simultaneous operation of the shears must lie. To each set will correspond a stress vector whose scalar product with each vector in the set gives the (positive) critical value. In general, an arbitrary strain will lie in a region generated by several sets of independent shears. It is required to show that the stress vector corresponding to at least one such set lies upon the yield surface.

§ 5. EXISTENCE THEOREM

Suppose n sets of five simultaneous shears exist which will impose a given strain geometrically. Consider the corresponding set of n stress vectors which operate these sets of shears. The minimum shear principle for a single crystal (Bishop and Hill 1951 a) can be stated in the form that if one of the vectors terminates on the yield surface, it will do less work in the given strain than any of the set terminating outside the surface.

Consider the set of shears for which the work is a minimum, and the corresponding stress vector. Either this lies upon the yield surface or else the critical shear stress is exceeded in some other glide direction. Let the set of (unit) shears be the vectors $\mathbf{d\gamma}_\alpha$ ($\alpha=1, 2, \ldots 5$). Since we are treating positive and negative directions of shear as separate vectors, the given strain $\mathbf{d\epsilon}$ can be expressed by

$$\mathbf{d\epsilon}=\sum_\alpha a_\alpha\,\mathbf{d\gamma}_\alpha,$$

where all the a_α are non-negative.

If τ_α are the critical shear stresses and $\boldsymbol{\sigma}$ is the stress state,

$$\boldsymbol{\sigma}\,.\,\mathbf{d\gamma}_\alpha=\tau_\alpha.$$

Further if $\mathbf{d\gamma}_6$ is the direction in which the critical value is exceeded,

$$\boldsymbol{\sigma}\,.\,\mathbf{d\gamma}_6>\tau_6.$$

It is proposed to show that a *positive* combination of this shear and four of the original five will suffice to constitute the given strain, i.e.

$$\mathbf{d\epsilon}=\sum_\alpha a_\alpha\,\mathbf{d\gamma}_\alpha=\sum_\beta a_\beta\,\mathbf{d\gamma}_\beta, \qquad \ldots\ldots\ldots \quad (7)$$

where $\beta=(1, 2, \ldots 6)$ with one of the indices $(1, 2, \ldots 5)$ excluded, and all $a_\beta \geqslant 0$.

Since the shears $\mathbf{d\gamma}_\alpha$ are independent,

$$\mathbf{d\gamma}_6=\sum_\alpha b_\alpha\,\mathbf{d\gamma}_\alpha, \qquad \alpha=1, 2, , \ldots 5;$$

the b_α may be positive, negative or zero.

Hence $\mathbf{d\gamma}_k=1/b_k\{\mathbf{d\gamma}_6-\sum_\alpha(b_\alpha\,\mathbf{d\gamma}_\alpha)_k\}$, where k takes the values $(1, 2, \ldots 5)$ and the subscript k outside the bracket indicates that k is omitted in the summation.

$$\sum_\alpha a_\alpha\,\mathbf{d\gamma}_\alpha=\sum_\alpha(a_\alpha\,\mathbf{d\gamma}_\alpha)_k+\frac{a_k}{b_k}\{\mathbf{d\gamma}_6-\sum_\alpha(b_\alpha\,\mathbf{d\gamma}_\alpha)_k\}$$

$$=\frac{a_k}{b_k}\mathbf{d\gamma}_6+\sum_\alpha\left\{b_\alpha\left(\frac{a_\alpha}{b_\alpha}-\frac{a_k}{b_k}\right)\mathbf{d\gamma}_\alpha\right\}_k.$$

Since the stress vector has a positive scalar product with all six unit shears, and $\mathbf{d\gamma}_6$ is a positive linear combination of the other five, not *all* b_α are negative. Consider the set b_α/a_α, $\alpha=1, 2, \ldots 5$. Since all the a_α are positive, at least one quotient will be positive and there will be a maximum value b_j/a_j (not necessarily unique).

Taking $k=j$, it is seen that $b_\alpha(a_\alpha/b_\alpha-a_k/b_k)$ is always non-negative, and hence the given strain can be imposed by a positive combination of $\mathbf{d\gamma}_6$ and four of the original five shears. Let $\boldsymbol{\sigma}_n$ be the stress required to achieve the critical shear stresses in this new set of shears. From (7) and the virtual work theorem, it follows that the work done by $\boldsymbol{\sigma}$ is the same in both the new and the original sets of shears. Since $\boldsymbol{\sigma}$ exceeded the critical shear stress in $\mathbf{d\gamma}_6$ and $\boldsymbol{\sigma}_n$ just attains it,

$$\boldsymbol{\sigma}_n\,.\,\mathbf{d\epsilon}<\boldsymbol{\sigma}\,.\,\mathbf{d\epsilon},$$

i.e. less work is required in the new set of shears to impose the given strain. But by hypothesis the original set corresponded to minimum work, and hence the assumption that σ is not a yield state must be wrong. The following theorem may be therefore enunciated. If a single set of five independent shears exist amongst the available glide systems, any arbitrary strain (with zero hydrostatic part) can be imposed both geometrically and physically.

§ 6. YIELD SURFACE OF A CRYSTAL

The maximum work principle for a single crystal states that the actual stress corresponding to a given strain does not do less work than any other stress state satisfying the yield conditions. Thus to find the stress required to operate a given strain, it is only necessary to find the stress vector lying on the yield surface maximizing the work. The yield surface is defined by an infinity of vectors, but it is not necessary to consider the infinity in maximizing the work. As we have seen, the stress surface is bounded by plane faces. If the strain vector corresponds to a single shear, any stress vector lying in the appropriate plane face of the yield surface will maximize the work, i.e. will operate the shear. A general strain requires five shears, which will be operated by stress vectors lying at the intersection of five plane faces. Since such stresses can also operate any selection of the relevant shears, it is clearly sufficient to consider only the 'vertices' of the stress surface in maximizing the work (as opposed to satisfying the stress equilibrium equations). The term 'vertex' is used by analogy with polyhedral surfaces in three dimensional space, but care must be exercised in identifying the geometrical properties of the vertices in the two spaces too closely. In the discussion below, the stress states defining the vertices of the yield surface of a face-centred cubic metal are derived.

In a face-centred cubic lattice, four glide-planes with three shear directions in each exist. The resolved shear stresses in terms of the stress components referred to the cubic axes are (multiplied by a factor $\sqrt{6}$)

$$\begin{array}{lll} A-G+H\ (a_1) & B+F-H\ (a_2) & C-F+G\ (a_3) \\ A+G+H\ (b_1) & B-F-H\ (b_2) & C+F-G\ (b_3) \\ A+G-H\ (c_1) & B+F+H\ (c_2) & C-F-G\ (c_3) \\ A-G-H\ (d_1) & B-F+H\ (d_2) & C+F+G\ (d_3) \end{array}$$

where $A=\sigma_{11}-\sigma_{33}$, $B=\sigma_{33}-\sigma_{11}$, $C=\sigma_{11}-\sigma_{22}$, $F=\sigma_{23}$, $G=\sigma_{31}$, $H=\sigma_{12}$. The letters and figures in brackets refer to the plane and glide direction respectively. (See Bishop and Hill 1951 b.)

In accordance with observation, we shall assume that the critical shear stress is the same on all glide planes, and for convenience it will be taken as $1/\sqrt{6}$ in both senses of shear. The yield surface is therefore defined by

$$A\pm G\pm H=\pm 1,\quad B\pm F\pm H=\pm 1,\quad C\pm F\pm G=\pm 1, \qquad . \quad . \quad (8)$$

where all combinations of signs are possible, giving 24 equations in all.

A stress state not exceeding the critical shear stress in any glide direction will satisfy the inequalities

$$|A \pm G \pm H| \leqslant 1, \quad |B \pm F \pm H| \leqslant 1, \quad |C \pm F \pm G| \leqslant 1.$$

Consider three rectangular Cartesian spaces with axes (A, G, H), (B, F, H) and (C, F, G). The stress components must be such that the vectors with components (A, G, H), (B, F, H) and (C, F, G) lie within or upon the octahedra given by (8). One such octahedron is shown in fig. 1. The faces are labelled to show the shears corresponding to stress vectors terminating in them. Vectors terminating at P, Q, R operate 1, 2, and 4 planes of type 1 respectively. Suppose the (A, G, H) vector terminates at P. This fixes the values of G and H, and it follows that the vectors in the other octahedra lie in sections by the places

Fig. 1

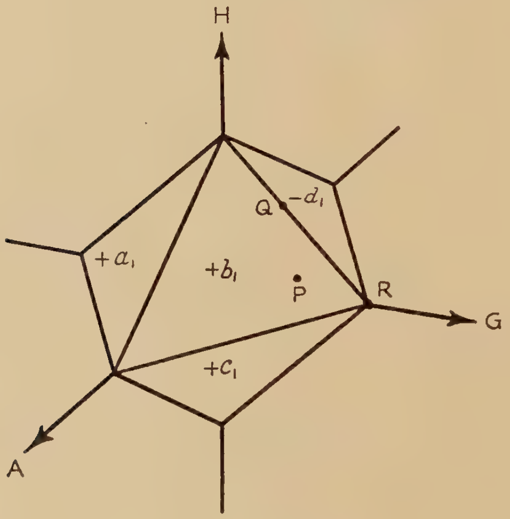

G=const., H= const. These are shown in figs. 2 (*a*) and 2 (*b*) for $A=1-g-h$, $G=g$, $H=h$. Since $A+B+C=0$, these two figures may be superposed as in fig. 3. A stress state not exceeding the yield conditions will be such that the vector in fig. 3 lies within the common shaded region. The sides are labelled to show the corresponding shears operated for $g, h>0$. When $g, h=0$, the shears in parentheses also operate.

If $(1-g-h)$, g, h lie within the open interval $(0, 1)$, only one plane of type 1 operates. From fig. 3 it can be seen that when $g=\frac{1}{2}$ *or* $h=\frac{1}{2}$, four more shears can be operated. Since, however, these are included in the sets operated by $g=\frac{1}{2}$ *and* $h=\frac{1}{2}$ (i.e. $A=0$), the stress states do not represent true vertices. It is therefore only necessary to consider stress states with at least one of A, G or H zero.

(i) Let $A=0$. A maximum number of four planes of type 1 operate.

The corresponding sections of the other two octahedra with $g \geqslant 0$ are shown in fig. 4 (*a*). All possible cases are covered by $g=0$, $g=\frac{1}{2}$ and $g=1$. The corresponding stress states (including the synonymous states in $B=0$ and $C=0$) are Nos. 4–6 and 13–28 inclusive in the table.

Fig. 2

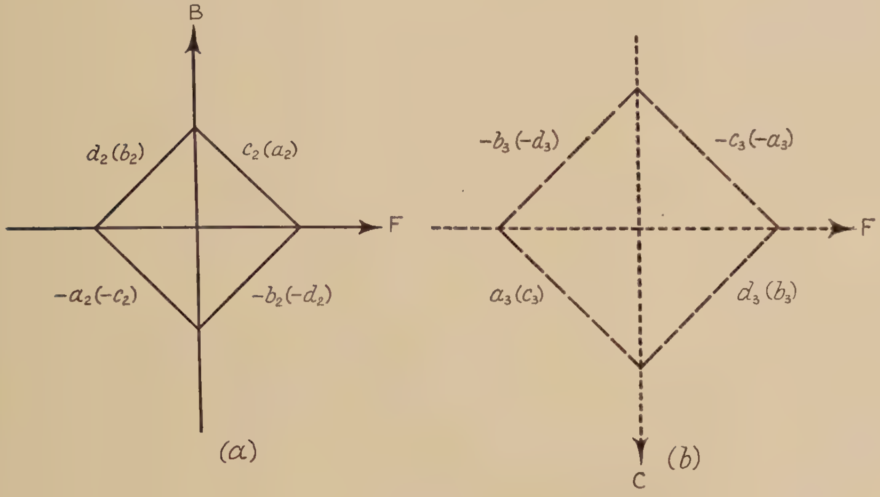

Fig. 3

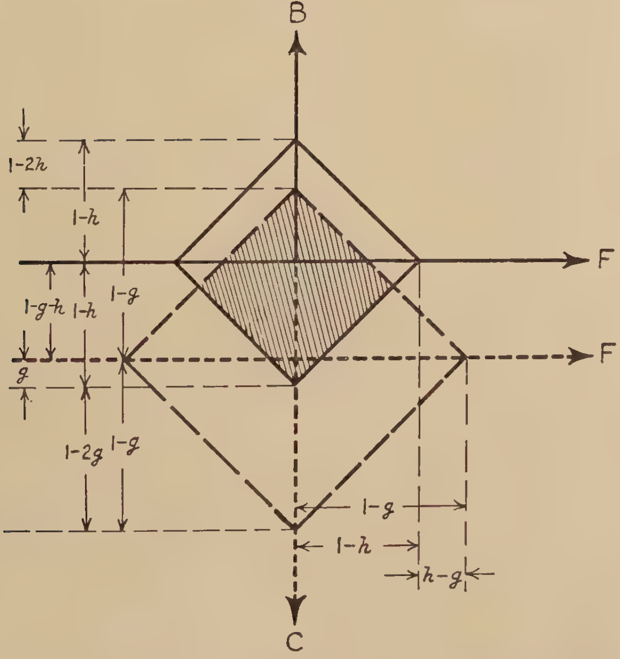

(ii) Let $G=0$. A maximum number of four planes of type 1 operate. Figure 4 (*b*) shows the corresponding sections of the other octahedra for $h \geqslant 0$. All possible cases are covered by $h=0$, $h=\frac{1}{2}$ and $h=1$, giving with synonymous states for $H=0$, Nos. 1–3 and 7–12.

This set of stress states (together with the negative values) defines the vertices of the yield surface. They were first determined by Hill (1949)* by means of a different method. Each of these states can operate either six or eight simultaneous shears, and in general several combinations of these will impose a strain both geometrically and physically as will be shown later. The yield surface for any lattice can, in principle, be similarly determined. If differential hardening occurs with strain, the yield surface will change in both size and shape.

Fig. 4

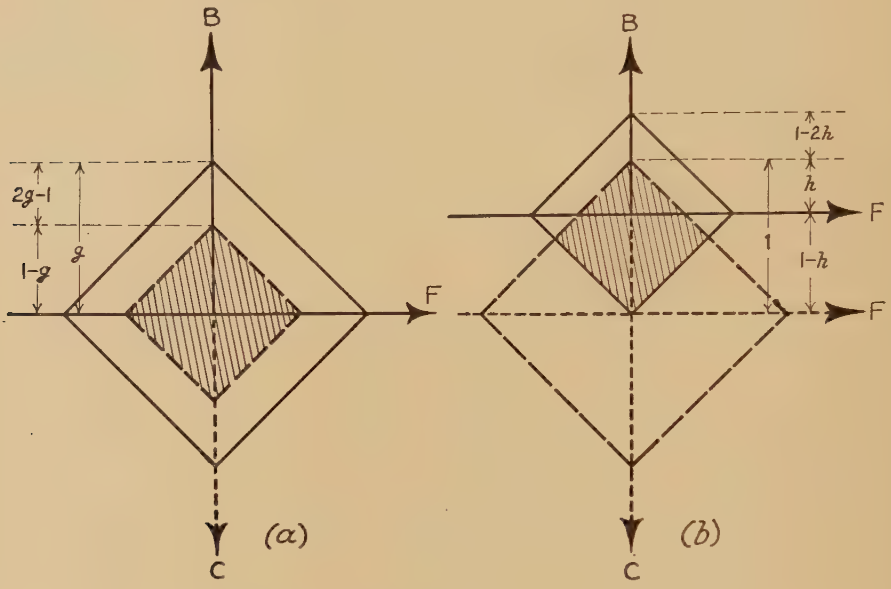

§ 7. UNIFORM ELONGATION IN A F.C.C. CRYSTAL

As an example of the use of the maximum work principle in conjunction with the tabulated stress states, it is proposed to examine the elongation of a single crystal with the transverse strains constrained to be equal. All orientations of the crystal cubic axes relative to the specimen axes are treated. This problem has been considered by Taylor (1938 a and b), who solved the sets of simultaneous equations expressing the strain in terms of five independent shears, and selected as the actual shears the set having a minimal sum of the absolute shear magnitudes.

If (x, y, z), (x', y', z') are the cubic and specimen axes respectively, and x' is the direction elongation,

$$d\epsilon'_{ij} = \begin{bmatrix} d\epsilon & 0 & 0 \\ 0 & -\tfrac{1}{2}d\epsilon & 0 \\ 0 & 0 & -\tfrac{1}{2}d\epsilon \end{bmatrix}.$$

---

* Private communication.

y' and z' are disposable orthogonal directions normal to x'; y' is taken to lie in the plane $z=0$. Taking θ as the meridional angle of the plane containing the x' and z axes from the plane $y=0$, and $\pi/2-\phi$ as the angle between the x' and z axes, symmetry considerations show that all orientations are covered by

$$0\leqslant\theta\leqslant\pi/4, \qquad 0\leqslant\phi\leqslant\tan^{-1}(\sin\theta).$$

No.	A	B	C	F	G	H
1	1	-1	0	0	0	0
2	0	1	-1	0	0	0
3	-1	0	1	0	0	0
4	0	0	0	1	0	0
5	0	0	0	0	1	0
6	0	0	0	0	0	1
7	$\frac{1}{2}$	-1	$\frac{1}{2}$	0	$\frac{1}{2}$	0
8	$\frac{1}{2}$	-1	$\frac{1}{2}$	0	$-\frac{1}{2}$	0
9	-1	$\frac{1}{2}$	$\frac{1}{2}$	$\frac{1}{2}$	0	0
10	-1	$\frac{1}{2}$	$\frac{1}{2}$	$-\frac{1}{2}$	0	0
11	$\frac{1}{2}$	$\frac{1}{2}$	-1	0	0	$\frac{1}{2}$
12	$\frac{1}{2}$	$\frac{1}{2}$	-1	0	0	$-\frac{1}{2}$
13	$\frac{1}{2}$	0	$-\frac{1}{2}$	$\frac{1}{2}$	0	$\frac{1}{2}$
14	$\frac{1}{2}$	0	$-\frac{1}{2}$	$-\frac{1}{2}$	0	$\frac{1}{2}$
15	$\frac{1}{2}$	0	$-\frac{1}{2}$	$\frac{1}{2}$	0	$-\frac{1}{2}$
16	$\frac{1}{2}$	0	$-\frac{1}{2}$	$-\frac{1}{2}$	0	$-\frac{1}{2}$
17	0	$-\frac{1}{2}$	$\frac{1}{2}$	0	$\frac{1}{2}$	$\frac{1}{2}$
18	0	$-\frac{1}{2}$	$\frac{1}{2}$	0	$-\frac{1}{2}$	$\frac{1}{2}$
19	0	$-\frac{1}{2}$	$\frac{1}{2}$	0	$\frac{1}{2}$	$-\frac{1}{2}$
20	0	$-\frac{1}{2}$	$\frac{1}{2}$	0	$-\frac{1}{2}$	$-\frac{1}{2}$
21	$-\frac{1}{2}$	$\frac{1}{2}$	0	$\frac{1}{2}$	$\frac{1}{2}$	0
22	$-\frac{1}{2}$	$\frac{1}{2}$	0	$-\frac{1}{2}$	$\frac{1}{2}$	0
23	$-\frac{1}{2}$	$\frac{1}{2}$	0	$\frac{1}{2}$	$-\frac{1}{2}$	0
24	$-\frac{1}{2}$	$\frac{1}{2}$	0	$-\frac{1}{2}$	$-\frac{1}{2}$	0
25	0	0	0	$\frac{1}{2}$	$\frac{1}{2}$	$-\frac{1}{2}$
26	0	0	0	$\frac{1}{2}$	$-\frac{1}{2}$	$\frac{1}{2}$
27	0	0	0	$-\frac{1}{2}$	$\frac{1}{2}$	$\frac{1}{2}$
28	0	0	0	$\frac{1}{2}$	$\frac{1}{2}$	$\frac{1}{2}$

If a_{ij} is the direction-cosine of the i specimen axis relative to the j cube axis,

$$a_{ij}=\begin{bmatrix} \cos\phi\cos\theta & \cos\phi\sin\theta & \sin\phi \\ -\sin\theta & \cos\theta & 0 \\ -\sin\phi\cos\theta & -\sin\phi\sin\theta & \cos\phi \end{bmatrix}.$$

The strain tensor relative to the cubic axes is given by

$$d\epsilon_{ij}=\sum_{kl} a_{ki}a_{lj}\, d\epsilon'_{kl},$$

whence

$$d\epsilon_{ij}=\frac{d\epsilon}{2}\cdot\begin{bmatrix}3\cos^2\phi\cos^2\theta-1 & 3\cos^2\phi\sin\theta\cos\theta & 3\sin\phi\cos\phi\cos\theta\\ 3\cos^2\phi\cos\theta\sin\theta & 3\cos^2\phi\sin^2\theta-1 & 3\sin\phi\cos\phi\sin\theta\\ 3\sin\phi\cos\phi\cos\theta & 3\sin\phi\cos\phi\sin\theta & 3\sin^2\phi-1\end{bmatrix}.$$

The work done by a stress σ_{ij} in a strain $d\epsilon_{ij}$ is

$$dW=\sum_{ij}\sigma_{ij}\, d\epsilon_{ij}.$$

Since $$d\epsilon_{xx}+d\epsilon_{yy}+d\epsilon_{zz}=0,$$

$$dW=-B\, d\epsilon_{xx}+A\, d\epsilon_{yy}+2F\, d\epsilon_{yz}+2G\, d\epsilon_{zx}+2H\, d\epsilon_{xy}.$$

From the maximum work principle, the yield stress state required to operate a given strain maximises the work. We have seen that the tabulated stresses form a complete set for this purpose. Hence the work done in a given orientation (specified by θ and ϕ) is the maximal value of the works done by the fifty-six stress states. It follows from the existence theorem that this state (not necessarily unique) operates sufficient shears to enable the strain to be enforced.

In fig. 5 the relevant stress states are shown: the bar above the numbers indicates that the stress state is the negative of that in the table. The boundaries between states are found by equating the works required by the states on either side. The work required to impose the strain is therefore known for all θ and ϕ. In region 6 for example, the work required is

$$dW=3\cos^2\phi\sin\theta\cos\theta\, d\epsilon.$$

In this region, the strains and shears are related by

$$\begin{aligned}\sqrt{6}\, d\epsilon_{11}&=-a_2-b_2-c_2-d_2,\\ \sqrt{6}\, d\epsilon_{22}&=a_1+b_1+c_1+d_1,\\ 2\sqrt{6}\, d\epsilon_{23}&=a_2-b_2+c_2-d_2,\\ 2\sqrt{6}\, d\epsilon_{31}&=-a_1+b_1+c_1-d_1,\\ 2\sqrt{6}\, d\epsilon_{12}&=a_1-a_2+b_1-b_2-c_1+c_2-d_1+d_2.\end{aligned}$$

Treating a_1, a_2 and b_1 as parameters,

$$\begin{aligned}2c_1&=\sqrt{6}\, d\epsilon_{22}+2\sqrt{6}\, d\epsilon_{31}-2b_1,\\ 2d_1&=\sqrt{6}\, d\epsilon_{22}-2\sqrt{6}\, d\epsilon_{31}-2a_1,\\ 2b_2&=-\sqrt{6}\, d\epsilon_{11}-\sqrt{6}\, d\epsilon_{22}-2\sqrt{6}\, d\epsilon_{12}+2a_1+2b_1-2a_2,\\ 2c_2&=-\sqrt{6}\, d\epsilon_{11}+2\sqrt{6}\, d\epsilon_{23}-2a_2,\\ 2d_2&=\sqrt{6}\, d\epsilon_{22}-2\sqrt{6}\, d\epsilon_{23}+2\sqrt{6}\, d\epsilon_{12}-2a_1-2b_1+2a_2.\end{aligned}$$

The stress system operates the shears in the senses $+a_1$, $+b_1$, $-c_1$, $-d_1$, $-a_2$, $-b_2$, $+c_2$, $+d_2$ and hence a_1, a_2 and b_2 must be chosen to satisfy these conditions.

Fig. 5

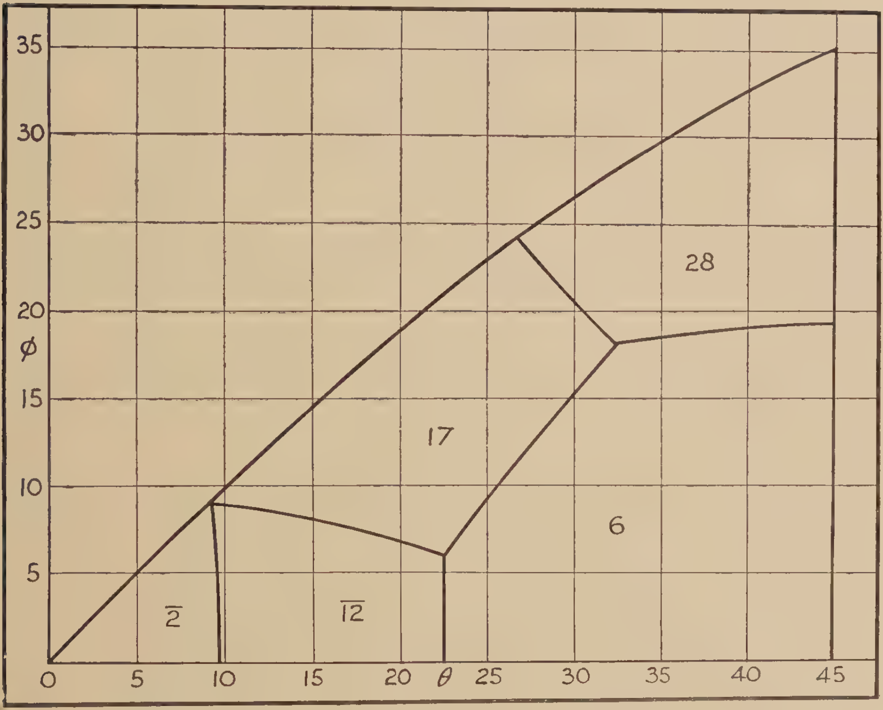

Consider for example the state $\theta=\pi/4$, $\phi=0$.

$$d\epsilon_{ij}=\begin{bmatrix} \frac{1}{4} & \frac{3}{4} & 0 \\ \frac{3}{4} & \frac{1}{4} & 0 \\ 0 & 0 & -\frac{1}{2} \end{bmatrix} . d\epsilon,$$

and

$$c_1=d\epsilon\sqrt{6}/8-b_1,$$
$$d_1=d\epsilon\sqrt{6}/8-a_1,$$
$$b_2=-d\epsilon\sqrt{6}+a_1+b_1-a_2,$$
$$c_2=-d\epsilon\sqrt{6}/8-a_2,$$
$$d_2=d\epsilon 7\sqrt{6}/8-a_1-b_1+a_2.$$

Clearly $a_1\geqslant d\epsilon\sqrt{6}/8$, $b_1\geqslant d\epsilon\sqrt{6}/8$, $a_2\leqslant d\epsilon\sqrt{6}/8$, with $a_1+b_1-a_2\leqslant d\epsilon 7\sqrt{6}/8$. Provided a_1, a_2 and b_1 satisfy these inequalities, this system of eight shears will impose the strain and is operable by a yield stress state. It appears therefore that this particular strain may be imposed by only one stress state, but that a triply infinite set of shears is available. It is generally true that a single stress state and a multiplicity of sets of shears can enforce an *arbitrary* strain (although *certain* strains may be imposed by several stress states).

ACKNOWLEDGMENTS

This paper has arisen from work on crystal plasticity in collaboration with R. Hill, to whom the author is indebted for his invitation to publish collaborated work and for his suggestions during the preparation of the paper. The author wishes to thank the Director of the Mechanical Engineering Research Organisation, D.S.I.R. of which he is a member, for his permission to publish the paper.

REFERENCES

BISHOP, J. F. W., and HILL, R., 1951 a, *Phil Mag.*, **42,** 414 ; 1951 b, *Ibid.*, **42,** 1298.
RÖHM, F., and KOCHENDÖRFER, A., 1951, *Z. Metallkde.*, **41,** 265.
TAYLOR, G. I., 1938 a, *J. Inst. Met.*, **62,** (i) 307 ; 1938 b, *S. Timoshenko Anniv. Vol.* (New York : Macmillan), p. 218.
TAYLOR, G. I., and ELAM, C. F., 1925, *Proc. Roy. Soc.* A, **108,** 28.

VII. *Second Neighbour Interaction in Regular Binary Assemblies*

By G. M. Bell
The Clarendon Laboratory, Oxford*

[Received September 15, 1952]

Abstract

A study is made of regular assemblies of species A and B, whose configurational energy is given by the expression $w_1N_{AB}(1)+w_2N_{AB}(2)$, $N_{AB}(1)$ and $N_{AB}(2)$ being the numbers of first and second neighbour A–B pairs respectively. Positive and negative values of w_1 and w_2 are treated and results apply to phase-separation, order–disorder and Ising ferromagnets and antiferromagnets at zero field. Generalized quasi-chemical approximations giving the correct ratio of total first and second neighbour pair numbers are used and the consistency is checked by the critical points in the limiting cases $w_1=0$ and $w_2=0$ and by the value of w_2/w_1 at which the critical temperature becomes zero. The simple cubic lattice is treated in detail and a critical temperature curve derived for the plane square lattice. Fluctuation effects are diminished for reinforcing first and second interactions and increased for opposing ones. The quadruplet approximation which has been used by certain authors is critically examined and it is pointed out that it would be consistent for the disordered state on the face-centred cubic lattice.

§1. Introduction

This paper will be concerned with the statistics of a regular binary assembly in which the interactions between first and second neighbours are appreciable. A method of constructing a generalized quasi-chemical approximation into which second neighbour interaction energies are incorporated will be described and certain criteria of consistency by which such an approximation can be tested will be developed. The assembly on a simple cubic lattice will be dealt with in detail.

In real condensed phases further neighbour interactions are not negligible, though they have often been assumed to be so in statistical studies. Even with an inverse sixth power law the ratio of the energy of a second neighbour pair to that of a first neighbour pair is 1 : 8 for a simple cubic lattice and 27 : 64 for a body-centred cubic lattice. It is considered that agreement between the computed and observed effects of superlattice formation could be considerably improved by taking account of the second as well as of the first interaction (Chang 1937, Fournet 1951). In materials where there are forces of the exchange type the further neighbour energies may be comparable with, or even larger than, the first (Seitz 1940, Bozorth 1947, 1952). A statistical method which gives proper weight to the effect of second neighbour interactions is therefore of considerable interest.

---

* Communicated by the Author.

Consider a lattice of N sites, each occupied by either a system of species A or a system of species B. Let the number of A be N_A and the number of B be N_B so that $N_\mathrm{A}+N_\mathrm{B}=N$. Let each system have z_1 first neighbours and z_2 second neighbours so that there is a total of $\frac{1}{2}z_1N$ first neighbour pairs and $\frac{1}{2}z_2N$ second neighbour pairs. Let the number of 'unlike' first neighbour pairs be $N_\mathrm{AB}(1)$ and the number of 'unlike' second neighbour pairs be $N_\mathrm{AB}(2)$. The configurational energy, E_c is linearly dependent on the various pair numbers and by a suitable choice of zero can be put into the form,

$$E_c=w_1N_\mathrm{AB}(1)+w_2N_\mathrm{AB}(2), \quad . \quad . \quad . \quad . \quad . \quad (1)$$

where $2(z_1w_1+z_2w_2)$ is the energy increment on exchanging an A and a B between pure A and B phases.

In the generalized quasi-chemical method (Guggenheim 1944, Yang 1945, Guggenheim and McGlashan 1951 a) an approximate configurational partition function is constructed by using a basic group of n sites, in which there are m_1 first neighbour pairs. To get the right total number of first neighbour pairs an assembly of $\frac{1}{2}Nz_1/m_1$ of these groups is used and, assuming their independence, a combinatorial factor is formed in terms of the probabilities, ψ_i, of the various configurations, i, on the sites of group. This is then multiplied by a normalizing factor $g_0(N_\mathrm{A}, N_\mathrm{B})$, given by

$$\ln g_0(N_\mathrm{A}, N_\mathrm{B})=(\tfrac{1}{2}nz_1/m_1-1)(N_\mathrm{A}\ln N_\mathrm{A}+N_\mathrm{B}\ln N_\mathrm{B}-N\ln N). \quad . \quad (2)$$

This is determined from the partition function when the interactions are zero and will thus be unaffected by the introduction of second neighbour energies.

Now suppose that the group contains m_2 second neighbour pairs ; the number of such pairs in $\frac{1}{2}Nz_1/m_1$ groups will be $\frac{1}{2}Nz_1m_2/m_1$ and for this expression to be equal to $\frac{1}{2}z_2N$ it is necessary that

$$m_2/m_1=z_2/z_1. \quad . \quad . \quad . \quad . \quad . \quad . \quad . \quad . \quad . \quad (3)$$

Consistent groups for which the relation (3) is satisfied will be used in this paper. Several attempts have been made (Chang 1937, Hill 1950, Guggenheim and McGlashan 1951 b) to extend the quasi-chemical approximation by using groups in which $m_2/m_1\neq z_2/z_1$ and these will be discussed below. As 'a posteriori' criteria of the consistency of the approximation the critical temperature values in the limiting cases $w_1=0$ and $w_2=0$ and the value of w_1/w_2 at which the critical temperature tends to zero will be used.

If $w_2=0$, $w_1>0$ and N_A and N_B are fixed the model represents a disordered binary mixture. If the lattice divides into equivalent sub-lattices a and b, such that all nearest neighbours of a given site are in the other sub-lattice, then, it is well known that this is equivalent to another binary mixture, with $N_\mathrm{A}=N_\mathrm{B}$ and a negative interaction $-w_1$. Let the ratio $N_\mathrm{A}/(N_\mathrm{A}+N_\mathrm{B})$ be denoted by x and the degree of order with respect to sublattices a and b by s, $\frac{1}{2}(1-s)$ being the proportion of systems in 'wrong' positions. Then the compositions of the conjugate phases of the disordered mixture are related to the equilibrium degree of order in the other model by

$$x=\tfrac{1}{2}(1+s), \qquad 1-x=\tfrac{1}{2}(1-s). \quad . \quad . \quad . \quad . \quad (4)$$

This can be shown by replacing each A on a b site by B and each B by A, leaving the configuration on sub-lattice a unchanged. If the lattice is such that all second neighbours of a given site are in the same sub-lattice as this site then this interchange will not affect the total second neighbour energy, $w_2 N_\mathrm{AB}(2)$. A model with interactions w_1, w_2 is thus equivalent to one with interactions $-w_1$, w_2 and eqn. (4) still applies (Bell 1952). Define a parameter ρ by $\rho=w_2/w_1$ where $w_1>0$ and $\rho=-w_2/w_1$ where $w_1<0$. The first and second interactions will now reinforce each other in both models when $\rho>0$ and oppose each other when $\rho<0$. The mathematical theory can be developed in terms of either model; the positive first interaction (disordered) case will be chosen here.

When N_A, N_B are not fixed the disordered model becomes a zero-field Ising 'ferromagnet', which is quantum-mechanically incorrect but permits statistical calculation over the whole temperature range. (For a full discussion, see Van Vleck 1945.) The relative magnetization is connected with the conjugate phase compositions by relations identical with (4). The ordered model is related to an 'antiferromagnetic' model of similar type. (For the 'first neighbour only' case with applied field, see Brooks and Domb 1951, Ziman 1951.)

§2. The Simple Cubic Lattice

In this lattice $z_1=6$, $z_2=12$, so that the ratio m_2/m_1 for the basic group must be equal to 2. The group employed consists of a central site with its six nearest neighbours so that $n=7$, $m_1=6$, $m_2=12$. It will be represented schematically by

$$\begin{array}{ccccc} & & \mathrm{X} & & \\ & & & + & \\ \mathrm{X} & & \mathrm{O} & & \mathrm{X} \\ & + & & & \\ & & \mathrm{X} & & \end{array}$$

where 'O' is the central site, the 'X' are its four nearest neighbours in one plane and '+' are the other two nearest neighbours. There are twenty types of configuration on these sites and the first ten of these, with their ' weights ' ω_i are given below :

(1)	(2)	(3)	(4)	(5)
A A A A A A A $\omega_1=1$	B B B A B B B $\omega_2=1$	A A B A A A A $\omega_3=6$	B B A A B B B $\omega_4=6$	A A B A B A A $\omega_5=3$
(6)	**(7)**	**(8)**	**(9)**	**(10)**
B B A A A A A $\omega_6=12$	B B A A A B B $\omega_7=3$	A A B A B B B $\omega_8=12$	A B B A B A A $\omega_9=12$	B B B A A A A $\omega_{10}=8$

Configuration $i+10$ is obtained from i by replacing each A by B and each B by A.

In order that the probability of occurrence of an A on both the central site and the outer sites should be x, and that the sum of the configuration probabilities, $\Sigma_i\omega_i\psi_i$, should be equal to unity, the following three relations exist.

$$x=\psi_1+\psi_2+6\psi_3+6\psi_4+3\psi_5+12\psi_6+3\psi_7+12\psi_8+12\psi_9+8\psi_{10}, \quad . \quad . \quad (5)$$

$$1-x=\psi_{11}+\psi_{12}+6\psi_{13}+6\psi_{14}+3\psi_{15}+12\psi_{16}+3\psi_{17}+12\psi_{18}+12\psi_{19}+8\psi_{20}, \quad (6)$$

$$\psi_2+\psi_3+5\psi_4+\psi_5+4\psi_6+2\psi_7+8\psi_8+6\psi_9+4\psi_{10}$$
$$=\psi_{12}+\psi_{13}+5\psi_{14}+\psi_{15}+4\psi_{16}+2\psi_{17}+8\psi_{18}+6\psi_{19}+4\psi_{20}. \quad . \quad . \quad . \quad (7)$$

The pair numbers $N_{\mathrm{AB}}(1)$ and $N_{\mathrm{AB}}(2)$ are given in terms of ψ_i by

$$N_{\mathrm{AB}}(1)=3N(\psi_2+\psi_{12}+\psi_3+\psi_{13}+5\psi_4+5\psi_{14}+\psi_5+\psi_{15}+4\psi_6+4\psi_{16}$$
$$+2\psi_7+2\psi_{17}+8\psi_8+8\psi_{18}+6\psi_9+6\psi_{19}+4\psi_{10}+4\psi_{20}), \quad . \quad (8)$$

$$N_{\mathrm{AB}}(2)=6N(2\psi_3+2\psi_{13}+2\psi_4+2\psi_{14}+2\psi_5+2\psi_{15}+6\psi_6+6\psi_{16}+2\psi_7+2\psi_{17}$$
$$+6\psi_8+6\psi_{18}+8\psi_9+8\psi_{19}+4\psi_{10}+4\psi_{20}). \quad . \quad . \quad . \quad . \quad . \quad (9)$$

The logarithm of a general term of the configurational partition function is

$$\frac{5N}{2}\{x\ln x+(1-x)\ln(1-x)\}-\frac{N}{2}\Sigma_i\omega_i\psi_i\ln\psi_i-\frac{1}{kT}\{w_1N_{\mathrm{AB}}(1)+w_2N_{\mathrm{AB}}(2)\}. \quad . \quad . \quad . \quad (10)$$

The seventeen probabilities $\psi_3, \ldots, \psi_{10}, \psi_{12}, \ldots, \psi_{20}$ are chosen as independent variables and the remaining three ψ_1, ψ_{11} and ψ_2 are given by (5), (6) and (7) respectively. Introduce the symbols η, ξ, α, β, ϕ defined by $\exp(-w_1/kT)=\eta$ $(w_1>0)$, $\exp(w_1/kT)=\eta$ $(w_1<0)$; $\exp(-w_2/kT)=\xi$;

$\psi_1=\alpha^6$; $\psi_2=\beta^6$; $\alpha\eta/\beta=\phi$. (α and β are real and positive.) Now differentiate (10) with respect to the independent variables

$$\left.\begin{array}{ll} & \psi_{12}=\eta^{12}\alpha^6\beta^{-6}\psi_{11} \\ \psi_3=\xi^4\alpha^5\beta & \psi_{13}=\eta^2\xi^4\alpha\beta^{-1}\psi_{11} \\ \psi_4=\xi^4\alpha\beta^5 & \psi_{14}=\eta^{10}\xi^4\alpha^5\beta^{-5}\psi_{11} \\ \psi_5=\xi^8\alpha^4\beta^2 & \psi_{15}=\eta^4\xi^8\alpha^2\beta^{-2}\psi_{11} \\ \psi_6=\xi^6\alpha^4\beta^2 & \psi_{16}=\eta^4\xi^6\alpha^2\beta^{-2}\psi_{11} \\ \psi_7=\xi^8\alpha^2\beta^4 & \psi_{17}=\eta^8\xi^8\alpha^4\beta^{-4}\psi_{11} \\ \psi_8=\xi^6\alpha^2\beta^4 & \psi_{18}=\eta^8\xi^6\alpha^4\beta\;{}^4\psi_{11} \\ \psi_9=\xi^8\alpha^3\beta^3 & \psi_{19}=\eta^6\xi^8\alpha^3\beta^{-3}\psi_{11} \\ \psi_{10}=\xi^6\alpha^3\beta^3 & \psi_{20}=\eta^6\xi^6\alpha^3\beta^{-3}\psi_{11} \end{array}\right\} \quad . \quad . \quad . \quad . \quad (11)$$

To obtain the conjugate phases in the disordered case a differentiation with respect to x is necessary,

$$\psi_{11}=\alpha^6(1-x)^5/x^5. \quad . \quad . \quad . \quad . \quad . \quad . \quad . \quad (12)$$

This also gives the equilibrium value of s in the ordered case and the relative magnetization in the Ising Model. Substituting (11) in (5), (6) and (7) and eliminating β and ψ_{11},

$$x/(1-x)=f_2f_3/(f_1f_4), \quad . \quad . \quad . \quad . \quad . \quad (13)$$

where

$$f_1(\phi)=\eta^6+5\eta^5\xi^4\phi+(2\eta^4\xi^8+8\eta^4\xi^6)\phi^2+(6\eta^3\xi^8+4\eta^3\xi^6)\phi^3$$
$$+(\eta^2\xi^8+4\eta^2\xi^6)\phi^4+\eta\xi^4\phi^5, \quad . \quad . \quad . \quad . \quad . \quad . \quad . \quad . \quad (14)$$

$$f_2(\phi)=\phi^6f_1(\phi^{-1}), \quad . \quad . \quad . \quad . \quad . \quad . \quad . \quad . \quad . \quad . \quad . \quad . \quad . \quad . \quad . \quad (15)$$

$$f_3(\phi)=\eta^6+6\eta^5\xi^4\phi+(3\eta^4\xi^8+12\eta^4\xi^6)\phi^2+(12\eta^3\xi^8+8\eta^3\xi^6)\phi^3$$
$$+(3\eta^2\xi^8+12\eta^2\xi^6)\phi^4+6\eta\xi^4\phi^5+\phi^6, \quad . \quad . \quad . \quad . \quad . \quad . \quad (16)$$

$$f_4(\phi)=\phi^6f_3(\phi^{-1}). \quad . \quad . \quad . \quad . \quad . \quad . \quad . \quad . \quad . \quad . \quad . \quad . \quad . \quad . \quad . \quad (17)$$

Using (12), $x/(1-x)$ can be eliminated to give

$$\phi^6f_1{}^4f_4{}^5-f_3{}^5f_2{}^4=0. \quad . \quad . \quad . \quad . \quad . \quad . \quad . \quad (18)$$

(18) is an equation in the single unknown ϕ and gives ϕ for any pair of values of η and ξ ; the conjugate phases are then given by (13).

Choosing the value 0·5 for ρ (18) was solved numerically for three values of η, 0·77, 0·79 and 0·81, and the corresponding values of x were then calculated from (13).

The critical temperature for $\rho=0{\cdot}5$ is given by

$$\eta_c=\exp\,(-w_1/kT_c)=0{\cdot}8344,$$

which was calculated from the equation given in the next section. In table 1 the ratios T/T_c are compared with those obtained from the present quasi-chemical approximation with $\rho=0$ (when it becomes identical with the quasi-chemical ‘ pair ’ approximation) and the zeroth-order approximation.

The zeroth-order method for the disordered case becomes accurate when the interaction energies are independent of the distance between the systems and it is thus to be expected that the effect of fluctuations will be diminished by a reinforcing second interaction. This is confirmed by table 1 which shows that the $2x-1$, T/T_c curve for $\rho=0{\cdot}5$ lies roughly half-way between that for $\rho=0$ and the zeroth-order curve.

Table 1

$2x-1$ $(=s)$	T/T_c (quasi-chemical)		T/T_c (zeroth-order)
	$\rho=0$	$\rho=0{\cdot}5$	
0·866	0·731	0·693	0·657
0·791	0·800	0·768	0·736
0·654	0·880	0·859	0·836

§3. THE CRITICAL TEMPERATURE

At the critical temperature the conjugate phases coalesce at $x=\frac{1}{2}$, so that, from (13) $\phi=1$ and (18) becomes an identity. The critical temperature can be obtained by putting $\phi=1+\delta$ in (18) and equating the coefficient of δ to zero. The resulting polynomial equation in η and ξ is

$$\begin{aligned}\xi^{16}(6\eta^4&+48\eta^5+216\eta^6+120\eta^7+24\eta^8)\\ &+\xi^{14}(48\eta^4+224\eta^5+288\eta^6+560\eta^7+192\eta^8)\\ &+\xi^{12}(-24\eta^4+44\eta^5+96\eta^6+272\eta^7+552\eta^8+108\eta^9)\\ &+\xi^{10}(-80\eta^4-336\eta^5-192\eta^7+112\eta^8+432\eta^9)\\ &+\xi^{8}(-2\eta^2-72\eta^3-32\eta^4-324\eta^6-20\eta^8+166\eta^{10})\\ &+\xi^{6}(-32\eta^2-48\eta^3-128\eta^4-80\eta^8+64\eta^{10})\\ &+\xi^{4}(-4\eta-100\eta^5-88\eta^7+56\eta^{11})+6\eta^{12}-24\eta^6=0. \quad . \quad (19)\end{aligned}$$

Where $\xi=1$ this reduces to

$$2\eta(3\eta-2)(1+\eta)^{10}=0. \quad . \quad . \quad . \quad . \quad . \quad . \quad . \quad . \quad (20)$$

The only positive solution of (20) is $\eta=2/3$ which is, as would be expected, the pair approximation result for $z=6$.

When the first interaction is zero the correlation between sub-lattices *a* and *b* is removed and the simple cubic lattice decomposes into a pair of face-centred cubic lattices. If the method discussed here is to be consistent the critical temperature must, as η tends to one, approach a value close to the pair approximation critical value for $z=12$. Putting $\eta=1$ (19) becomes

$$(46\xi^8+64\xi^6-28\xi^4-18)(9\xi^8+16\xi^6+6\xi^4+1)=0. \quad . \quad . \quad . \quad (21)$$

The first bracket on the left-hand side gives the only positive root and on equating it to zero the critical equation for the face-centred lattice using a group with $n=6$, $m=12$ is obtained. This yields a value 0·8300 for ξ_c which is quite near the pair approximation's 10/12 or 0·8333.

For purposes of comparison the critical equation for the plane square lattice in which $z_1=z_2=4$ has been deduced. A group of a central site with its four nearest neighbours, giving $m_1=m_2=4$ and twelve basic configurations, was used and the following critical equation obtained:

$$\xi^8(2\eta^3)+\xi^6(10\eta^4+8\eta^3+2\eta^2)+\xi^4(4\eta^2+4\eta^3+20\eta^4+20\eta^5)$$
$$+\xi^2(-1-4\eta-9\eta^2-5\eta^4+4\eta^5+11\eta^6)-4\eta^3+2\eta^4=0. \quad . \quad . \quad (22)$$

Where $\xi=1$ this reduces to

$$(2\eta-1)(1+\eta)^6=0, \quad . \quad . \quad . \quad . \quad . \quad . \quad . \quad . \quad (23)$$

whose only positive root is $\frac{1}{2}$, confirming that for $w_2=0$ the ordinary quasi-chemical pair approximation is regained.

The two equivalent sub-lattices are also of the plane square type so that the accurate critical values of η where $\xi=1$ and ξ where $\eta=1$ are both 0·414 (Kramers and Wannier 1941). Where $\eta=1$ (22) becomes

$$2(\xi^4+4\xi^2-1)(\xi^4+6\xi^2+1)=0. \quad . \quad . \quad . \quad . \quad . \quad (24)$$

The only positive root is given by the first bracket on the left-hand side and on equating it to zero the critical equation for the 'quadruplet approximation' for $z=4$ is obtained. Where $w_1=0$ the critical value of ξ is thus 0·486 while that of η with $w_2=0$ is 0·500 so that the effects of first and second interactions appear reasonably well-balanced in this approximation.

§ 4. Critical Temperature and Energy Values

Pairs of values of η and ξ satisfying (19) and (22) were obtained by giving η a definite value and finding the positive root of the resulting polynomial equation in ξ. Since there was never more than one change of sign in the coefficients of this equation the positive root obtained was unique by Descartes' Rule of Signs. Values of $\ln 2/\ln \eta_c^{-1}$ are plotted against ρ $(=\ln \xi_c/\ln \eta_c)$ in fig. 1. Where $w_1>0$ this gives a curve of $(kT_c \ln 2)/w_1$ against w_2/w_1.

If w_1 is kept constant the critical temperature, T_c, in both the simple cubic and the plane square cases decreases smoothly to zero as w_2 decreases. The curves thus resemble that derived by Domb and Potts (1952) for the plane square lattice, using a series approximation, and show no sign of the 'kinking' observable in that derived by Chang for the simple cubic lattice (1937). Chang used a quasi-chemical approximation different from that employed here.

The curve for the simple cubic lattice meets the ρ axis at $-1/4$; as T_c approaches zero the critical values of ψ_5 and ψ_{15} approach those of ψ_1 and ψ_{11}. This corresponds to the fact that where $\rho<-1/4$ an ordered state with A and B systems in alternate layers is more stable at the absolute zero than pure A or B phases.

Where $w_1<0$, $\rho=-w_2/w_1$ and the ordinate in fig. 1 represents $(kT_c \ln 2)/-w_1$, T_c being now the critical temperature for long-range order with respect to the face-centred cubic sub-lattices a and b. The ordered state at $T=0$ when $\rho<-\frac{1}{4}$ now consists of rows of A and B arranged so that each row of A is surrounded by four rows of B and vice versa; this was shown by Luttinger (1951) to be the state of least energy where $-w_2>-\frac{1}{4}w_1>0$. The fact that the T_c curve cuts the axis at the correct value of ρ represents a further check on the consistency of the approximation used here.

The T_c curve for the plane square lattice cuts the axis at $-\frac{1}{2}$. Where $\rho<-\frac{1}{2}$ an arrangement of alternate rows of A and B is the most stable state at absolute zero for both positive and negative values of w_1.

Fig. 1

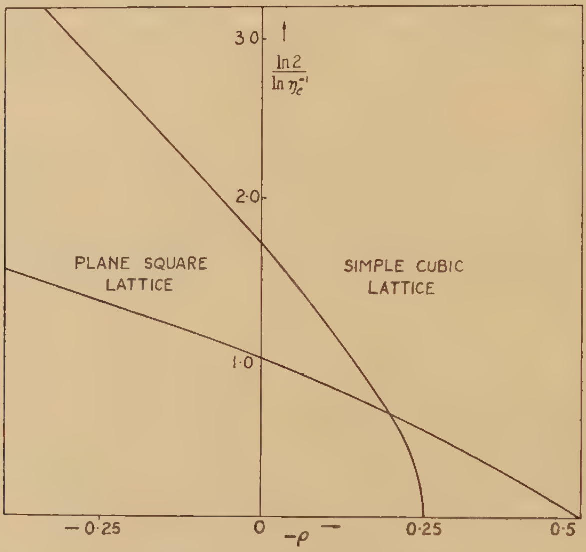

Critical temperature curves.

For $\rho>0$ the significance of the critical temperature results is best seen by plotting $T_c{}^0/T_c$, $T_c{}^0$ being the zeroth order critical temperature, against $z_2\rho/(z_1+z_2\rho)$. The quantity $z_2\rho/(z_1+z_2\rho)$ has the value 0 where $w_2=0$, 1 where $w_1=0$ and $\frac{1}{2}$ where $z_2w_2=z_1w_1$.

$kT_c=w_1/\ln \eta_c{}^{-1}$ and $T_c{}^0=\frac{1}{2}w_1(z_1+z_2\rho)/k$ so that for the simple cubic lattice

$$T_c{}^0/T_c=3(\ln \eta_c{}^{-1}+2\ln \xi_c{}^{-1}). \qquad (25)$$

The critical values of $N_{\mathrm{AB}}(1)$ and $N_{\mathrm{AB}}(2)$ may be obtained from (8), (9) and (11). Defining W as the critical value of the configurational energy

$$W/RT_c=\{N_{\mathrm{AB}}(1)\ln \eta_c{}^{-1}+N_{\mathrm{AB}}(2)\ln \xi_c{}^{-1}\}/N. \qquad (26)$$

The zeroth-order critical energy W^0 is given by

$$W^0=N(z_1w_1+z_2w_2)/4. \qquad (27)$$

Since

$$W^0/RT_c{}^0=1/2, \qquad (28)$$

$$(W^0/RT_c{}^0)/(W/RT_c)=RT_c/2W. \qquad (29)$$

Curves of T_c^0/T_c and $RT_c/2W$ are plotted against $2\rho/(1+2\rho)$ in fig. 2 and both show that the effect of fluctuations is diminished when there are reinforcing first and second interactions. It appears from these results and from those given in § 2 that the differences between values calculated for appreciable ρ and those calculated for $\rho=0$ are a considerable fraction of the differences between the latter and the zeroth order values, e.g. for $\rho=1/8$, corresponding to an inverse sixth power law, $(W^0/RT_c^0)/(W/RT_c)$ has diminished from 1·027, its value at $\rho=0$, to 1·016.

Fig. 2

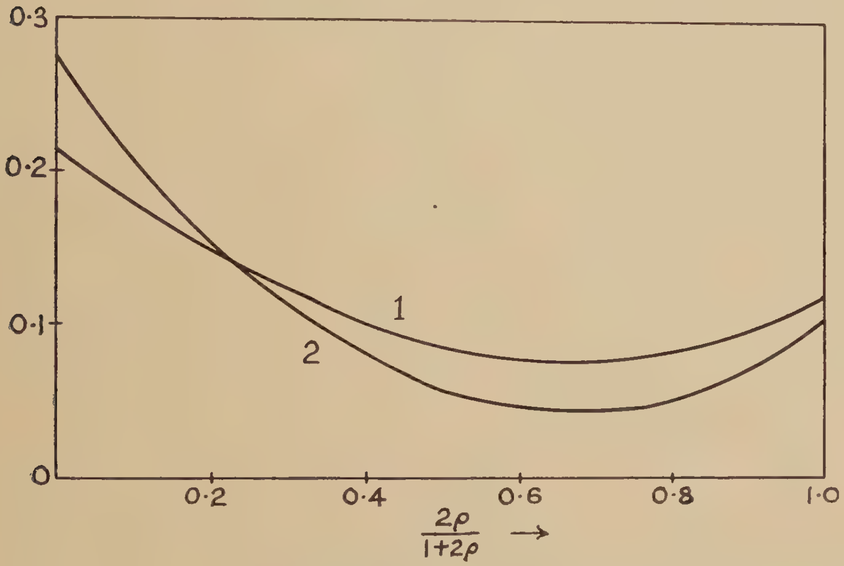

Critical temperature and energy curves.

$$(1)\ \frac{T_c^0}{T_c}-1. \qquad (2)\ 10\left\{\frac{W^0}{RT_c^0}\bigg/\frac{W}{RT_c}-1\right\}.$$

W^0 is the total configurational energy increase from $T=0$ to $T=\infty$ so that W/W^0 is the fraction of this increase which has taken place at $T=T_c$. W/W^0 is plotted in fig. 3 against $2\rho/(1+2\rho)$ over the whole range from -1 to 1 in which transitions of the type defined by (19) are possible. The values for $\rho>0$ again illustrate that the division of the configurational energy between reinforcing first and second neighbour interactions diminishes fluctuation effects. The opposite occurs where $\rho<0$ and W/W^0 decreases rapidly to zero at $2\rho/(1+2\rho)=-1$ or $\rho=-1/4$. Van Santen (1951) considered that low values of W/W^0 for appreciable further neighbour interaction are necessary to account for the observed magnitudes of latent heat of melting for ionic solids.

Chang (1941) showed, by means of Kirkwood's method, that an increase in critical short-range order must occur for negative values of ρ. Defining the short-range order

$$\sigma=\frac{N_{\mathrm{AA}}(1)+N_{\mathrm{BB}}(1)-N_{\mathrm{AB}}(1)}{\frac{1}{2}z_1N}, \quad . \quad . \quad . \quad . \quad . \quad (30)$$

it is found from (19) that, at the critical point for the simple cubic lattice, where

$$\begin{array}{ll} \rho=0 \quad , & \sigma=0{\cdot}2000, \\ \rho=-0{\cdot}0745, & \sigma=0{\cdot}2330, \\ \rho=-0{\cdot}1421, & \sigma=0{\cdot}2811. \end{array}$$

Fig. 3

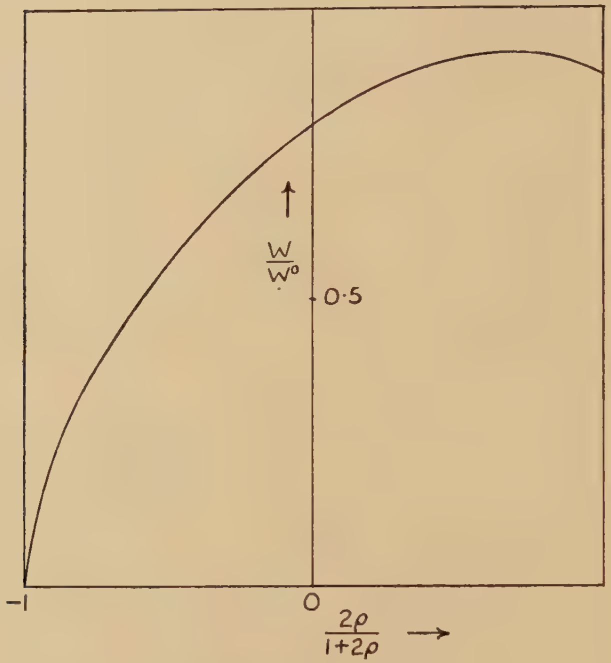

Critical energy ratios.

§5. Other Quasi-Chemical Methods

Chang (1937) applied the Bethe method to the simple cubic lattice for the $\rho<0$ case using a basic group consisting of a central site, an inner layer of six first neighbours and an outer layer of their eighteen first neighbours. Hence, $n=25$, $m_1=36$ and $m_2=72$. A complete consideration of this group would give the next approximation to that employed above but would be extremely laborious. However, Chang only considered 24 of the 72 second neighbour links giving an effective z_2 of 4 instead of 12.

The ‘ quadruplet ’ approximation with $n=m_1=4$, $m_2=2$ has been applied to the simple and body-centred cubic lattices for the positive values of ρ corresponding to an inverse sixth power law by Guggenheim and McGlashan (1951 b).

These authors recognize that, since the effective value of z_2 is always $\frac{1}{2}z_1$, the approximation is inconsistent when $z_2\neq\frac{1}{2}z_1$. The critical equation is, in the notation used here,

$$\eta^4+2\eta^2(4\xi/z_1+\xi^2)-3+8/z_1=0. \qquad . \quad . \quad . \quad . \quad . \quad (31)$$

Where $\xi=1$ the quadruplet approximation for first neighbours is regained but the results of the inconsistency appear when η is put equal to 1 and (31) becomes

$$\xi^2+4\xi/z_1-1+4/z_1=0. \quad . \quad . \quad . \quad . \quad . \quad . \quad . \qquad (32)$$

For $z_1=4$ the effective value of z_2 is 2 and there is no positive solution of (32). For $z_1=6$ the effective z_2 is 3 and (32) gives the solution $\xi=1/3$. For $z_1=8$ the effective z_2 is 4 and (32) gives $\xi=1/2$. Now the body-centred cubic lattice can be divided into two equivalent simple cubic sub-lattices, such that any site and its second neighbours lie in the same sub-lattice. The limiting value of ξ as w_1 tends to zero ought, therefore, to be near 2/3. For all values of z_1 the critical temperature given by (31) will go to zero at $\rho=-1$, though the correct values are $\rho=-1/4$ and $\rho=-2/3$ for the simple and body-centred cases respectively (Luttinger 1951). It is thus obvious that the quadruplet method, with its low effective z_2, underestimates the second neighbour effects and, in fact, Guggenheim and McGlashan come to the conclusion that these are of trivial importance in relation to measurable quantities. However, differences between results calculated on the quadruplet approximation with and without the second neighbour perturbation do not always seem to be negligible in comparison with the differences between the latter and the zeroth-order results (Guggenheim and McGlashan 1951 b, table 3).

Hill (1950) uses the quadruplet approximation for the plane square lattice and to correct for the inconsistency he regards the factor ξ as

$$\exp\,(-2z_2w_2/z_1kT),$$

instead of $\exp\,(-w_2/kT)$. However, in the limit $w_1=0$ there is again no finite critical temperature and, although Hill does not suggest using the approximation in the region of large ρ, this fact does not indicate that the correction is very effective in the plane square case. It is of some interest to apply our criteria to the modified quadruplet approximation for the simple and body-centred cubic cases. For $z_1=6$, $z_2=12$, $w_1=0$, $\exp\,(-w_2/kT_c)=0{\cdot}7598$, a value which corresponds to an effective z_2 of about 8; T_c becomes zero at the correct value, $-1/4$, of ρ. For $z_1=8$, $z_2=6$, $w_1=0$, $\exp\,(-w_2/kT_c)=0{\cdot}6300$, a value which corresponds to an effective z_2 of between 5 and 6; T_c again becomes zero at the correct value of ρ, which is now $-2/3$. The correction thus results in a considerable improvement in these two cases.

The quadruplet approximation has not been applied to the face-centred cubic lattice where, since $z_2=6=\frac{1}{2}z_1$, it gives the right ratio of second to first neighbour pairs. This lattice is composed of four simple cubic sub-lattices such that a given site and its second nearest neighbours all lie in the same sub-lattice. Thus, as w_1 tends to zero the critical temperature should tend to that of the simple cubic lattice. Putting $z_1=12$ in (32) we obtain the positive root 2/3.

Where $w_1>0$, $w_2<0$ and $\rho<-1$ pure A and B phases (ferromagnetic state) are less stable at $T=0$ than a state in which there is a completely ordered arrangement of A and B on each sub-lattice, the sub-lattices being thus uncorrelated (Smart 1952, table 2).

Equation (31), in making the T_c curve cut the ρ axis at -1, is thus correct for the $w_1>0$ case on the face-centred cubic lattice. Hence, by this criterion and by that of the limiting values at $w_1=0$ and $w_2=0$, the quadruplet approximation is a consistent one for the disordered phase separation or ferromagnetic case on the face-centred lattice. Since this lattice cannot be decomposed into two equivalent sub-lattices there is no simple connection between the equilibrium states for $w_1>0$ and those for $w_1<0$, these latter being rather complicated (Anderson 1950, Smart 1952).

ACKNOWLEDGMENTS

In conclusion, I should like to thank Dr. C. Domb for encouragement and advice received during the course of this work and Prof. G. S. Rushbrooke for helpful discussions.

REFERENCES

ANDERSON, P. W., 1950, *Phys. Rev.*, **79,** 705.

BELL, G. M., 1952, *Thesis* (D.Phil.), Oxford.

BOZORTH, R. M., 1947, *Rev. Mod. Phys.*, **19,** 74 ; 1952, *Ferromagnetism* (New York : D. Van Nostrand Inc.), p. 443.

BROOKS, J. E., and DOMB, C., 1951, *Proc. Roy. Soc.* A, **207,** 343.

CHANG, T. S., 1937, *Proc. Roy. Soc.* A, **161,** 546 ; 1941, *J. Chem. Phys.*, **9,** 169, 174.

DOMB, C., and POTTS, R. B., 1951, *Proc. Roy. Soc.* A, **210,** 125.

FOURNET, G., 1951, *Comptes Rendus*, **232,** 155.

GUGGENHEIM, E. A., 1944, *Proc. Roy. Soc.* A, **183,** 213.

GUGGENHEIM, E. A., and MCGLASHAN, M. L., 1951 a, *Proc. Roy. Soc.* A, **206,** 335 ; 1951 b, *Trans. Faraday Soc.*, **47,** 929.

HILL, T. L., 1950, *J. Chem. Phys.*, **18,** 988.

KRAMERS, H. A., and WANNIER, G. H., 1941, *Phys. Rev.*, **60,** 252.

LUTTINGER, J. M., 1951, *Phys. Rev.*, **81,** 1015.

SEITZ, F., 1940, *Modern Theory of Solids* (New York : McGraw-Hill Inc.), Sec. 144.

SMART, J. S., 1952, *Phys. Rev.*, **86,** 968.

VAN SANTEN, J. H., 1950, *Philips Res. Rep.*, **5,** 282.

VAN VLECK, J. H., 1945, *Rev. Mod. Phys.*, **17,** 27.

YANG, C. N., 1945, *J. Chem. Phys.*, **13,** 66.

ZIMAN, J. M., 1951, *Proc. Phys. Soc.* A, **64,** 1108.

VIII. *The Interaction of Negative μ-mesons with Uranium Nuclei*

By W. Galbraith and W. J. Whitehouse
Atomic Energy Research Establishment, Harwell, Berks.*

[Received July 2, 1952. Revised September 26, 1952]

Abstract

A coincidence experiment is described in which an attempt is made to detect fissions of uranium nuclei resulting from the capture of negative μ-mesons in the cosmic radiation. The result shows that fission is not the most probable process following meson capture, and an upper limit of 0·25 is set for the probability of this fission process occurring. A interpretation of the result is suggested in terms of the competition between fission and neutron emission in the protoactinium isotope ^{238}Pa which is formed in the capture process.

§ 1. Introduction

The processes which occur when a negative μ-meson is captured by a nucleus are usually explained in terms of the so-called charge-exchange reaction, in which the meson interacts with one of the protons of the nucleus, giving rise to a neutron and a neutral particle which may be a neutrino

$$\mu^- + \mathrm{P} = \mathrm{N} + \nu.$$

The amount of excitation energy imparted to the resultant nucleus, in a charge-exchange reaction in which a neutrino is emitted, has been calculated by Tiomno and Wheeler (1949) using three different nuclear models. The three calculations give results of the same order of magnitude and the free particle model, which is most applicable in the present case, predicts a most probable excitation of $\sim$ 14 Mev and a maximum of $\sim$ 22 Mev. Rosenbluth (1949) finds a value which is almost exactly in agreement with Tiomno and Wheeler, but Taketani, Nakamura and Sasaki (1949) calculate the nuclear excitation to be about 6 Mev for large Z and about 14 Mev for small Z. Lang (1952) has given reasons for concluding that the excitation energy is about 1·5 times that predicted by Tiomno and Wheeler.

The excitation of the nucleus to the predicted extent would be expected to result in the emission of neutrons, and these have been observed, from lead, by Sard *et al.* (1951), Groetzinger and McClure (1950) and Sard and Crouch (1952). The number of neutrons emitted is about two, which is in reasonable agreement with theoretical prediction based upon the

---

* Communicated by the Authors.

evaporation formula of Weisskopf. George and Evans (1951), using photographic emulsions underground, have shown that only about 9% of the captured mesons produced disintegrations accompanied by the emission of charged particles, and that 90% of these visible stars had one prong and 10% two prongs. This, according to the calculations of Fujimoto and Yamaguchi, is consistent with a nuclear excitation of about 15 MEV. The charge-exchange reaction as given above is therefore supported by a considerable body of experimental evidence.

Wheeler (1949) has pointed out that the capture of a μ^--meson by a uranium nucleus might be expected to lead to fission by one of two possible processes : (*a*) The meson is first trapped and moves in stable orbits round the nucleus. The calculated energy released in the 1s–2s transition is 7 MEV uncorrected and 5–6 MEV if allowance is made for the dumb-bell shape of the nucleus immediately prior to fission. If this energy, instead of being radiated as a hard X-ray, could be transferred to the nucleus, fission might result. (*b*) In heavy elements, the meson is captured by the nucleus before it decays. As has been shown above the excitation energy imparted to the nucleus is of the right magnitude to induce fission.

The observation of fission induced by the capture of μ^--mesons, if it occurs, would be intrinsically difficult, since it would have to be observed in the presence of the natural α-activity and also of spontaneous fission. The rate of capture by uranium of μ^--mesons from the cosmic radiation is calculated to be about 7×10^{-3} per gramme per hour, while the measured spontaneous fission rate is $24{\cdot}8\pm0{\cdot}9$ per gramme per hour, and the α-emission is about 10^8 per gramme per hour. Simple calculations showed, however, that coincidences between the passage of mesons through counter trays and the occurrence of fissions in an ionization chamber could be observed, and that the background of random coincidences would be negligibly small. If the majority of the captured mesons had given rise to fissions, the number observed, though small, would have been statistically significant. In fact, the number of events recorded was very much below the calculated maximum, which indicates that fission is not the most probable consequence of μ^--meson capture by a uranium nucleus.

§ 2. EXPERIMENTAL ARRANGEMENT

A fuller account of the apparatus and of the precautions taken to ensure reliability has been given elsewhere (Galbraith and Whitehouse 1952) and only the essentials will be described here.

The general arrangement of the trays of Geiger-Müller counters is shown in fig. 1. The upper trays A and B, which had areas of 4900 cm^2 and 3060 cm^2 respectively, detected the passage of penetrating charged particles into the apparatus. The tray D was connected in anti-coincidence, and, although it could not be made as efficient as is usual, owing to the necessity of supports for the ionization chamber, served to reduce the background of random coincidences by a large factor. The flat, cylindrical ionization chamber C contained about 8 grammes of uranium in the form of thin foils of U_3O_8. The measured rate of spontaneous fission in this chamber was 115 per hour, and this, in conjunction with the known spontaneous fission rate (§ 1), gave the effective weight of uranium, from which fissions could be observed, as $4{\cdot}7 \pm 0{\cdot}5$ grammes. The events of direct interest are the passages of charged particles through A and B but not through D, accompanied by a fission in coincidence. Such events are denoted by (AB–D : C).

The function of the lead between the two upper trays A and B was to prevent the production of false (AB–D : C) events due to the discharge of the counters by γ-rays emitted in spontaneous fission. The thickness of lead was chosen to decrease the γ-counting rate in A by so large a factor that this effect was excluded. Subsidiary experiments, in which a Po–α–Be neutron source was used to increase the fission rate in the chamber, were carried out to verify this point.

Fig. 1

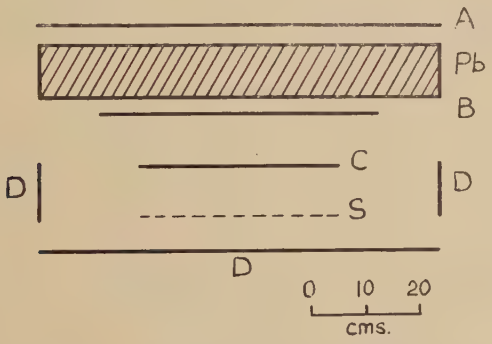

Arrangement of counter trays and ionization chamber. A, B and D indicate the central planes of the trays of counters. C indicates the mean position of the uranium foils. S indicates the approximate position of the shower tray.

The tray S marked in fig. 1, which consisted of eight counters coupled alternately in two groups of four, was used in part of the experiment to ensure that the apparatus was not sensitive to dense electron showers.

A block diagram of the electronic apparatus is given in fig. 2. When an (AB : C) event occurred the fission pulse was displayed on a cathode ray oscilloscope and photographed, as a precaution against spurious events. The other events (AB–D : C) were recorded on pen recorders. The resolving times in the coincidence unit were set at one micro-second, and subsidiary experiments were carried out to ensure that the pulses from all the units, particularly those from the ionization chamber, arrived within this time, and that no coincidences were lost. Daily checks were made of the reliability of the whole equipment. The spontaneous fission rate and the (AB–D) rate were recorded continuously as a further check on the operation of the equipment. The whole apparatus was driven from a motor generator to reduce the possibility of spurious counts due to surges in the mains.

The apparatus was first set up at ground level under a $\frac{1}{16}$ in. steel roof, and later moved below a concrete roof, 3 ft. thick.

Fig. 2

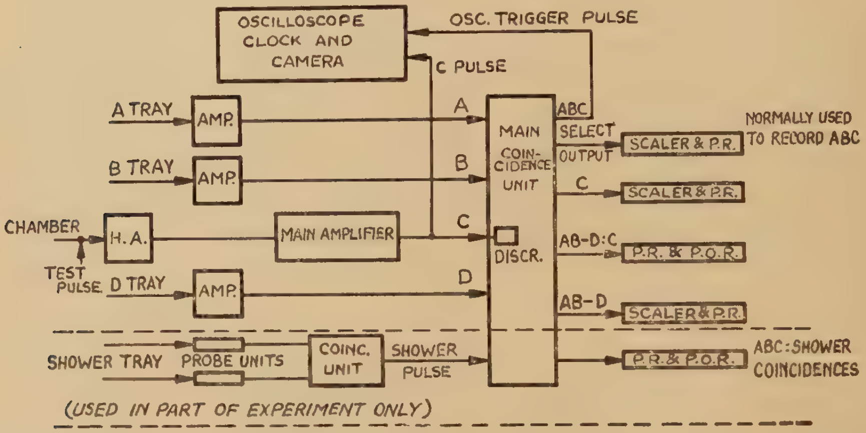

Block diagram of electronic apparatus (P.O.R.=Post Office Register; P.R.=pen recorder. The ‘ select output ’ scaler and recorder, normally used to record ABC coincidences, could be used to measure the A, B, D, AB, ABD and AB–D rates).

§ 3. Calculated Rates

3.1. *Rate of Capture of μ^--mesons*

The flux of penetrating charged particles at sea level was not measured in this experiment. Instead the result of Greisen (1942, as reported by Rossi 1948), who found a value of 46 particles per cm^2 per hour, was used. Of these about 99% are μ-mesons and 1% fast protons (Mylroi and Wilson 1951). Further, 45% of the mesons are negatively charged (Owen and Wilson 1951). A calculation of the geometrical efficiency of our counter trays shows that 90% of the particles which pass through the uranium also pass through the trays. Allowing for the combined detection efficiency of the trays A and B (93%), we estimate that the effective flux of μ -mesons through the uranium is 17 per cm^2 per hour.

The fraction of μ-mesons stopped by uranium may be calculated from the absorption in lead, which has been measured several times (Koenig 1946, Rossi 1948, Kraushaar 1949, York 1952). We have used the most conservative value, that of Koenig, who found that 1 g per cm^2 of lead stopped 0·033% of the mesons. Assuming the mass absorption of the two elements to be the same, and the effective mass of uranium to be 4·7 g (§ 2) the rate of absorption of μ^--mesons, and hence the maximum possible rate of μ-meson fission, is 27 per 1000 hours. For that part of the experiment which was carried out under concrete the meson flux was attenuated by about 15%, but the energy spectrum was very little changed, and the proportional absorption of mesons was the same as above ground.

3.2. *Proton Reactions*

The flux of fast protons with momentum great enough to penetrate the lead between the trays and enter the chamber ($\sim 10^9$ ev) is about 0·2 per cm^2 per hour (Mylroi and Wilson *loc. cit.*). If we assume that the cross-section for interaction is the geometrical cross-section of the nucleus and that every interaction results in a fission, we obtain, for the present apparatus at ground level, a maximum rate of 7 proton-induced fissions per 1000 hours. Below the concrete roof the proton flux is reduced by a factor of about 5, if an attenuation length of 140 g per cm^2 is assumed (Mylroi and Wilson *loc. cit.*), and the number of proton-induced fissions is therefore hardly observable.

3.3. *Other Mechanisms*

There are a number of indirect processes by which fast protons may initiate (AB–D : C) or (ABD : C) events. Most of these depend upon the production of a star in the material of the apparatus and the subsequent induction of a fission by a secondary particle from the star. Approximate calculations indicate that the fission rates from these processes are much smaller than those from μ-meson capture above ground, while below the concrete they are virtually absent.

Another type of reaction which might conceivably lead to fission is the direct electromagnetic interaction which occurs when a fast charged particle passes close to the nucleus. The results of George and Evans (1950) indicate that the cross-section for this interaction is $\sim 10^{-29}$ cm^2 per nucleon, and a simple calculation shows that fissions caused by this effect would be too infrequent to be detected by the present apparatus.

3.4. *Accidental Rates*

The accidental rates can be calculated from the usual formula ($R_a=2\tau R_1R_2$), in which R_a is the accidental rate, τ is the resolving time of the coincidence unit (1 μ sec), R_1 is the spontaneous fission rate in the chamber and R_2 is either the (ABD) or the (AB–D) rate. The calculated accidental rates are shown in the table.

§4. RESULTS

The results of all the runs are recorded in the table. The following conclusions may be drawn from them.

Runs I and II. Together these indicate that the rate of meson-induced fission is significantly below the calculated rate, but the interpretation is complicated by the fact that the number of (ABD : C) events is above the calculated random rate. This may be due to the indirect processes mentioned in § 3.3.

Run	Experimental details	Total hours	ABD : C coincidences		AB–D : C coincidences		Calculated maximum number of fissions	
			Observed number of events*	Calculated random number	Observed number of events	Calculated random number	μ^--meson	proton
I	Uranium foils above ground	730	18	6	11	1	20	5
II	As I with shower tray added	480	8	4	6	1	13	3
I and II	Sum of I and II	1210	26 (<33, >20)	10 (<15, >6)	17 (<23, >12)	2 (<5, >0)	33 (<41, >22)	8 (<13, >5)
I and II	After subtracting background		16 (<22, >11) True rate		15 (<21, >10) True rate			
III	Chamber not between counter trays; control run	850	6	6	2	1	0	0
IV	As I, but lead foils substituted for uranium; control run	470	4	0	0	0	0	0
V	As I, but below 3 ft. concrete	1340	10 (<15, >6)	8 (<13, >5)	5 (<8, >2)	2 (<5, >0)	31 (<39, >24)	2 (<5, >0)
V	After subtracting background		2 (<5, >0) True rate		3 (<6, >1)			

* This rate is not recorded directly, but is obtained by subtracting the observed AB–D : C rate from the AB : C rate.

NOTE : If the number is given as x (<y, >z) this means that the observed value during the run was x, y is the mean number of counts on the high side for which there is a 0·1 probability of observing x, and z is the mean number on the low side for which there is also a 0·1 probability of observing x, assuming these numbers to have a Poisson distribution.

Run II. No coincidences were observed between (AB : C) events and electron showers.

Runs III and IV. These are satisfactory control runs, in which the rates are in agreement with the calculated random rates. The count of 4(ABD : C) events in run IV is not large enough to justify any definite conclusions about the fission of lead by cosmic ray particles, but it would not be inconsistent with fission by fast protons at a rate determined by the geometrical cross-section.

Run V. The number of (AB–D : C) events is so much less than the calculated rate of absorption of μ^--mesons that the experiment provides no evidence for fission by μ-mesons in uranium. The statistical accuracy is such that the upper limit of the probability of fission following the capture of a μ^--meson in ^{238}U can be set at 0·25.

§5. DISCUSSION

At first sight the results of this experiment seem to be at variance with predictions based upon the charge-exchange reaction. It seems probable, however, that an explanation for the result can be made in the following way.

Experimental evidence has accumulated which indicates that fission competes unfavourably with neutron emission at moderate excitation energies. It has been shown that the photofission cross-section of ^{238}U is only a fraction of the cross-section for neutron emission at energies of the order of 20 MEV (Charbonnier, Scherrer and Wäffler 1949, Goward, Jones, Watson and Lees 1951) in spite of the fact that the photofission threshold, 5·1 MEV, is lower than the threshold for the (γ, n) reaction, 5·9 MEV (Koch, McElhinney and Gasteiger 1950, Anderson and Duffield 1952). Thus it appears probable that neutron emission is favoured with respect to fission even when the fission barrier is less than the binding energy of the neutron.

Price and Kerst (1952) estimate, from their observations of the photo-neutron yield, that only about half of the ^{238}U nuclei undergo fission when bombarded with 22 MEV γ-rays, the rest losing most of the excitation energy by neutron emission. For ^{232}Th they find the probability of fission occurring is only 0·24 for the same excitation energy. Levenger and Bethe (1952) show that the photo-neutron yield for ^{238}U observed experimentally by other workers is consistent with a value of 0·23 for the probability that fission occurs in place of neutron emission. We would expect that the probability of fission occurring in the compound nucleus ^{238}Pa, which is formed when a μ-meson is captured by ^{238}U, will be even smaller, since its Z^2/A value is less than that for ^{238}U. The upper limit of 0·25 observed in the present experiment for the probability of fission occurring would then appear to be in reasonable agreement with the above considerations.

If this explanation of the failure to observe μ-meson fission is correct, there is no conflict between the result of the present experiment and other work on μ-meson capture.

ACKNOWLEDGMENTS

We wish to express our thanks to Mr. F. H. Wells who designed and supervised the construction of the coincidence unit, to Mr. I. A. Nelsey for the preparation of the uranium foils and to Mr. F. R. Barclay for assistance in the experiments. We are grateful to the Director A.E.R.E. for permission to publish this work and to Dr. E. Bretscher, Head of the Nuclear Physics Division, for his continued interest in it.

REFERENCES

ANDERSON and DUFFIELD, 1952, *Phys. Rev.*, **85,** 728.
CHARBONNIER, SCHERRER and WÄFFLER, 1949, *Helv. Phys. Acta*, **22,** 385.
CROUCH and SARD, 1952, *Phys. Rev.*, **85,** 120.
FUJIMOTO and YAMAGUCHI, 1949, *Prog. Theor. Phys.*, **4,** 468.
GALBRAITH and WHITEHOUSE, 1952, *A.E.R.E. Report* NR 987.
GEORGE and EVANS, 1950, *Proc. Phys. Soc.* A, **63,** 1248 ; 1951, *Ibid.*, **64,** 193.
GOWARD, JONES, WATSON and LEES, 1951, *Proc. Phys. Soc.* A, **64,** 95.
GREISON, 1942, *Phys. Rev.*, **61,** 212.
GROETZINGER and MCCLURE, 1951, *Phys. Rev.*, **81,** 969.
KOCH, MCELHINNEY and GASTEIGER, 1950, *Phys. Rev.*, **77,** 329.
KOENIG, 1946, *Phys. Rev.*, **69,** 590.
KRAUSHAAR, 1949, *Phys. Rev.*, **76,** 1045.
LANG, 1952, University of Liverpool, paper to be published.
LEVENGER and BETHE, 1952, *Phys. Rev.*, **85,** 577.
MYLROI and WILSON, 1951, *Proc. Phys. Soc.* A, **64,** 404.
OWEN and WILSON, 1951, *Proc. Phys. Soc.* A, **64,** 417.
PRICE and KERST, 1950, *Phys. Rev.*, **77,** 806.
ROSENBLUTH, 1949, *Phys. Rev.*, **75,** 532.
ROSSI, 1948, *Rev. Mod. Phys.*, **20,** 537.
SARD, CROUCH, JONES, CONFORTO and STEARNS, 1951, *Nuovo Cimento*, **8,** 326 (this paper contains references to earlier work by Sard *et al.*).
TAKETANI, NAKAMURA and SASAKI, 1949, *Phys. Rev.*, **76,** 852.
TIOMNO and WHEELER, 1949, *Rev. Mod. Phys.*, **21,** 153.
WHEELER, 1949, *Rev. Mod. Phys.*, **21,** 133.
YORK, 1952, *Phys. Rev.*, **85,** 998.

IX. *The Production of τ-Mesons in Ice*

By A. J. HERZ, P. E. HODGSON and R. M. TENNENT
Imperial College of Science and Technology, London, S.W.7 *

[Received August 13, 1952]

SUMMARY

Nuclear-research emulsion has been exposed to the cosmic radiation under various thicknesses of ice. Three events interpreted as the decay of τ-mesons have been observed, and measurements on their tracks show that these particles decay into three π-mesons of total kinetic energy (73 ± 6) MeV and have mass $(965 \pm 12) m_e$. They are found with a frequency of about 0·0008 τ-mesons per star in emulsion exposed under ice. The emulsion was examined for nuclear disintegrations produced by heavy mesons, and for τ-mesons decaying in flight, but no such events were found. The life time is shown to be longer than 10^{-9} sec.

§1. INTRODUCTION

IN 1949, Brown, Camerini, Muirhead, Powell and Ritson (1949) observed a single event which indicated the existence of a particle having a mass about a thousand times that of the electron, and decaying into three singly-charged particles. This particle was called the τ-meson, and its existence was confirmed when, during an investigation of the attenuation of cosmic radiation in ice, Harding (1950) found two events interpreted as the decay of τ-mesons (numbers 1 and 2 in this paper).

A second batch of plates has been exposed in the ice and examined for further evidence of τ-mesons. One more (number 3) was found (Hodgson 1951).

The measurements on all the τ-mesons so far observed at Imperial College have been repeated and extended, and the results are given in this paper together with the evidence about the mass, mode of decay, frequency of production, and life time of these particles. The plates have also been examined for evidence of slow heavy mesons producing nuclear disintegrations.

§2. EXPERIMENTAL PROCEDURE

Boxes of plates coated with Ilford G5 nuclear-research emulsion were exposed vertically in a steel pipe sunk into the ice on the Jungfraujoch plateau (see Harding 1951). Particles 1 and 2 were found in 200-μ-thick emulsion, number 3 in 400-μ emulsion.

---

* Communicated by E. P. George.

§ 3. THE MASS OF THE τ-MESON

(*a*) *Gap measurements on the tracks of the τ-mesons*

The results of gap measurements on the tracks of particles 1 and 2 have been published (Hodgson 1950). However, as the tracks had faded considerably, it was not possible to find an accurate value of the mass of the τ-meson from them. The track of the remaining τ-meson dips too steeply for any measurements to be made by this method.

(*b*) *Multiple scattering of the τ-mesons*

Measurement of the multiple scattering on the track of particle 2 gave a value of $(1870 \pm 500) m_e$ for its mass. This is rather high, but it is not inconsistent with the more accurate value found below. The tracks of the other τ-mesons were not suitable for scattering measurements.

(*c*) *The energy balance of the decay process*

The most accurate value of the mass of the τ-meson is obtained by assuming the decay scheme and adding the rest masses of the secondary particles to the mass equivalent of their kinetic energies (see § 4.) The best value found in this way is $m_\tau = (965 \pm 12) m_e$, in excellent agreement with the figure of $(966 \pm 8) m_e$ given by Fowler, Menon, Powell and Rochat (1951). In both these investigations, the mass of the secondary π-mesons was assumed to be $(274 \pm 2) m_e$ (Alvarez 1950). Since this paper was written another τ-meson has been reported by Ceccarelli, Dallaporta, Merlin and Rostagni (1952) who find a mass of $(991 \pm 15) m_e$ which is consistent with our value.

§ 4. THE DECAY OF THE τ-MESON

In all the examples of τ-meson decay observed so far, the tracks of the three secondary particles are coplanar to within 2°, indicating that not more than three particles are emitted. The possibility of the emission of a neutral fourth particle of low energy or small mass cannot be excluded definitely, but it will be disregarded in the analysis to follow.

The grain densities of all the tracks of secondary particles suitable for measurement were found, and they are given in table 1 as a multiple of the minimum grain density of singly-charged particles. Owing to fading, the values quoted for the first two events are not as reliable as those for the third.

The relative masses of the secondary particles were found from their directions of emission and the grain densities of their tracks by the methods of Fowler *et al.* (1951), and they are given in table 1. These results show that the secondary particles are of equal mass to an accuracy of about 10 per cent.

The absolute values of the masses of those secondaries having a sufficient length of track in the emulsion were determined from measurements of grain density and multiple scattering, and the results are shown in table 1. These masses are in the range 200 to 400m_e, indicating that the secondary particles are μ- or π-mesons. But since one of the secondaries in the event observed by Brown *et al.* (1949) was identified as a π-meson, and since it has been shown above that the secondary particles are all of the same mass, we can conclude that all the secondary particles are π-mesons. Provided that all the τ-mesons observed have the same decay scheme, the probability that one or two of the secondaries are μ-mesons is negligible.

Table 1

	τ-Meson		
	1	2	3
$I/I_{\min}$ of Secondaries	1·62±0·30 2·90±0·90 3·52±0·50	— 2·36±0·20 —	1·90±0·25 2·00±0·15 4·72±0·70
Relative Masses of Secondaries	1·00 0·96±0·25 1·05±0·20	— — —	1·00 0·93±0·12 1·09±0·17
Absolute Masses of Secondaries (m_e)	— — 300±70	— — —	260±100 330±140 260±110
Relative Momenta of Secondaries*	1·00 0·59±0·18 0·51±0·11	— — —	1·00 0·95±0·10 0·49±0·06
Relative Momenta of Secondaries†	1·00 0·57 0·53	1·00 0·96 0·91	1·00 0·88 0·54
Energies of Secondaries in MeV	45·0±12 17·5± 8 13·3± 3	25±5 24±4 20±4	33·5±5‡ 31·0±4 9·0±1·5
Total Kinetic Energy of Secondaries in MeV	76±15	69±8	73·5±7

* From grain densities.

† From angles of emission.

‡ M. G. K. Menon of Bristol University has measured the energies of the secondary particles using the scattering technique, and he finds them to be 33±10, 27±6 and 8±1 MeV respectively.

Knowing the secondary particles to be π-mesons, their energies were found from the grain densities of their tracks ; they are given in table 1. The relative momenta of the secondaries are also given, and they agree well with the values calculated from the angles of emission.

The values for the total kinetic energy of the secondary particles agree within the limits of experimental error, supporting the view that τ-mesons decay into just three particles. The mean value of the total kinetic energy of the secondaries is (73 ± 6) MeV, in agreement with that given by Fowler *et al.* (1951).

In the case of the second τ-meson, two of whose secondaries were too short even for grain-density measurements, the total kinetic energy of the secondary particles was found from the angles of emission and the energy of the third particle.

§ 5. THE RATE OF PRODUCTION OF τ-MESONS

During his investigation of the attenuation of the cosmic radiation in ice, Harding (1950, 1951) observed two τ-mesons among 3673 stars of three or more tracks in plates exposed in the ice at depths between 0 and 9 metres, which gives a ratio of τ-mesons to stars of $0{\cdot}0005^{+0{\cdot}0007}_{-0{\cdot}0004}$. In the second exposure, made at depths between 2·5 and 3·5 metres of ice, one τ-meson was found among 1300 stars and 170 π–μ decays and meson-induced stars, giving τ-meson frequencies of $0{\cdot}0008^{+0{\cdot}0018}_{-0{\cdot}0006}$ per star and $0{\cdot}006^{+0{\cdot}014}_{-0{\cdot}005}$ per meson of the type given above.

Fowler *et al.* (1951) examined plates exposed under 30 cm of lead, and found one τ-meson accompanied by 750 π-mesons, that is $0{\cdot}0013^{+0{\cdot}003}_{-0{\cdot}001}$ per π-meson.

The errors given here were computed from the fiducial limits given by Regener (1951), and it can be seen that the frequencies under ice and under lead are of the same order of magnitude. However, the difference between the figures suggests that τ-mesons are more frequently found under ice than under lead, and if this were confirmed by further experimental evidence it would provide support for the hypothesis (Hodgson 1951) that τ-mesons are more likely to be produced in hydrogen than in other elements. This may be understood if it is assumed that τ-mesons, or their parents if they are secondary particles, if created in nucleon–nucleon collisions in larger nuclei, have a high probability of reabsorption in the nucleus in which they were produced.

The τ-mesons made angles of 85°, 169° and 133° respectively with the upward vertical when they entered the emulsion. These data are insufficient to allow positive conclusions about the zenith-angular distribution of the particles to be drawn.

§ 6. THE LIFE TIME OF τ-MESONS

The fact that the frequency with which τ-mesons are found to stop in plates surrounded by ice is comparable to that in plates surrounded by lead, or even greater, is the more surprising because for charged particles of short life time the probability of coming to rest increases with the density of the medium in which they are slowed down. This probability has been calculated for particles of various energies, using the methods described by Herz (1951), and an analysis based on the results is given in this section.

If we assume that all the τ-mesons found came from the ice, we can calculate how many had to be present just outside the pipe for every one stopping in the plates. At that point the particles would have had a kinetic energy of about 55 Mev.

However, certainly not all the τ-mesons were created just outside the pipe, and it is therefore of interest to find out how many would have to be produced per particle stopped if production took place at some higher energy. Now, so far, there has not been any positive experimental evidence to suggest that τ-mesons are ejected from nuclear interactions with kinetic energies sufficiently low to make them identifiable (Camerini, Fowler, Lock and Muirhead 1950, Daniel, Davies, Mulvey and Perkins 1952). Furthermore, although the accuracy of mass determinations is low in cloud-chamber work, it seems safe to say that τ-mesons occur only very rarely amongst the non-relativistic decay products of *V*- and *K*-particles, if at all.

We shall thus assume for the purpose of this calculation that most of the τ-mesons are produced with kinetic energies equal to their rest energy (about 500 Mev) or greater, and that they are not very abundant at that energy (if they were, one would expect a fair number to be produced at lower energies also). Table 2 shows how many particles would be needed at 500 Mev for every one stopping in the plates; the number needed at 55 Mev (just outside the pipe) is given for comparison. The figures strongly suggest that the life time is longer than 10^{-9} sec unless most of the particles are produced with low energies.

Table 2

Attenuation Cross Section	T in Mev	Life Time in Seconds			
		10^{-7}	10^{-8}	10^{-9}	10^{-10}
Negligible	55	1·003	1·023	1·26	9·76
Geometrical	55	1·022	1·043	1·28	9·95
Negligible	500	1·068	1·93	713	$3{\cdot}4\times10^{28}$
Geometrical	500	6·68	12·1	4460	$2{\cdot}1\times10^{29}$

A further approach to the problem can be made by comparing the experimental upper limit to the number of decays in flight of τ-mesons accompanying those stopped with the expected number, assuming various life times. Clearly, if more particles are produced than are found to stop, the particles which do not survive must disappear either by decay in flight or by nuclear interaction. However, no event of either type, involving an identifiable τ-meson, has yet been found in the experiments reported here (see also §7). In order to be certain about this, 0·27 cm^3 of emulsion was specially examined under high magnification, and, using the fiducial limits given by Regener (1951), we can conclude from that alone that the number of decays in flight was not more than 120 per τ-meson stopped. If we accept the result that no τ-meson decayed in flight in the emulsion of the second exposure which was searched specially for this type of event, the experimental upper limit becomes 1·9 decays in flight per particle stopped.

Assuming that all τ-mesons are produced with kinetic energy 500 MEV, the number expected to decay in flight in the emulsion was calculated. The results are given in table 3; they may be in error by a factor of about three because of the simplifying assumptions made. Comparison of the calculated figures with the experimental upper limit again leads to the conclusion that the life time must be longer than 10^{-9} sec.

Table 3. Expected Number of Decays in Flight of Particles Entering the Emulsion with Kinetic Energies between 130 and 490 MEV, per τ-meson Stopped

Life Time in sec	10^{-8}	10^{-9}	10^{-10}
No nuclear interaction	0·3	250	$2{\cdot}2\times10^{29}$
Interaction cross section taken as geometrical	0·6	900	$1{\cdot}3\times10^{30}$

§7. THE NUCLEAR INTERACTIONS OF HEAVY MESONS

Investigations of very-high-energy nuclear interactions by Daniel *et al.* (1952) have shown that few, if any, τ-mesons are produced in them. If these particles were produced directly, we should expect them to interact strongly with nuclear matter, in which case only those charged positively which are repelled by nuclei would be found to decay spontaneously after coming to rest. The negatively charged heavy mesons, presumably produced together with the positive ones, will interact with nuclei when they come to rest in the emulsion, causing disintegrations. It is therefore of great importance to search for more events of the type observed by Leprince-Ringuet (1949) and Fry and Lord (1952) which can be interpreted as the nuclear interaction of a heavy meson.

All the stars in the present batch of emulsion were therefore examined, but no event was found which could have been produced by a slow negative heavy meson. This does not, however, show that such events do not occur, for the track of an incoming heavy meson would show little multiple scattering and might easily be mistaken for that of a slow outgoing proton unless a considerable length of track was available for examination.

If τ-mesons do not interact strongly with nuclear matter, all the events could be attributed to the decay of both negative and positive particles. This would suggest that τ-mesons are the decay products of still heavier particles which are themselves produced in nuclear interactions.

ACKNOWLEDGMENTS

We should like to thank Professor Sir George Thomson and Dr. E. P. George for a number of discussions and for the helpful suggestions they have made. We are most grateful to Dr. M. G. K. Menon for repeating some of our measurements and giving us his results. Thanks are also due to the authorities of the Hochalpine Forschungsstation Jungfraujoch for making the exposures possible. Our team of searchers did their best to find more τ-mesons.

REFERENCES

ALVAREZ, L., 1950, *Proc. Harwell Nuclear Physics Conf.*, p. 1.
BROWN, R. H., CAMERINI, U., FOWLER, P. H., MUIRHEAD, H., POWELL, C. F., and RITSON, D. M., 1949, *Nature, Lond.*, **163,** 82.
DANIEL, R. R., DAVIES, J. H., MULVEY, J. H., and PERKINS, D. H., 1952, *Phil. Mag.*, **43,** 753.
CAMERINI, U., FOWLER, P. H., LOCK, W. O., and MUIRHEAD, H., 1950, *Phil. Mag.*, **41,** 413.
CECCARELLI, M., DALLAPORTA, N., MERLIN, M., and ROSTAGNI, A., 1952, *Nature, Lond.*, **170,** 454.
FOWLER, P. H., MENON, M. G. K., POWELL, C. F., and ROCHAT, O., 1951, *Phil. Mag.*, **42,** 1040.
FRY, W. F., and LORD, J. J., 1952, *Phys. Rev.*, **87,** 533.
HARDING, J. B., 1950, *Phil. Mag.*, **41,** 405 ; 1951, *Ibid.*, **42,** 651.
HERZ, A. J., 1951, *Proc. Bristol Conference on V-Particles and Heavy Mesons*, p. 25.
HODGSON, P. E., 1950, *Phil. Mag.*, **41,** 725 ; 1951, *Ibid.*, **42,** 1060.
LEPRINCE-RINGUET, L., 1949, *Rev. Mod. Phys.*, **21,** 42.
REGENER, V. H., 1951, *Phys. Rev.*, **84,** 161.

X. *The Interaction of Dislocations and Boundaries*

By A. K. Head
H. H. Wills Physical Laboratory, University of Bristol*

[Received October 16, 1952]

Abstract

The image forces on a screw dislocation due to a grain boundary, or a free surface on which is a surface film, are evaluated. For the case of an oxide layer on aluminium it is shown that there is an equilibrium position for the dislocation, at a depth in the metal approximately equal to the thickness of the oxide film. The behaviour of an edge dislocation is approximately the same.

§ 1. Introduction

It has been shown (Eshelby 1951) that there exists a close analogy between screw dislocations and electrostatic line charges. In particular, the interaction of a screw dislocation with changes in the elastic constants of the medium is analogous to the electrostatic problem of a line charge in a medium of non-homogeneous dielectric constant.

The solution of electrostatic problems by the method of images (Jeans 1911) can thus be applied directly to the analogous dislocation problem.

§ 2. Grain Boundary

As a model for a grain boundary, consider an infinite isotropic elastic medium of shear modulus μ_1, for $x>0$, and modulus μ_2 for $x<0$. Then the interaction between a screw dislocation of unit strength at $x=a$, $y=0$ and the boundary can be represented by the following images. For $x<0$ the stress field is the same as that due to a dislocation of strength $2\mu_1/(\mu_2+\mu_1)$ at $x=a$, $y=0$ in an infinite medium. For $x>0$ the stress field is the same as that due to the original unit dislocation plus a dislocation of strength $(\mu_2-\mu_1)/(\mu_2+\mu_1)$ at the image point $x=-a$, $y=0$. Thus the dislocation will be attracted to the image (i.e. to the boundary) if $\mu_2<\mu_1$, and repelled if $\mu_2>\mu_1$. This is a long range force which varies as a^{-1}. For a real crystal boundary there is an additional short range force due to the misfit of the two atomic lattices at the boundary (Nabarro 1952).

§ 3. Surface Film on Free Surface

Consider a semi-infinite isotropic elastic medium of shear modulus μ_1 for $x>0$ and modulus μ_2 for $-b<x<0$, with a free surface at $x=-b$. Then a screw dislocation of unit strength at $x=a$, $y=0$ will induce a stress field for $x>0$ which can be described by an infinite set of images at $y=0$, with values of x, and strengths, as follows :—

---

* Communicated by F. C. Frank.

Position of image : value of x	Strength of image
$-a$	κ
$-(a+2b)$	$-(1-\kappa^2)$
$-(a+4b)$	$-(1-\kappa^2)\kappa$
$-(a+6b)$	$-(1-\kappa^2)\kappa^2$
$-(a+8b)$	$-(1-\kappa^2)\kappa^3$
etc.	etc.

where $\kappa=(\mu_2-\mu_1)/(\mu_2+\mu_1)$.

If $\mu_2<\mu_1$ then the dislocation is attracted to the boundary for all values of a. If $\mu_2>\mu_1$ the dislocation is attracted to the boundary for large values of a and repelled for small values of a. Thus there will be a position where the dislocation is in stable equilibrium, this being when the stress due to all the images is zero at the position of the dislocation. If this position of equilibrium is $x=d$, then, writing $n=d/b$, the condition of zero image stress at $x=d$ is

$$0=\kappa-(1-\kappa^2)\left[\frac{n}{n+1}+\frac{n}{n+2}\kappa+\frac{n}{n+3}\kappa^2+\frac{n}{n+4}\kappa^3+\ldots\right].$$

On multiplying this series by κ^{n+1} and differentiating a geometric progression is obtained. Summing this and then integrating gives as the equation for the equilibrium position of the dislocation

$$0=\kappa-n(1-\kappa^2)\kappa^{-n-1}\int_0^{\kappa} t^n\,(1-t)^{-1}\,dt.$$

This has been solved numerically for $n=0{\cdot}5$, 1, 2 and the corresponding values of μ_2/μ_1 are given in the following table :—

n	μ_2/μ_1
Small	$1+2n$
0·5	2·20
1	3·65
2	6·76

For the case of an oxide film on aluminium, this analysis can be expected to be approximately true as the elastic anisotropy of aluminium is small (Boas 1947). The elastic constants of bulk aluminium oxide (Bhimasenachar 1950) are from three to four times the elastic constants of aluminium. If the oxide layer on the metal has the same elastic constants as the bulk oxide then, by table 2, the equilibrium position of a dislocation would be at a depth in the metal approximately equal to the thickness of the surface layer.

§ 4. EDGE DISLOCATION

An exact analysis (Head, unpublished) of the interaction of an edge dislocation with the model grain boundary leads to a rather complicated result. However, a good approximation (with a maximum error of 15%) is that an edge dislocation is influenced by the boundary in the same way as a screw dislocation, i.e., as if there were a dislocation of strength $(\mu_2-\mu_1)/(\mu_2+\mu_1)$ at the image point. The more complicated case, of interaction with a surface film, does not appear to be readily soluble. The following physical reasoning suggests that there will be a position of equilibrium if $\mu_2>\mu_1$. For when the dislocation is close to the surface, the surface film will be effectively infinitely thick and the dislocation will be repelled if $\mu_2>\mu_1$. And if the dislocation is far from the surface, then the effect of the surface film will be small and the dislocation will be attracted as to a free surface. In between will be a position of equilibrium, but its location can only be surmized to be approximately that for a screw dislocation.

ACKNOWLEDGMENT

This paper is published by permission of the Department of Supply, Commonwealth of Australia, of which the author is an officer.

REFERENCES

BHIMASENACHAR, J., 1950, *Proc. Nat. Inst. Sci., India*, **16,** 241.
BOAS, W., 1947, *Physics of Metals and Alloys* (Melbourne : University Press), p. 51.
ESHELBY, J. D., 1951, *Phil. Trans.* A, **244,** 101.
JEANS, J. H., 1911, *The Mathematical Theory of Electricity and Magnetism* (Cambridge : University Press), p. 200.
NABARRO, F. R. N., 1952, *Advances in Physics*, **1,** 315.

XI. *Neutron Total Cross Sections between* 30 *and* 153 Mev

By A. E. Taylor and E. Wood
Atomic Energy Research Establishment, Harwell*

[Received November 17, 1952]

Abstract

The neutron total cross sections of carbon, aluminium, copper, cadmium and lead have been determined as a function of energy in the range 30 to 139 Mev. The lead total cross section shows a dip at about 60 Mev and corresponding dips in the cadmium and copper cross sections appear to occur between 30 and 40 Mev. The neutron total cross section of hydrogen has been measured as $56{\cdot}9 \pm 1{\cdot}8 \times 10^{-27}$ cm^2 at a neutron energy of 126 ± 2 Mev.

§1. Introduction

Neutron total cross sections of several elements at 153 Mev have been determined previously (Taylor, Pickavance, Cassels and Randle 1951 a). Carbon, aluminium, copper, cadmium and lead have now been studied in the energy range 30 to 139 Mev and the cross section of hydrogen has been measured at 126 ± 2 Mev using the method previously described (Taylor, Pickavance, Cassels and Randle 1951 b). Some of the preliminary results for lead have already been briefly communicated (Taylor and Wood 1952).

Other determinations of the neutron total cross sections of a number of elements in this same range of energies have been reported at 42 Mev (Hildebrand and Leith 1950), at 83 Mev (Cook, McMillan, Peterson and Sewell 1949), at 95 Mev (DeJuren and Knable 1950) and at 115 Mev (DeJuren and Moyer 1951). Additional measurements of the carbon total cross section have been reported (Mott, Guernsey and Nelson 1952, Taylor *et al.* 1951 b).

The values of the total cross sections presented in this paper are not in disagreement with those obtained by other investigators. However, by using a narrower energy band than in the work at 42, 83, 95 and 115 Mev, it has been possible to look for more detail in the variation of cross section with energy. This investigation has shown a dip in the lead cross section at about 60 Mev and has indicated the occurrence of corresponding dips for cadmium and copper between 30 and 40 Mev. It has not been possible to follow the variation of cross section with energy below 30 Mev since the counting rates became very small.

Since several parts of the apparatus used in these measurements were similar to those described in the previous experiment (Taylor, Pickavance, Cassels and Randle 1951 c), the details will not be repeated here.

---

* Communicated by the Authors.

§ 2. Experimental

(i) *Principle*

The attenuation of a neutron beam was measured using a ‘good’ geometry arrangement. The neutron beam was produced by proton bombardment of an internal cyclotron target and was then collimated by a series of holes in the concrete shielding. There were five sets of holes in the two shielding walls (fig. 1, Taylor *et al.* 1951 c), each set corresponding to a particular target radius. It was possible to vary the effective energy of the neutron beam at a particular radius by decreasing the magnetic field and

Fig. 1

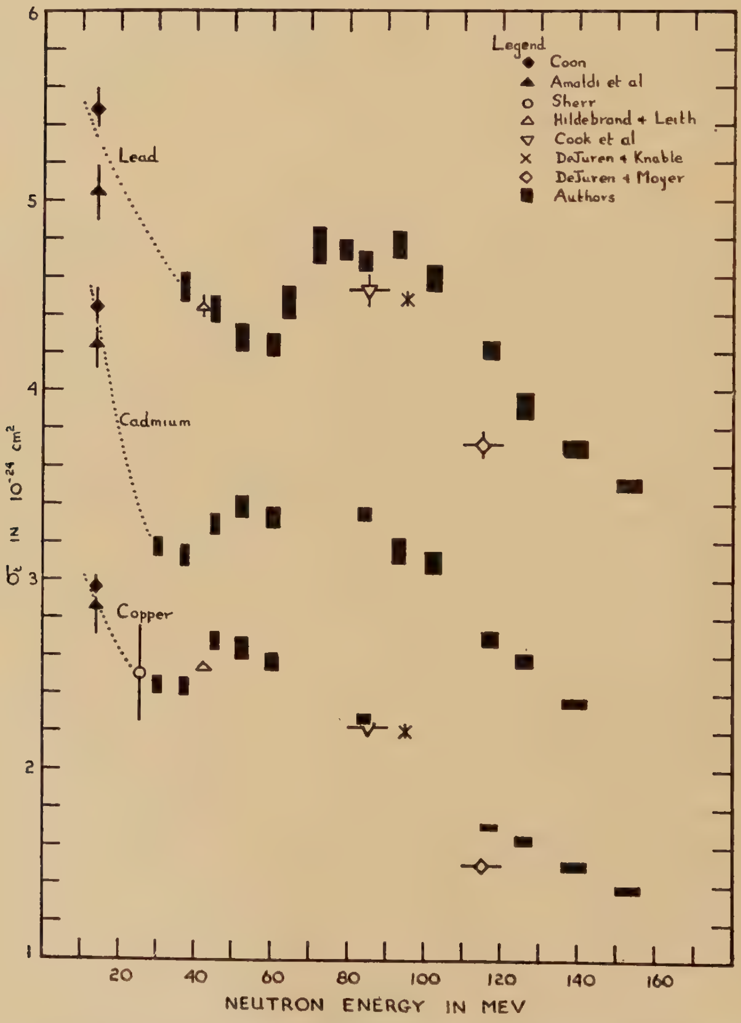

Variation of the neutron total cross section with energy for lead, cadmium and copper in the energy range 14 to 156 MeV.

by altering the target material. For instance the p–n threshold in beryllium is about 2·0 MeV whereas the threshold in carbon is about 20 MeV. A triple coincidence counter telescope detected the neutrons by counting the recoil protons emerging from a polyethylene disc placed in the collimated neutron beam.

Fig. 2

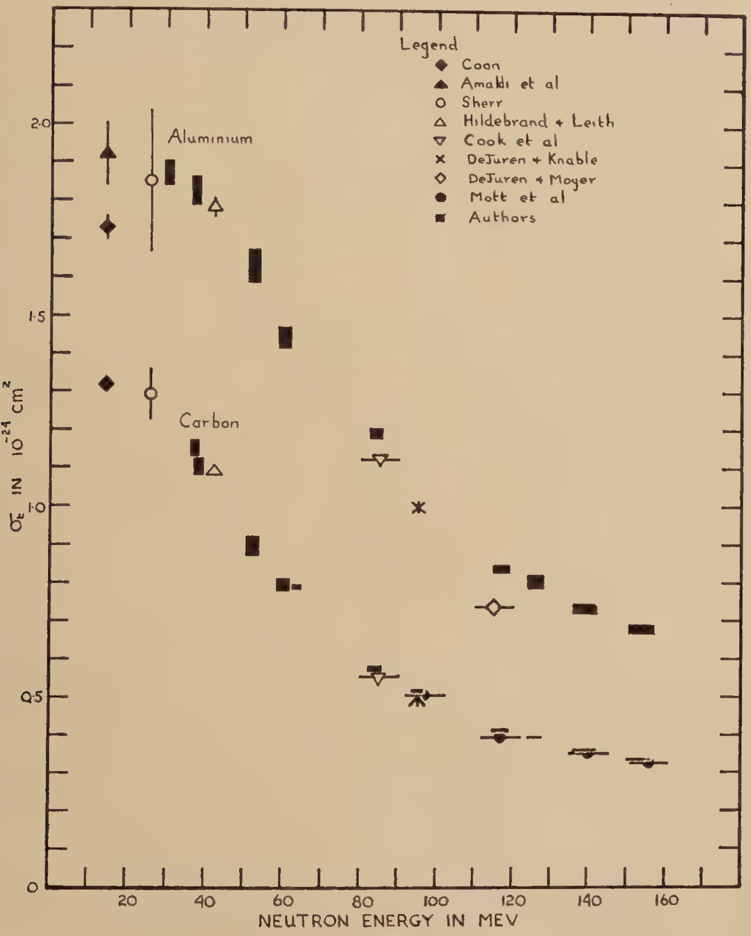

Variation of the neutron total cross section with energy for aluminium and carbon in the energy range 14 to 156 MeV.

The upper energy limit of the neutrons detected was governed by the position of the target in the cyclotron, by the value of the magnetic field and by the threshold energy required for the production of neutrons by protons. A lower energy limit was set by placing absorbers between the counters, so that only recoil protons with energy greater than a given value were detected. The band of neutron energies used varied from about

10 MeV at the lower energies of the investigation to about 20 MeV at the higher energies. Thus a relatively narrow band of neutron energies was used.

(ii) *Geometrical Layout*

The neutron beam, after emerging through a thin window in the cyclotron tank, was collimated by a 1 inch diameter hole in a steel bar 2 feet in length. This steel bar was inserted in one of five 2 inch diameter holes in the main concrete shielding wall, which was 6 feet thick (fig. 1 of the earlier report). The 1 inch diameter collimator was placed 26 feet from the internal target and the attenuators, $2\frac{1}{2}$ inches in diameter, were a further 8 feet behind the collimator. Exposure of an x-ray film at the position of the attenuators, showed that the beam was closely defined to $1\frac{1}{4}$ inch diameter. The polyethylene disc $2\frac{1}{2}$ inches in diameter, and the counter telescope were placed 30 feet behind the attenuators in the shielded tunnel. The target, attenuators and polyethylene disc were aligned by means of a theodolite.

(iii) *Attenuators*

The attenuators were machined to $2\frac{1}{2}$ inches in diameter and the various lengths were chosen to correspond to about two mean free paths for the particular neutron energy. A remotely controlled sample changer, operated from the counting room, held the five attenuators in position and also had a position for measurements with the unattenuated beam. The sample changer repeatedly positioned the attenuators to an accuracy of 1/32 inch. Chemically pure materials were used for the attenuators.

(iv) *Neutron Detector*

A triple coincidence counter telescope, using gas counters operated in the proportional region, was used to detect recoil protons emerging from the polyethylene disc placed in the collimated neutron beam. The counters, which were placed at a small angle to the main neutron beam, were rectangular in cross section, but otherwise similar to those used in the experiment at 153 MeV (Taylor *et al.* 1951 c). A similar arrangement of amplifiers, coincidence unit and scalers was used to measure the triple coincidences. As previously, random triple coincidences were estimated by measuring the coincidences between double coincidence pulses and the delayed third channel pulses. The random triple coincidence rate was never more than 1% of the true triple coincidence rate.

The thickness of the polyethylene disc used at any energy was chosen so that it was a small fraction of the total absorber in the telescope. Carbon absorbers were placed between the second and third counters in order to set a lower energy limit to the recoil protons detected.

(v) *Neutron Monitor*

The intensity of the incident neutron beam was monitored by a single boron fluoride counter immersed in a block of paraffin wax and placed behind a concrete block in the shielding wall. Tests were made under steady cyclotron conditions of the variation of counting rate with discriminator voltage and counter voltage, and conditions were set for minimum variation.

§3. NEUTRON ENERGY BAND AND THE EFFECTIVE ENERGY

Only at the highest energies of this investigation was there any appreciable contribution from the carbon content of the polyethylene, $(CH_2)_n$, to the detected protons. This arose from using an energy band greater than the 13 MeV threshold of the $^{12}C(np)^{12}B$ reaction. However, even at these energies the contribution was less than 3% of that coming from the hydrogen content. At the lower energies the contribution was less than 1%.

Neutron Total Cross Sections in 10^{-27} cm^2

Element	H	C	Al	Cu	Cd	Pb
Energy MeV						
30±1			1871±31	2442±39	3171±46	
37±1		1150±20	1825±35	2428±42	3119±48	4541±72
*38±1	223±7·6	1100±20				
45±1				2672±42	3288±50	4424±66
52±1·5		892±22	1627±41	2630±50	3376±52	4274±67
60±1·5		789±12	1439±25	2559±40	3324±48	4236±52
*63±1·6	126±3	784±5				
64±1·5						4463±82
72±1·5						4762±94
79±1·5						4742±52
84±1·5		571±6	1188±11	2260±22	3341±31	4685±48
93±1·5					3146±61	4762±66
*95±1·5	73·9±3	508±5				
102±2					3083±52	4593±64
117±2		408±4	833±8	1702±10	2686±37	4214±44
126±2	56·9±1·8	390±3	799±17	1627±22	2568±30	3917±64
139±3		355±3	729±11	1490±20	2349±19	3691±41
*153±3	46·4±1·2	330±3	677±11	1376±18		3499±26

* Previous results with energies corrected.

Since 97% or more of the protons counted were hydrogen recoils, the proton lower energy limit of the telescope corresponded to a definite and known neutron energy. By measuring the number of recoil protons as a function of absorber thickness and using a range–energy relation, it was possible to calculate the effective neutron energy. This measurement also provided a check of the maximum neutron energy against the value expected from the position of the target in the cyclotron, the value of the magnetic field and the threshold energy required for production of neutrons by protons. The agreement between the maximum neutron energy estimated from the range–energy relation and the expected value gave an estimate of the possible error in the absolute value of the effective energy.

Thus not only was a narrow energy band of neutrons used, but also the effective neutron energy was known within close limits.

A comparison of the range in carbon and aluminium of the external proton beam has suggested that the effective energy of the previous experiment quoted as 156±3 MEV may be nearer 153±3 MEV.

§4. EXPERIMENTAL PROCEDURE

The experiment was performed by placing each attenuator in turn in the neutron beam and comparing the counting rate with that obtained when no attenuator was present. This cycle of operations was then repeated until the desired statistical accuracy had been obtained. The cross sections obtained from each individual cycle showed no greater statistical deviation from the weighted mean than that expected from the total number of counts recorded.

The final result was taken as the weighted mean of the individual cycles.

§5. RESULTS

The values of the total cross sections obtained in the neutron energy range 30 to 139 MEV for carbon, aluminium, copper, cadmium and lead are given in the table together with results previously obtained.

A small correction has been added to the measured cross section in order to take account of those neutrons which were elastically scattered into the detector. The lengths of the attenuators and the geometrical arrangement were such that this correction was less than the experimental standard deviation.

The cross sections obtained in this investigation, together with those obtained by other investigators in the same energy region, are shown in the figures.

§6. DISCUSSION

The lead cross section shows a dip at intermediate energies, the difference between the value at 79 MEV and the miminum value at 60 MEV being ten times the standard deviation on either point. Assuming that the variation of the lead cross section with energy is correctly depicted by the values obtained in this experiment, the lower values shown at 83 and 95 MEV (Cook *et al.* 1949, DeJuren and Knable 1950) can be partially accounted for by the broader neutron energy band used in those determinations.

Including the 25 MEV results (Sherr 1945) and the 14 MEV results (Amaldi, Bocciarelli, Cacciapuoti and Trabacchi 1947, Coon 1952) as shown in the figures, a similar but slightly smaller dip is indicated in the cross section of cadmium and copper between 30 and 40 MEV. Also the value of the aluminium cross section at 14 MEV (Coon 1952) is lower than the value at 30 MEV by four times the standard deviation on either point, again indicating the possibility of a dip below 30 MEV.

A partial explanation of the shape of these curves is suggested in an accompanying letter by Lawson (1953).

ACKNOWLEDGMENTS

The authors wish to express their thanks to the Director, Atomic Energy Research Establishment, for his interest and for permission to publish the results of this work.

Grateful thanks are due to Mr. L. Bird for his valuable assistance in constructing the remotely controlled sample changer and in helping to take the measurements. Thanks must also be tendered to the cyclotron operating crew for their co-operation, and also to many colleagues for their helpful interest.

REFERENCES

AMALDI, E., BOCCIARELLI, D., CACCIAPUOTI, B. N., and TRABACCHI, G. C., 1947, *Report of an International Conference on Fundamental Particles* (London : Physical Society).

COOK, L. J., MCMILLAN, E. H., PETERSON, J. M., and SEWELL, D. C., 1949, *Phys. Rev.*, **72,** 1264.

COON, J. H., GRAVES, E. R., and BARSCHALL, H. H., 1952, *Phys. Rev.*, **88,** 562.

DEJUREN, J., and KNABLE, M., 1950, *Phys. Rev.*, **77,** 606.

DEJUREN, J., and MOYER, B. J., 1951, *Phys. Rev.*, **81,** 919.

HILDEBRAND, R. H., and LEITH, C. E., 1950, *Phys. Rev.*, **80,** 842.

LAWSON, J. D., 1953, *Phil. Mag.*, **44,** 102.

MOTT, G. R., GUERNSEY, G. L., and NELSON, B. K., 1952, *Phys. Rev.*, **88,** 9.

SHERR, R., 1945, *Phys. Rev.*, **68,** 240.

TAYLOR, A. E., PICKAVANCE, T. G., CASSELS, J. M., and RANDLE, T. C., 1951a, *Phil. Mag.*, **42,** 751 ; 1951 b, *Ibid.*, 328 ; 1951 c, *Ibid.*, 20.

TAYLOR, A. E., and WOOD, E., 1952, *Phys. Rev.*, **87,** 907.

XII. CORRESPONDENCE

A Diffraction Effect illustrating the Transparency of Nuclei to High Energy Neutrons

By J. D. Lawson
Atomic Energy Research Establishment, Harwell*

[Received November 17, 1952]

The transparency of nuclei to high energy neutrons has been strikingly demonstrated by recent cross section measurements by Taylor and Wood described in a companion paper (1953).

According to the ‘ continuum ’ nuclear model of Bethe (1940), later extended by Fernbach, Serber and Taylor (1949), the nucleus can be roughly represented by a sphere possessing a complex refractive index to the neutron waves. The real part of the refractive index is due to the nuclear potential well, and the imaginary part represents a loss of neutrons by absorption or inelastic scattering. The value of V, the depth of the potential well, is determined by the neutron binding energy and the energy of the highest momentum state of the nucleons on the assumption that they form a degenerate Fermi gas ; it is of order 30 Mev (Fermi 1950). The absorption coefficient may be represented by an imaginary potential iV' but its value is not important to the present argument so long as V' is not large compared with V, and is small compared with the incident neutron energy E.

From this model it is easy to find the change of phase of the neutron wave if a slab of nuclear matter of depth D is placed with its faces parallel to the wavefront. Now if a sphere of diameter D, with a refractive index not very different from unity, is introduced instead of a slab there will be behind it a circular region of diameter approximately equal to D where the average value of the phase retardation is rather less than that which would be caused by a slab of thickness D. In the case of the sphere the diffraction scattering will be a maximum when this phase change is an odd multiple of π, and a minimum when it is an even multiple.

The phase change caused by the slab is given by $\phi=D(k_1-k_0)$ where k_1 and k_0 are the propagation constants inside and outside it. From the elementary relation $E=\frac{1}{2}Mv^2=h^2/2M\lambda^2$ we find $k_0=2\pi/\lambda_0=2\sqrt{2\pi}M^{1/2}E^{1/2}/h$ and $k_1=2\sqrt{2\pi}M^{1/2}\,|E+V+iV'|^{1/2}/h$. Now if V and V' are small compared with E, $k_1-k_0=(2\sqrt{2\pi}M^{1/2}E^{1/2}/h)(V/2E)$, so that for the slab $\phi/\pi=(k_1-k_0)D/\pi=\sqrt{2}DM^{1/2}V/hE^{1/2}\approx 10^{13}D/E^{1/2}$ where D is in cm, and E in Mev. For the sphere the phase change will be given by $\phi/\pi=10^{13}\epsilon D/E^{1/2}$ where ϵ is a constant rather less than 1. A phase change of $n\pi$ will therefore occur at an energy given by $E=10^{26}\pi^2\epsilon^2D^2/n^2$. Taking rough values of 0·6 for ϵ and $2{\cdot}8\times10^{-13}\,\mathrm{A}^{1/3}$ for D, the value of E for which $n=1$ is shown in the table for various elements.

---

* Communicated by the Author.

Element	C	Al	Cu	Cd	Pb
Value of E for which $\phi=\pi$	14	26	46	64	100

It will be seen that these coincide, as nearly as might be expected from these very naive considerations, with the peaks in the cross section curves as measured by Taylor and Wood. The formula predicts other maxima and minima at lower energies than those shown, but at such energies the conditions for the validity of these considerations are not expected to hold.

I wish to thank Dr. J. M. Cassels and Mr. A. E. Taylor for illuminating discussions on this problem.

REFERENCES

BETHE, H. A., 1940, *Phys. Rev.*, **57**, 1125.
FERMI, E., 1950, *Nuclear Physics* (University of Chicago), p. 159.
FERNBACH, S., SERBER, R., and TAYLOR, T. B., 1949, *Phys. Rev.*, **75**, 1352.
TAYLOR, A. E., and WOOD, E., 1953, *Phil. Mag.*, **44**, 95.

A New Parameter for Use in Discussions of the Shell Model of the Nucleus

By N. FEATHER, F.R.S.
The University, Edinburgh*

[Received November 4, 1952]

IT is well known that the shell model and the liquid-drop model of the nucleus derive from approximations to a theory of nuclear structure which are distinct and to a large extent mutually contradictory. Each model, however, has had considerable success in correlating the results of experiment in a wide field. It is the object of this note to draw attention to a method of using certain experimental results which focuses attention on the differences between the properties of real nuclei and those predicted by the v. Weizsäcker formula (taken as representing the liquid-drop model). If the shell model is to be preferred to the other, then obviously it must be capable of providing a plausible explanation of these differences.

As in a previous note (Feather 1952), we use $B_p\binom{A}{Z}$; $B_n\binom{A}{Z}$ to represent, respectively, the energies of binding of the last proton and the last neutron in the nucleus $\binom{A}{Z}$, and we define a quantity ${}_D\Delta_p(Z)$ by the relation

---

* Communicated by the Author.

$${}_D\Delta_p(Z)=B_p\binom{2Z+D}{Z}-B_p\binom{2Z+D-1}{Z}.$$

Here D is the isotopic number of the nucleus $\binom{A}{Z}$ and ${}_D\Delta_p(Z)$ is a measure of the extent to which the energy of binding of the last (Z^{th}) proton in this nucleus exceeds that of the last proton in $\binom{A-1}{Z}$. Using a result established in the above-mentioned note (Feather 1952), we also have

$$B_p\binom{2Z+D}{Z}-B_p\binom{2Z+D-1}{Z}=B_n\binom{2Z+D}{Z}-B_n\binom{2Z+D-1}{Z-1},$$

so that ${}_D\Delta_p(Z)$ likewise measures the extent to which the energy of binding of the last ($(Z+D)^{\text{th}}$) neutron in the nucleus $\binom{A}{Z}$ exceeds that of the $(Z+D)^{\text{th}}$ neutron in $\binom{A-1}{Z-1}$. The parameter of interest for the discussion of nuclear models is now ${}_D\Delta'_p\,(Z)$, where

$${}_D\Delta'_p(Z)={}_{D-2}\Delta_p(Z+1)-{}_D\Delta_p(Z).$$

It will be observed that ${}_D\Delta'_p(Z)$ represents the increase, for unit increase in the proton number Z (from Z to $Z+1$), in the difference between the energies of binding of the last proton in nuclei of mass numbers A and $A-1$, respectively (as also the corresponding quantity in respect of neutron binding energies). Other formal properties of ${}_D\Delta'_p(Z)$ are as follows:

(i) If $T_\beta^-\binom{A}{Z}$ represents the total energy of negative β-disintegration, ground-state to ground-state, for the species $\binom{A}{Z}$, then

$${}_D\Delta'_p(Z)=T_\beta^-\binom{2Z+D}{Z}-T_\beta^-\binom{2Z+D-1}{Z}-T_\beta^-\binom{2Z+D-1}{Z-1}$$
$$+T_\beta^-\binom{2Z+D--2}{Z-1}.$$

Here we may note that the four species involved in this relation comprise one example each of the neutron-proton parity types $e-e$, $o-o$, $e-o$, $o-e$, whatever the parities of Z and D.

(ii) Assuming the four-constant v. Weizsäcker formula for the 'exact' nuclear mass (that is omitting any spin or parity-type term) the terms in α and γ ('volume' and 'surface' effects) vanish identically in the general expression for ${}_D\Delta'_p(Z)$—and the term in β ('asymmetry' effect) vanishes identically when $D=1$.

(iii) On the same assumption, and with accepted values for the v. Weizsäcker constants α, β, γ and δ, for all values of D the numerical magnitude of ${}_D\Delta'_p(Z)$ is negligibly small for all but the very smallest values of Z (e.g. for $D=2$, $Z=7$; $D=3$, $Z=16$; $D=51$, $Z=90$ calculated values of ${}_D\Delta'_p(Z)$ are, respectively, 0·052, 0·0096 and 0·0008 Mev).

Since ${}_D\Delta'_p(Z)$ can rarely be known from experiment to better than ±0·05 Mev, it will be seen from (iii) that experimental values of this parameter significantly different from zero point to a failure of the v. Weizsäcker liquid-drop model formula completely to account for the facts in individual cases—and it will be seen that this conclusion is effectively valid over the whole range of D and Z.

A survey of experimental data leading to the calculation of more than 600 neutron and proton binding energies has recently been completed, and an account will shortly be published with full discussion using the parameter ${}_D\Delta'_p(Z)$ and other criteria. For the purposes of this note it is sufficient to state that the 'experimental' curves of ${}_D\Delta'_p(Z)$ against Z (D constant) show interesting, and obviously significant, features. Thus the 5 points which are available for $D=1$ can be represented within the limits of experimental uncertainty by the straight line $\Delta'=0$, but the 12 points available for $D=2$ represent positive values of Δ' ranging from 0·4 to 4·0 Mev. Experimental values of Δ' considerably different from zero are less numerous as D (and Z) increases—thus the 9 points for $D=47$ fall on the line $\Delta'=0$ almost within the limits of error—but variations in Δ' (D constant) as large as 1·5 Mev certainly persist as far as $D=15$.

Reference

Feather, N., 1952, *Phil. Mag.*, **43**, 133.

The Surface of Beryl and Cadmium Iodide Crystals

By H. F. Kay and Barbara Appelbe
H. H. Wills Physical Laboratory, University of Bristol*

[Received November 4, 1952]

Optical microscope studies of the prism faces of beryl crystals (Griffin 1951) revealed unimolecular 7·9 Å steps of surprisingly high visibility which nevertheless varied considerably over different areas of the crystal surface. This strongly suggested the presence of surface features peculiar to the step, which were just smaller than the resolution of the optical apparatus employed. The electron microscope was employed to investigate these surface features by standard replica techniques.

The prism faces $(10\bar{1}0)$ of beryl crystals were found to be covered with small pits which are attributed to some etching process having occurred subsequent to growth. The high visibility of the steps is due to the higher concentration of pits along the step edges. Figure 1 (figs. 1, 2,

---

* Communicated by the Authors.

Plate 1, figs. 3, 4, Plate 2) is an electron micrograph of a single-stage shadowed formvar plastic replica taken from a prism face, and shows this concentration of the pits along lines representing the step-edges. The variation in optical visibility results from changes in size ($2\,\mu$ to $0{\cdot}05\,\mu$), depth ($0{\cdot}4\,\mu$ to $0{\cdot}02\,\mu$) and distribution of the pits.

In general, no characteristic regularity of shape or linking together seems to occur, for quite different types of corrosion can be seen even on different areas of the same face, but higher resolution two-stage methylmethacrylate silica replicas of a frequently occurring type of pit show that here at least they appear to be of more definite shape and are striated parallel to the basal plane at intervals of $\sim$ 350–400 Å. Figures 2 and 3 show two examples of this kind.

Replicas of the terminal faces (0001) of beryl revealed multimolecular steps and the absence of the general pitting such as occurred on the prism faces. Mottled patches approximately a few microns in extent were found to be scattered over the terminal surface and these are possibly finely pitted areas, the pits themselves being on the limit of the horizonal resolution of the plastic replicas. The absence of pits along the step edges on the terminal faces explains the paradox, observed optically (Griffin 1951), that the visibility of the multi-molecular steps is much less than that of the unimolecular steps on the prism faces.

The growth of cadmium iodide crystals as revealed by the optical microscopy (Forty 1952) is consistent with the spiral mechanism predicted by the dislocation theory. Electron optical observations were undertaken on these crystals to try and elucidate the nature of the large dislocation sources observed. Owing to their high molecular weight, the crystals could not be examined directly by electron transmission, and replica techniques were employed to study the surface features. The small cadmium iodide crystals were grown between microscope slide and a cover-slip from a drop of warm saturated solution. A polystyrene in benzene replica was then taken of the crystals on the slide. Although polystyrene replicas were found to be the strongest, they almost invariably broke along the step edges due to the fact that the step heights, usually up to 2 000 Å, were much greater than the thickness of the replica. Figure 4 shows a crystal whose growth is activated by two dislocations of opposite hand and of multiple strength, the centres of which are marked by hexagonally shaped prismatic holes approximately $\frac{1}{3}\,\mu$ in diameter, and having three of their edges parallel to the growth steps. (See inset.) Forty (1952) has seen indications of such hollow dislocation centres in optical photographs of cadmium iodide and they have been predicted on purely theoretical grounds by Frank (1951).

REFERENCES

Forty, A. J., 1952, *Phil. Mag.*, **43**, 72.
Frank, F. C., 1951, *Acta Crystallogr.*, **4**, 497.
Griffin, L. J., 1951, *Phil. Mag.*, **42**, 775.

Fig. 1

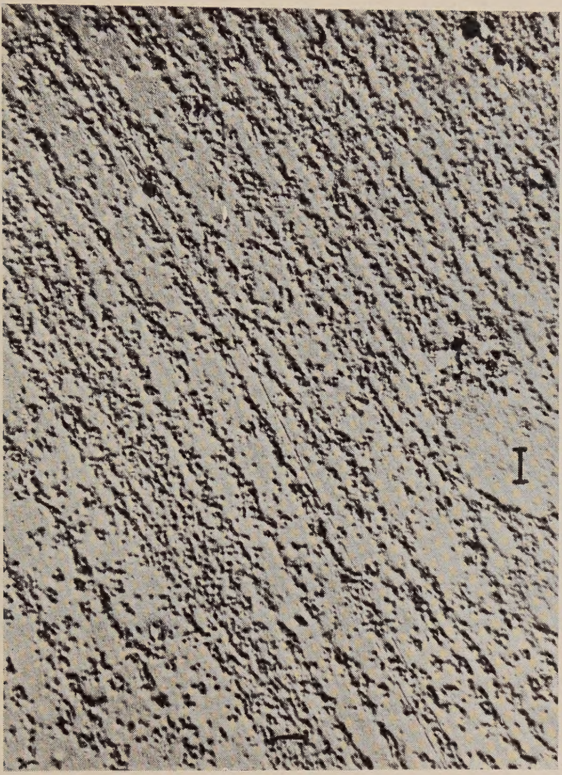

The surface of a prism face of a beryl crystal. Formvar replica shadowed with gold-palladium at 10°. The indicators represent 1 micron.

Fig. 2

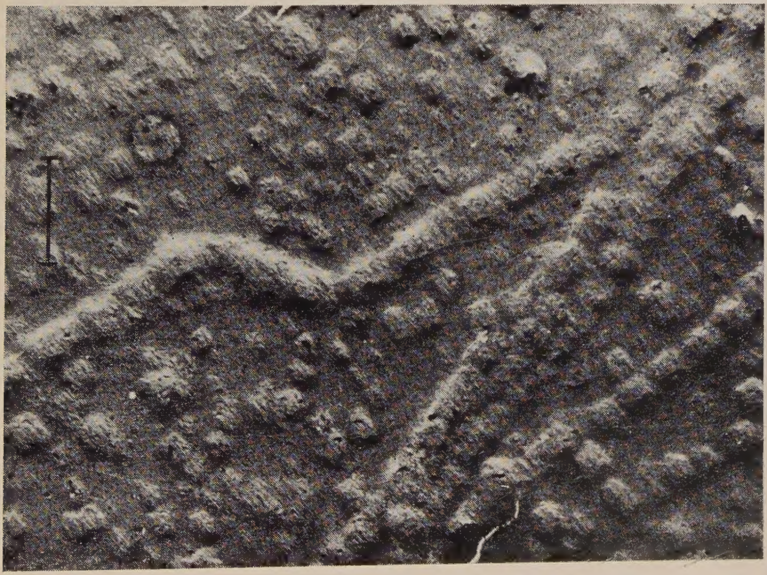

Another type of pitting seen on the prism face of beryl crystals. Methyl-methacrylate silica replica shadowed with gold-palladium at 10°.

Econometrics. By G. Tintner. (Chapman and Hall.) Price 46*s*.

This book will be of value to those who know both a little economics and a little mathematical statistics, although the standard of exposition is not as high as the subject deserves. The first part of the book is introductory. The second deals with multivariate analysis. The last, modestly entitled ‘ Some topics in time series analysis ’, efficiently treats problems of importance to economists which are not discussed in other text-books, and is therefore of great value to the student or the lecturer.

Throughout the book the examples are apposite and helpful, while the footnotes would make a full and useful bibliography—the absence of which is to be regretted. H. A. T.

A Short Table of the Bessel Functions $I_{n+\frac{1}{2}}(x)$, $(2/\pi)K_{n+\frac{1}{2}}(x)$. Prepared by C. W. Jones on behalf of the Mathematical Tables Committee of the Royal Society. (Cambridge University Press.) Price 6*s*. 6*d*.

The functions tabulated here are, with the corresponding ranges of argument and order,

$x^{-n-\frac{1}{2}}I_{n+\frac{1}{2}}(x)$	x=0(0·1)5 ;	n=0(1)10
$(2/\pi)x^{n+\frac{1}{2}}K_{n+\frac{1}{2}}(x)$	x=0(0·1)5 ;	n=0(1)10
$e^{-x}I_{n+\frac{1}{2}}(x)$	x=5(0·1)10 ;	n=0(1)10
$(2/\pi)e^{x}K_{n+\frac{1}{2}}(x)$	x=5(0·1)10 ;	n=0(1)10

which for obvious reasons are more convenient to tabulate than the Bessel functions themselves. Seven or eight significant figures are given almost everywhere and modified second differences are provided L. H.

Metallurgical Equilibrium Diagrams. By W. Hume-Rothery, J. W. Christian and W. B. Pearson. (The Institute of Physics, London.) [pp. 310.] Price 50*s*.

This is a good book ; but the title may be a little misleading. It deals primarily with the experimental methods employed on establishing the diagrams and not at all with the results of such investigations. There is in addition a brief theoretical introduction. The authors have interpreted these terms of reference generously and have ranged far in search of material. There are large sections on thermometry and thermal analysis and less extensive chapters on x-ray, dilatometric and magnetic methods, and on the techniques of metallography. The book includes 239 diagrams, 202 references to the literature and a copious index. Although intended primarily for research students in metallurgy, it will prove valuable to all metallurgists and metal physicists and indeed to all workers concerned with laboratory experiments at high temperatures.

Progress in Metal Physics, Vol. III. By B. Chalmers (*Editor*). (London : Pergamon Press Ltd., 1952.) [Pp. 334.] Price 48*s*.

The high standard of previous volumes is maintained in this latest group of reviews of progress in certain fields of metal physics. The subjects covered in this volume are crystallography of transformations, low temperature properties, electron theory, twinning, ferromagnetism, x-ray strain measurements, re-crystallization, and grain boundaries. A. K. H.

[The Editors do not hold themselves responsible for the views expressed by their correspondents.]